Molecular Analysis of Adenylyl Cyclase:

Bacillus anthracis Edema Factor Exotoxin

Dissertation

To obtain the Degree of Doctor of Natural Sciences
(Dr. rer. nat.)
From the Faculty of Chemistry and Pharmacy
University of Regensburg

Presented by

Hesham Hamada Taha Mohammed

From Cairo - Egypt

2009

The experimental part of this work was carried out between September 2006 and October 2009 at the Department of Pharmacology and Toxicology at the University of Regensburg under the supervision of Prof. Dr. R. Seifert.

The PhD – thesis was submitted on: October 2009

The colloquium took place on: 27. November 2009

Board of Examiners:	Prof. Dr. J. Schlossmann	(Chairman)
	Prof. Dr. R. Seifert	(1st Expert)
	Prof. Dr. S. Elz	(2nd Expert)
	Prof. Dr. A. Göpferich	(Examiner)

First and foremost, I would like to thank God for blessing me with this opportunity to pursue my PhD in the Germany. I thank Him for supporting me through the best and toughest years of my life.

Next, I am extremely thankful and grateful to my supervisor Prof. Dr. Roland Seifert for his invaluable guidance, support and for sharing his expertise and research insight. Prof. Seifert taught me the accuracy in the work and seeking for the excellence. Thanks for believing in me during the toughest times and boosting my morale to do better every day. Thanks for helping me develop my presentation, writing and research skills. I am deeply grateful to him and I wouldn't have been able to fulfil this dream without his constant encouragement and support. I hope that I have the chance to continue work with him forever.

I am deeply grateful to Prof. Dr. Frieder Kees for helping me initiating the project, for helping me in the protein purification and helping me realize what I was capable of and encouraged me.

I would like to thank Prof. Dr. J. Schlossmann, Prof. Dr. S. Elz and Prof. Dr. A. Göpferich (Institute of Pharmacy, University of Regensburg, Germany) for being part of the examination board.

I would like to thank also due all the collaborators at various stages of my PhD studies. I also wish to thank Dr. Wei-Jen Tang (Ben-May Institute of Cancer Research, University of Chicago, Chicago, IL, USA) for kindly providing us with EF, EF3, EF3F586A bacteria and various mutants EF3 proteins.

I would also like to thank Dr. Stefan Dove (Department of Pharmaceutical and Medicinal Chemistry II, University of Regensburg, Germany) for providing me with all the help on molecular modeling. I would like also to acknowledge Dr. Burkhard könig and my colleague Dr. Jens Geduhn (Institute of Organic Chemistry, University of Regensburg, Germany) for providing us with various purine and pyrimidine substituted nucleotides.

I would like to acknowledge and extend my appreciation to the following persons who have made the completion of this thesis is possible:

Dr. R. Schupfner (Center for Chemical Analysis, University of Regensburg, Germany) for the support in handling of radiochemicals.

Dr. E. Schneider and Dr. K. Wenzel-Seifert (Institute of Pharmacy, University of Regensburg, Germany) for inspiring scientific discussions.

Mrs. R. Prenzyna, Mrs. A. Seefeld, Mrs. S. Brüggemann, and Mrs. K. Wohlfahrt (Institute of Pharmacy, University of Regensburg, Germany) for support, understanding and expert technical assistance.

My colleagues Mrs. H. Appl, Ms. I. Brunskole, Mr. M. Desch, Ms. M. Erdorf, Ms. S. Geiger, Mr. B. Hieke, Ms. M. Hübner, Ms. N. Pop, Ms. K. Salb, Ms. E. Schinner, Mr. D. Schnell, Ms. A. Schramm and Dr. M. Göttle for contributing to the friendly atmosphere in our group.

I don’t have enough words to describe how grateful I am to my parents. Without them, my dream to become a researcher would always be unfulfilled. They have been the guiding angels in my life, helped me realize what I was capable of. They encouraged me, helped me achieve my goals and to stay focused, in short, I owe them all my success.

I thank all my family, my sisters (Shereen, Ashgan), my brother (Mohammed) for being very supportive and proud of my achievements. In particular, I would specially like to acknowledge my father-in-law Mr. Abdelwahab for his constant encouragement that will always help me remain grounded and work even harder to achieve my goals.

I would like to thank my colleagues at the Department of Biochemistry, Faculty of pharmacy, Al-Azher University, Egypt for the continuous encouragements. Also, I would like to thank the Egyptian government, Ministry of Higher Education, and Cultural affairs mission for the financial support of the scholarship.

Lastly, and most importantly, I thank Hager, my wife, and my kids for being my source of strength without them this journey would have been incomplete. I am extremely grateful to my wife for always being there for me, for believing in me and my capabilities, and for her love.

Abstracts and Publications

Parts of this thesis were published or presented as posters or short lectures:

Original Publications:

2008

Taha, H.M., Schmidt, J., Göttle, M., Suryanarayana, S., Shen, Y., Tang, W.J., Gille, A., Geduhn, J., König, B., Dove, S., Seifert, R. (2009) Molecular analysis of the interaction of anthrax adenylyl cyclase toxin, edema factor, with 2´(3´)-*O*-(*N*-(methyl)anthraniloyl)-substituted purine and pyrimidine nucleotides. Mol Pharmacol 75: 693-703.

2009

In preparation:

Taha, H.M., Shen, Y., Tang, W.J., Gille, A., Geduhn, J., König, B., Dove, S., Seifert, R. (2009) Molecular analysis of the interaction of anthrax adenylyl cyclase toxin, edema factor, with bis-2´, 3´-*O*-(*N*- (propyl)/(methyl)anthraniloyl)-substituted purine and pyrimidine nucleotides.

Poster presentations:

2008

Molecular analysis of the interaction of anthrax adenylyl cyclase toxin, edema factor, with 2´(3´)-*O*-(*N*- (methyl)anthraniloyl)-substituted purine and pyrimidine nucleotides
Taha, H.M., Geduhn, J., König, B., Dove, S., Seifert, R.
Symposium aus Anlass der Verabschiedung von Prof. Dr. med. K. Resch und des Dienstantritts von Prof. Dr. med. R. Seifert als Direktor des Instituts für Pharmakologie an der Medizinischen Hochschule Hannover, Hannover (Germany), November 2008

2009

Synthesis of a hydrolytically stable, fluorescent-labeled ATP analog as a tool for probing adenylyl cyclases
Emmrich T.[1], El-Tayeb A.[2], **Taha H.M.[3]**, Seifert R.[3], Müller C. E.[2], Link A[1].
DPhG-Doktorandentagung Für Studenten und Doktoranden, Irdning (Austeria), November 2009.

Short Talk:

2009

Molecular analysis of the interaction of anthrax adenylyl cyclase toxin, edema factor, with Bis-2´, 3´-*O*-(*N*- (propyl)/(methyl)anthraniloyl)-substituted purine and pyrimidine nucleotides.
50. Jahrestagung der Deutschen Gesellschaft für Experimentelle und Klinische Pharmakologie und Toxikologie (DGPT), Mainz (Germany), March 2009

Contents

Chapter I

I. General Introduction

1. Adenylyl Cyclases

1.1 Mammalian Adenylyl Cyclases

The modulation of AC activity is the key step in intracellular cAMP regulation by extracelluar stimuli. In mammals, the major ACs are integral plasma membrane proteins; they catalyze the synthesis of cAMP and pyrophosphate (PP_i) by conversion of adenosine 5'-triphosphate (ATP) (1-4). In intracellular signaling pathways adenosine 3',5'-cyclic monophosphate (cAMP) is a key player as second messenger in the response to first messenger signaling molecules such as neurotransmitters, hormones, and odorants. Until recently, the signaling by this archetypal second messenger was thought to be straightforward, but fifty years after its discovery by Earl Sutherland, cAMP regulation has become very complex. By direct activation of nucleotide-gated ion channels and stimulation of protein phosphorylation *via* activation of protein kinase A (PKA), cAMP is known to be involved in modulation of membrane potential and the rate of cell division (5-7). Independently of any phosphorylation, cAMP also induces protein-protein interactions, *e.g.* in signaling of Rap1 proteins (8, 9). The high complexity of synthesis and degradation of the second messenger is also due to a multiplicity of phosphodiesterases and adenylyl cyclase (AC) isoforms.

ACs act as effector enzymes integrating extracelluar signals by G-protein coupled receptors (GPCRs) to a variety of intracellular signaling pathways (10, 11). The classic receptor-G-protein-AC signal transduction cascade is characterized by a large excess of G-proteins compared to receptor and effector molecules. Therefore, G-proteins are the major amplification factor of the GPCR signal (12, 13), and the AC molecules are the limiting component for maximum second messenger production in response to hormone stimulation (14, 15). Although ACs do not contribute extensively to the amplification of intracellular signaling, they participate in diverse manners to integrate signaling pathways and cross-talks in different cell systems (16, 17).

Mammalian ACs are transmembrane proteins with the exception of one soluble form of AC (sAC) identified in testis (18). Nine different AC isoforms have been identified in mammals that differ in tissue distribution, activation and inhibition by different mediators (19, 20).

1.2 Bacterial Adenylyl Cyclase Exotoxins

In addition to mACs, several microorganisms such as *Bacillus anthracis, Bordetella pertussis and Pseudomonas aeroginosa*, release AC toxins that play an important role in disrupting several host intracellular signaling pathways. These exotoxins enter host cells *via* different mechanisms and cause a dramatic increase in cAMP levels (21-23).

1.2.1 Anthrax Adenylyl Cyclase Toxin, Edema Factor

One such toxin is Edema Factor, released by *Bacillus anthracis* that alters water homeostasis and causes edema by increasing cAMP levels (24, 25). Though mACs and EF are structurally distinct, both these enzymes are important cAMP modulators and they both constitute potential drug targets. By regulating cAMP levels, mACs play an important role in several diseases such as congestive heart failure, and bronchial asthma (19, 20). By increasing cAMP levels, EF contributes significantly to cutaneous and systemic forms of anthrax (26, 27).

Anthrax disease

Anthrax, caused by *Bacillus anthracis*, is a deadly epizootic disease primarily affecting cattle and consequently humans that come in contact with infected animals or animal products (28, 29). Occupational exposure to infected animals or their products - such as skin and meat - is the usual pathway for humans. Persons, who work with imported animal hides, tissues or furs from high incidence areas and workers, who are exposed to dead animals and animal products, are at the highest risk to become infected, especially in countries where anthrax is more common. Human anthrax is more common in developing countries of Asia and Africa compared to the developed countries (30).

Anthrax cases have been described as early as 16th century BC in Egypt and several publications describing anthrax were published in the 1800s (31, 32). More recently, anthrax spores were used during the terrorist attacks in the US in 2001 giving a new meaning to the word bioterrorism (33).

Bacillus anthracis is a large Gram-positive bacterium that forms spores when coming in contact with oxygen (Fig. 1). The spores which carry the virulent factors are highly resistant to a wide range of climatic and environmental conditions such as high temperature, UV light and high pH (34-36). The spores carry three exotoxins namely Edema Factor (EF), Lethal Factor (LF) and Protective Antigen (PA) and a poly-γ-D glutamyl capsule, all of which are released when the spores come in contact with host cells. Crystallographic, biochemical, kinetic and structural studies have greatly improved our understanding of the mode of action of these toxins.

Fig. 1: ***a) Coloured scanning, electron micrograph (SEM) of bacillus anthracis*** **(37),** ***b) Gram-stain of bacillus anthracis*** **(38), c)** ***Original photomicrograph of Bacillus anthracis by Robert Koch*** **(38).**

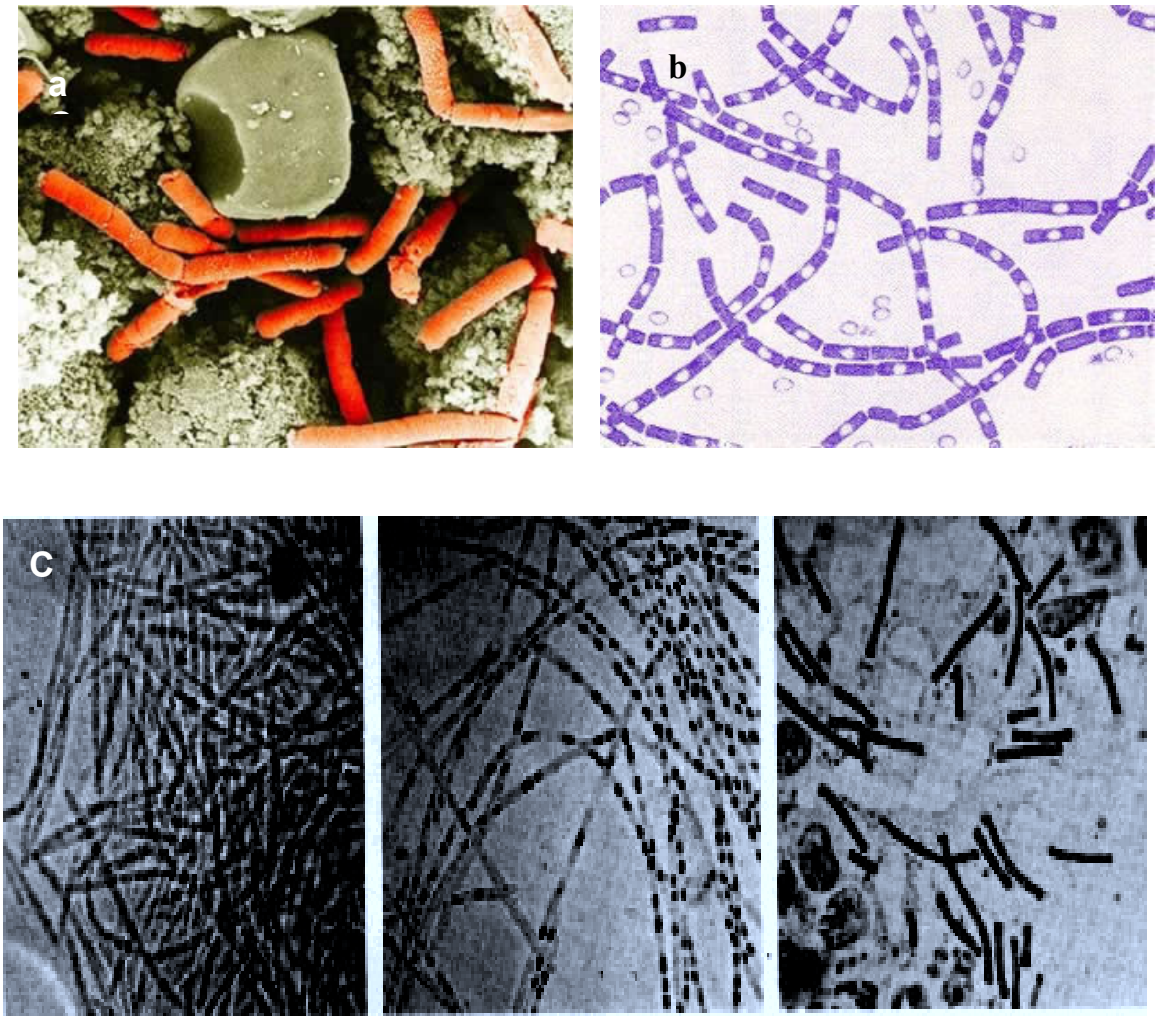

Anthrax is primarily classified into three types depending on the mode of entry of the spores into the host. These anthrax forms are (a) cutaneous anthrax, (b) inhalational anthrax and (c) gastrointestinal anthrax. There are also some minor and rare forms of anthrax such as anthrax sepsis and renal and ophthalmic forms of anthrax (32).

Cutaneous anthrax

Cutaneous anthrax is the most common manifestation of anthrax in humans, accounting for more than 95 percent of cases occurs due to introduction of endospores into the body through a cut, break or abrasion on the skin. In most cases, cutaneous anthrax in humans is due to the handling of infected animals or their products. There have also been reports of some rare cases of cutaneous anthrax due to biting of flies that have fed on anthrax-infected animals. The incubation period of spores is typically between 1-12 days (39). The signs and the symptoms appear with the development of papule on the skin which slowly turns into a vesicle showing necrosis, edema and a characteristic black eschar (lesion) (Fig. 2). The cutaneous form of anthrax can be effectively treated with antibiotics and can be fatal if left untreated. About 20 percent of untreated cases of cutaneous anthrax will result in death. Anthrax is not spread from person to person by casual contact, coughing and sneezing; the only way anthrax can be transmitted is by direct contact with the drainage from an open sore (32, 40, 41).

Inhalational anthrax

Inhalational anthrax, also called pulmonary anthrax, is the most lethal form of anthrax. The spores inhaled and, after a brief journey to the lungs, reach the alveolar sac. the immune cells, macrophages, become aware of the presence of anthrax endospores and start to engulf them (42). The macrophages travel to the lymph gland where the immunity against the future infection is prepared. However, the spores are not destroyed but germinate to vegetative bacteria called bacilli. The Initial symptoms start with fever and cough. Within a few hours, more serious symptoms such as dyspnea (shortness of breath), cyanosis (blue coloration of the skin) and respiratory failure develop leading to septicemia, shock and death. Current models for inhalational anthrax assume that bacilli, multiply and lyse cells, then

spread through lymph nodes causing extensive septicemia (Fig. 3). Inhalational anthrax cases have a high mortality rate and broad-spectrum antibiotic therapies have not been very helpful (40, 43, 44).

Gastrointestinal anthrax (GI anthrax)

The gastrointestinal form of anthrax accounts for less than 5% of all anthrax infections. Gastrointestinal anthrax occurs due to ingestion of spores through contaminated food or water. This form of anthrax has a high mortality rate. Two subforms i.e. the oropharyngeal form where spores get deposited in the upper GI tract, and the intestinal or abdominal form with deposition of spores in the lower GI tract, have been reported. The latter form is characterized by an acute inflammation of the intestinal tract. First symptoms of nausea, loss of appetite, vomiting and fever are followed by abdominal pain, vomiting of blood and severe watery or bloody diarrhea. Intestinal anthrax results in death in 25-60 percent in cases (45). Extensive edema and necrosis occurs in both forms of GI anthrax. If detected early, GI anthrax can be treated with antibiotics. Once spores invade the bloodstream, they cause toxemia, septicemia and death (46).

Fig. 2: ***Cutaneous anthrax; examples for the cratered center surrounded by dying tissue,*** **a (47), b (48), c (49)**

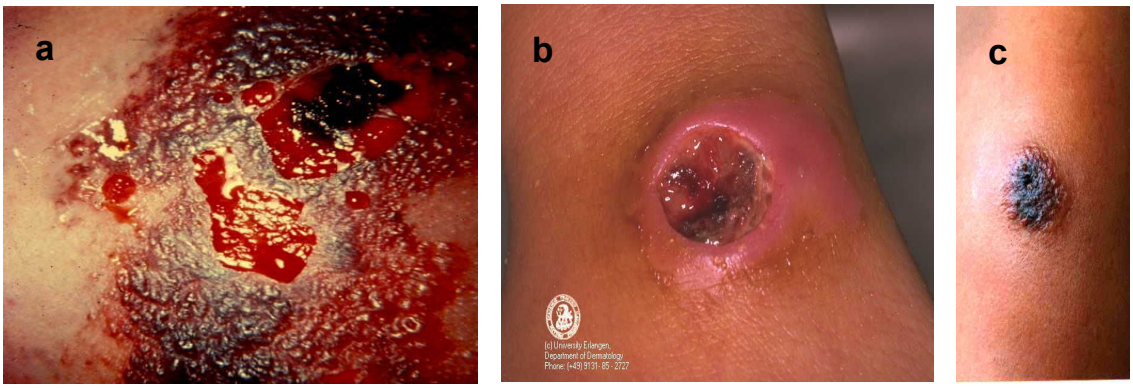

Fig. 3: Inhalational anthrax - Chest X-rays may show a widened mediastinum and pleural effusions (50).

Diagnosis, treatment and prevention

The symptoms of systemic anthrax infection resemble septic shock and kill the patient within days. For example, inhalational form of anthrax is a deadly disease; the bacilli and their exotoxins diffuse through the body before the immune system has had a chance to eradicate the invaders. Laboratory diagnosis of anthrax includes Gram and polychrome methylene blue staining of the specimen from potentially infected patients to identify the polypeptide capsules of *Bacillus anthracis. Bacillus anthracis* from body fluids can also be cultured in blood agar and identified as large colonies, white or grey in color. It can also be diagnosed by measuring specific antibodies in the blood of infected persons. The anthrax skin test is performed by injecting an attenuated strain and is positive in 85% of cases immediately after infection (32, 51, 52).

The first vaccine for anthrax was developed by Louis Pasteur by injection of an attenuated *Bacillus anthracis* strain. Protective antigen (PA) was discovered as one of the toxins responsible for virulence by Gladstone (53). By the 1950s, the AVA vaccine was developed with PA and small amounts of Edema factor (EF) and lethal factor (LF) from an attenuated strain adsorbed to aluminum hydroxide. AVA, the only vaccine for anthrax approved for use in humans, was licensed by the FDA in the 1970s. AVA with the trade name BioThrax® is manufactured by Bioport Corp (Lansing, MI, USA), parent company of Emergent Biosolutions (Rockville, MD, USA). Due to problems related to purity, differences in reactivity and manufacturing, a next

generation vaccine called rPA is being clinically tested to determine its safety and reactivity. rPA is a recombinant protective antigen purified from an asporogenic *Bacillus anthracis* strain. rPA was clinically tested by VaxGen Inc (Brisbane, CA, USA) and later acquired by Emergent Biosolutions (Rockville, MD) in 2006 (54). Due to the rapid growth of *Bacillus anthracis* in vital organs the pathogenesis of anthrax is mediated by the combination of bacteremia and toxemia (55-57). Anthrax bacteria are sensitive to a broad spectrum of antibiotics; thus antibiotics are the primary treatment of this infectious disease. However, antibiotics are ineffective against either toxemia or antibiotic-resistant strains (58-60). In addition to vaccines, post-exposure treatment for anthrax is aggressive and comprises timely antibiotic therapy with penicillin, doxycyclin and other broad spectrum antibiotics such as fluoroquinolone compounds.

Approaches to develop next-generation drugs and vaccines for anthrax are exploring new avenues such as inhibitor design for receptor binding, toxin assembly, endocytosis, and enzymatic activity of toxins and targeting virulence of the poly-γ-D glutamyl acid capsule (61-63).

Prevention is effective by surveillance and regular check-up of humans working closely associated with animals and military personnel working in higher-risk areas where anthrax spores may be used for potential biological warfare. Timely immunization of animals and humans is also a key to preventing anthrax infections in case of a suspicious exposure to anthrax spores (64, 65).

1.2.1.2 Anthrax – Biological warfare and incidence in developing countries

Bacillus anthracis spores have been used as bioweapons and several significant incidents occurred during the last few centuries. Ideal characteristics of biological weapons are quick low-cost-production in large quantities, easy cultivation of the microbes, high infectivity, high potency, fast-acting without a long lag time between dispersal and debilitating illness and delivery as an aerosol. Often, the biological weapons can be manufactured quickly and easily – the primary difficulty is not the production of the biological agent but delivery in an infective form to a vulnerable target (66-68). Anthrax spores were purportedly used to kill millions of people and cattle during the movement of Huns across Eurasia in 80 AD (69). In

1941, the British Government tested the effect of anthrax spores as a bioweapon in Gruinard Island near Scotland. The island was uninhabited until 1986 after several attempts were made to sterilize the soil (70). In 1979, 96 cases of anthrax including 68 deaths resulted due to accidental release of anthrax spores from a military facility in Russia (71). In 1993, an attenuated strain of anthrax was sprayed from the top of a building by the Aum Shinrikyo, a doomsday cult in Tokyo (72-74). In 2001, anthrax spore-laced letters caused widespread panic among people in the United States and worldwide. The event of the 2001 bioterrorism-related anthrax attack in the United States highlighted an urgent need for a valuable, more effective adjunct to conventional antibiotic treatment to improve survival rate and quality of life of patients suffering from anthrax due to future acts of bioterrorism (75). For cases of pulmonary anthrax antibiotic treatment used for victims of this attack resulted in a survival rate of slightly better than 50%. Due to its high potency, hardiness and resistance to a wide range of conditions, anthrax is classified as Category A bioterrorism agent by the US Centers for Disease Control and Prevention (CDC). It is estimated that a 50 kg of anthrax aerosol spray would result in millions of deaths and, therefore, the potential devastating effects of anthrax cannot be underestimated (76).

Naturally occurring anthrax is still a major problem in several countries such as India, Turkey, Greece and countries in the African continent. Until 2006, at least 205 cases of anthrax have been reported in parts of Southern India especially in the under-developed regions (76, 77). Actually, there is no doubt that, lack of awareness and lack of vaccinations for both humans and livestock are the primary reasons for high incidence of anthrax infection.

In view of the potential use of anthrax as a bioweapon and the high incidence of naturally occurring infections, there is an urgent need for the development of efficient, accessible and cost-effective drugs, vaccines and other therapeutics to prevent and cure anthrax.

1.2.1.3 Anthrax tripartite toxin and mechanism of toxin translocation into host cells

Virulence factors of *Bacillus anthracis* are encoded on two plasmids: - pXO1 which contains genes responsible for synthesizing the exotoxins EF, lethal factor (LF), and protective antigen (PA), and pXO2 which carries genes that synthesize the poly-γ-D glutamyl capsule. *Bacillus anthracis* toxin is a member of the bacterial binary A-B toxin family where the B moiety acts as a transporter helping the A moiety to translocate into the cytosol. The A moiety exerts its deleterious effects after it enters the cytosol. In the case of *B.anthracis*, PA acts as a transporter protein and translocates EF and LF into the host cell (28, 78) (29, 79, 80) .

Protective antigen (PA) is an 83 kDa protein that binds to specific receptors referred to as ANTXR1 (tumor endothelial marker 8) and ANTXR2 (Capillary morphogenesis protein 2), on host cells. Both ANTXR1 and ANTXR2 are widely expressed in cells and consist of regions similar to the von Willebrand factor type A domain and the Integrin I domain, thus binding to collagen and collagen/laminin respectively. LRP6, a cell surface protein, can also act as a coreceptor. By interacting directly or indirectly with ANTXR1 and ANTXR2, LRP6 can stimulate PA binding to ANTXR1 and ANTXR2 (81-87). After PA83 is bound to ANTXR1 or ANTXR2, it is cleaved by a member of the furin family of proteases. The N terminal region of PA83 is cleaved, releasing PA20 extracellularly, and PA63 is bound to the receptors (88). PA63 then self oligomerizes to form a ring-shaped heptamer referred to as prepore conformation. EF and LF bind competitively with high affinity to the PA63 heptameric prepore conformation. Several studies have shown that a maximum of three molecules of EF and/or LF can be accommodated by the PA63 heptamer.

The recognition sites of the interaction of EF and LF with PA63 heptamer have been mapped and both EF and LF are positioned with their N termini at the entrance of the PA63 prepore and therefore can translocate in the N- to C terminal direction. The PA63 heptamer with bound LF and or EF then undergoes receptor-mediated endocytosis and is transferred into an intracellular acidic compartment. The low pH in the endosomal compartment results in structural rearrangements, giving rise to the PA63 pore conformation that can now insert itself in the endosomal membrane. The

PA63 pore is typically a 14-strand transmembrane β barrel with a water-filled central cavity of about 15 Å in diameter (79, 88-90). EPR (Electron Paramagnetic Resonance) studies have shown that seven F427 residues from the PA63 heptamer form a "Φ" (phi) clamp exposing their aromatic rings in the lumen. The Φ clamp causes partial unfolding and translocation of EF and LF through the pore coupled to a positive membrane potential across the membrane (91).

Fig. 4: Schematic representation of PA binding, assembly, endocytosis and translocation of EF and LF inside the cytosol.

PA83 binds to specific receptors on the membrane. Furin endoproteases present on the cell membrane cleave PA83, releasing PA20 extracellularly, and PA63 bound to the receptor. PA63 self-oligomerizes to form a ring-shaped heptamer termed the prepore complex that can bind to EF and or LF. Prepore complex with bound EF and or LF is then endocytosed to an intracellular acidic compartment. The lower pH in the endosome triggers structural rearrangements causing a change in conformation from prepore to pore causing partial unfolding and translocation of EF and LF into the cytosol.

Fig. 4: Schematic representation of PA binding, assembly, endocytosis and translocation of EF and LF inside the cytosol.

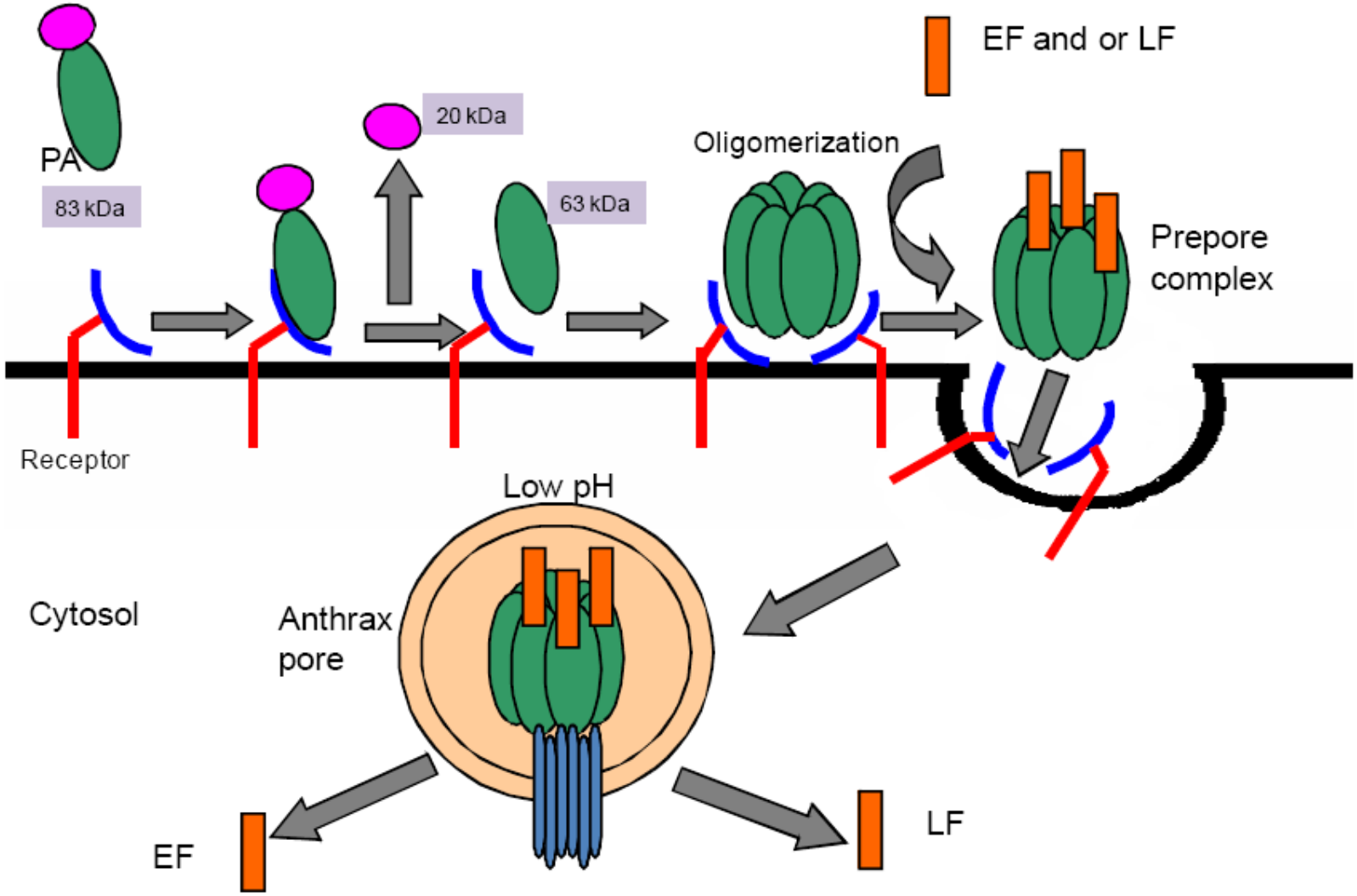

1.2.1.4 Anthrax toxin components and their function

Protective antigen (PA), 83 kDa protein, is divided into four domains. Domain 1 has a recognition site for Furin-like family endoproteases and part of domain 1 is cleaved giving rise to PA20 that is released extracellularly and PA63 which can self oligomerize. Domain 2 undergoes pH-dependent conformational changes and helps in oligomerization, conversion from prepore to pore forms and translocation of EF and LF into the cytosol. Domain 2 from seven PA63 monomers forms the transmembrane β barrel and consists of the Φ clamp for unfolding and translocation of EF and LF. Furthermore, it has been shown that K397 from one PA domain 2 can form a salt bridge with D426 of the neighboring PA domain 2 thus giving rise to a loop bringing the F427 residues closer to form the Φ clamp. Mutational studies have shown that Domain 3 is also important for oligomerization of PA63. Domain 4 consists of the receptor-binding domain and is important for the interaction of PA with its cellular receptors ANTXR1 and ANTXR2 (92-95).

Lethal factor (LF) is a 90 kDa zinc-dependent metalloprotease that can cleave the proline-rich N-terminal of mitogen–activated protein kinase (MAPK) kinases (MEKs). LF can cleave and inactivate all MEKs except MEK 2. Since MEKs serve as important substrates for downstream signaling, proteolytic inactivation of MEKs by LF inhibits the MAP kinase signal transduction pathways that include p38, JNK and ERK. The crystal structure of LF with bound substrate and inhibitor has shown the presence of four domains. The N-terminal domain 1, or LF-N, is the protective antigen binding domain and has residues similar to EF-N. Domain 2 and Domain 3 serve as sites for substrate recognition. The C terminal domain 4 consists of the zinc metalloprotease site (79, 96, 97). Though several studies have shown that EF and LF can bind only to PA63 heptamers, recent evidence suggests that LF and LF-N (N-terminal region of LF) can bind to PA63 monomer, albeit with lower affinity. It has also been shown that PA20 interacts with LF-N, though a functional role for this interaction has not been determined (89, 98). It has also been demonstrated that low concentrations of LF bind to PA63 and higher concentrations inhibit PA63 assembly (99).

Edema Factor (EF) is a 93 kDa calmodulin (CaM)-activated adenylyl cyclase that can convert ATP to cAMP (23). Increased cAMP levels can cause several changes by activating downstream targets such as PKA, in turn disrupting intracellular signaling pathways and impairing host defences (43). EF is thought to be primarily responsible for the cutaneous form of anthrax (23, 100). A detailed analysis of the structure and intracellular activation of EF will be discussed in the following sections.

ET (EF with PA) and LT (LF with PA) can together or separately impair host defences by promoting bacterial invasion (101). Both ET and LT suppress innate immune responses and impair human neutrophil activity (102, 103). ET and LT inhibit the generation of superoxides and reactive oxygen species (ROS) by NADPH oxidase activity of human neutrophils needed to cause bacterial killing (104). ET increased cAMP levels of lymphocytes can cause changes in important gene expression resulting in suppression of the immune response. ET can also inhibit chemotaxis in endothelial cells by activating downstream effectors such as Epac and RAP1 (105). Also, the PA binding domain of EF is not essential for potency of ET (106). Furthermore, ET can inhibit platelet aggregation and cause hemorrhage, an important symptom of anthrax (107). Anthrax toxin can induce hemolysis in the presence of polymorphonuclear cells (PMNs), an activity primarily mediated by PA, with synergistic effects provided by LF and EF (108). EF and LF are capable of inducing hemolysis (lysis of blood cells) in the presence of neutrophils (108).

1.2.1.5 Edema Factor – structure and intracellular activation

EF can be possesses two domains, a 30 kDa N-terminal protective antigen binding domain and a 63 kDa CaM sensitive adenylyl cyclase domain or EF3 (26, 109). The PA-binding domain is homologous to the N terminal region of LF (110). EF3 can be further divided into N terminal EF3 (EF3-N) and a C terminal EF3 (EF3-C). EF3-N is homologous to AC exotoxins from *Bordetella pertussis* and *Pseudomonas aeuroginosa.* It is resistant to protease digestion. EF3-C is sensitive to protease digestion in the absence of CaM (109).

After PA-mediated entry of EF into the cells, EF binds to calmodulin (CaM). CaM is a highly conserved calcium sensor protein. CaM has a molecular weight of

16.5 kDa and consists of N- and C-terminal globular domains which are connected by a flexible, central α-helix (Fig. 5), and is ubiquitously expressed in cells. CaM binds and modulates activities in a large number of targets that include enzymes, pumps and ion channels in a calcium-dependent manner, thus playing an important role in several intracellular processes such as signal transduction and gene transcription (111, 112).

X-ray and NMR studies have shown that CaM exists as a flexible dumbbell-shaped structure with two globular end domains; each globular domain comprises two helix-loop-helix calcium-binding motifs. Calcium binding to CaM induces conformational changes from a closed state with a highly negatively charged surface to an open conformation. In the closed state, the two helices of each Ca^{2+}-binding helix-loop-helix motif are almost anti-parallel, whereas in the open conformation the two helices are nearly perpendicular. These conformational rearrangements lead to the exposure of a large, hydrophobic binding pocket (113, 114).

Fig. 5: A) 3-d-structure of Ca^{2+}-free calmodulin (115)**. B) 3-d-structure of calmodulin in complex with Ca^{2+}-ions (blue spheres)** (116, 117)**.**

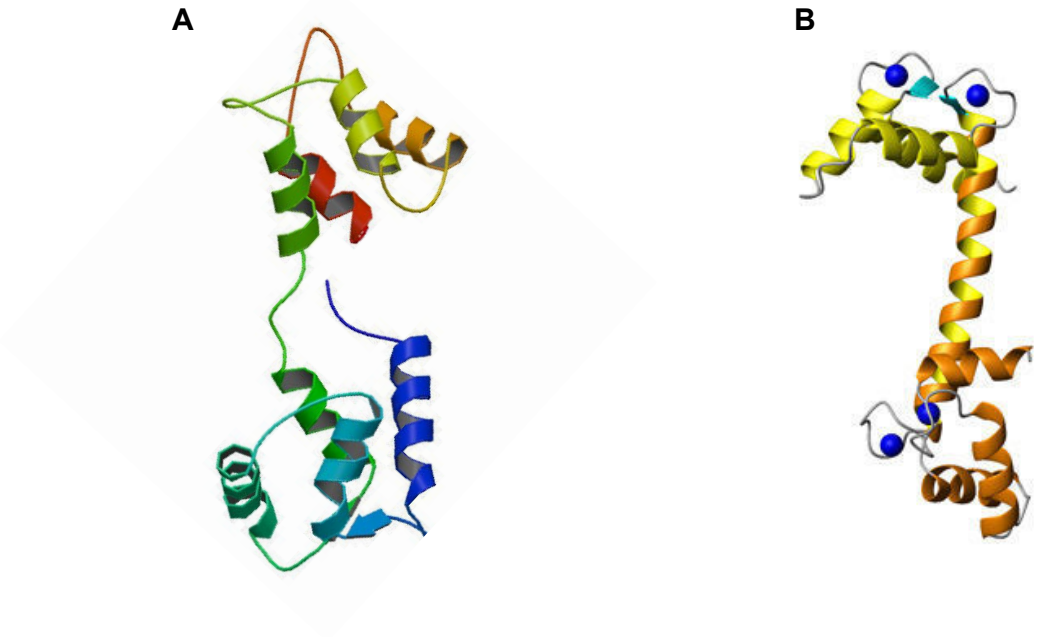

CaM binding causes large conformational changes in the structure of EF. The structure of EF is crucially dependent on binding of its cofactor. In the absence of calmodulin, EF shows no catalytic activity.

The crystal structure of EF with and without CaM and inhibitor, solved by Drum et al (2001), showed that the C terminus of EF consists of three domains, CA, CB and a helical domain. A linker region connects CA to the helical domain and CA and CB together form the catalytic core of the enzyme. In the CaM-free EF structure, CA, the helical domain and switch C form a contiguous, positively charged surface that is likely to make initial electrostatic contacts with the highly negatively charged CaM. The unusually large binding surface between EF and CaM stabilize the various structural rearrangements that activate EF. EF activation by CaM is a multistep process, which is initially mediated by CaM-binding residues that are exposed in the CaM-free state. One such residue, Lys 525, has been identified as a binding 'hot spot' through alanine-scanning mutagenesis of EF residues located in the interface between helix H and CaM. Whereas mutations in nearby residues Lys 523, Gln 526 and Val 529 have little effect on CaM activation, the Lys525Ala mutation markedly increases (200-fold) the CaM concentration for half-maximum response (EC50), with only a small reduction in the velocity of the enzyme-catalysed reaction at infinite concentration of substrate (V_{max}).

CaM is almost completely wrapped by a clamp formed by CA, linker and the helical domain in such a manner that it causes a 30˚ rotation and a 15 Å movement of the helical domain. In addition, three regions, switch A, B and C in EF also undergo large conformational changes due to CaM binding. Switch A (residues 502-551) consists of amino acid residues important for CaM- and nucleotide binding. Switch B (residues 578-591) contains residues important for ATP binding and catalysis. Switch C (residues 630-659) consists of residues from the linker region and swings almost 33 Å when CaM binds to EF. The EF-CaM interaction is stabilized and strengthened by a large number of both hydrophobic and hydrophilic contacts. FRET (Fluorescence resonance energy transfer) experiments have also shown that CaM binds to EF in an extended conformation unlike its binding to a number of other proteins (109, 118).

There are several mechanisms by which activators are known to activate enzymes. The activation of EF by CaM is conceptually most similar to the activation of G_{α} proteins by regulator of G-protein signalling. In this case, as in EF, the catalytic machinery is present near the site of catalysis, but is disordered in the inactive state. The most surprising aspect of EF activation by CaM is that the conformational switches associated with activation do not involve residues that participate in chemical catalysis. The catalytic base, the metal-binding site, and all of the amino acids thought to be involved in stabilizing the pentavalent transition state are virtually identical in the active and inactive states of the enzyme. These residues are significantly more exposed to solvent (and substrate) in the inactive state than in the active state. The switch that gives rise to a 1,000-fold increase in enzyme activity involves residues that bind and position the substrate, not those that perform the catalytic reaction (25).

Fig. 6: Schematic illustration of EF and EF3 proteins

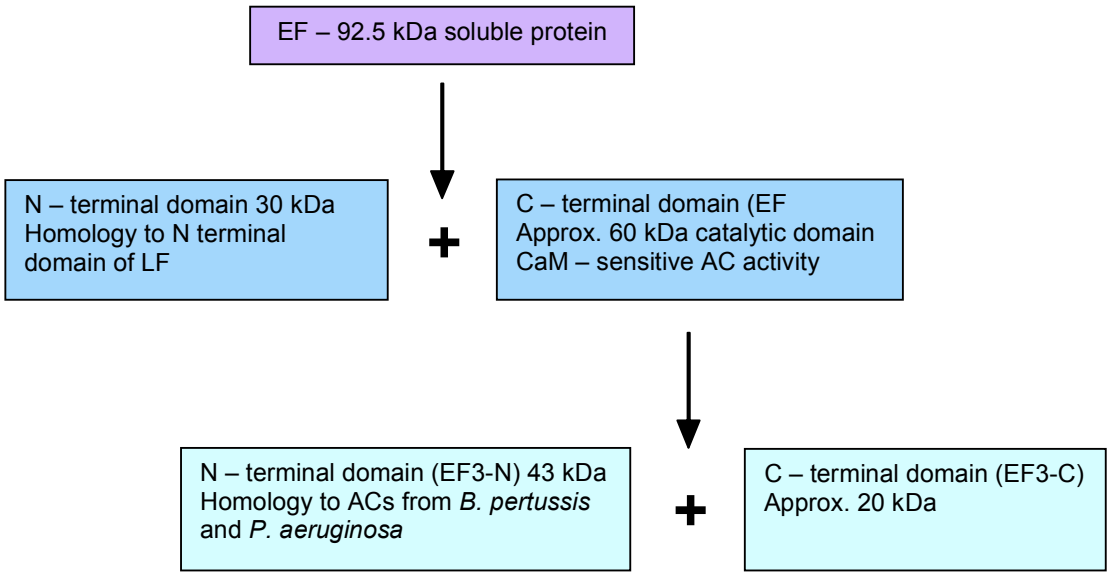

Fig. 7: Crystal structure of EF (a) EF alone (b) EF with bound CaM and 3'dATP (25).

CA and CB domains of EF are shown in green and the helical domain is shown in yellow. Switch A, B and C regions are shown in blue, orange and magenta respectively. CaM is shown in red and metal ions and 3'-d-ATP are shown in purple. CaM is wrapped by the helical domain and the switch A, C and CA regions. The CA and CB domains form the catalytic core of EF (25).

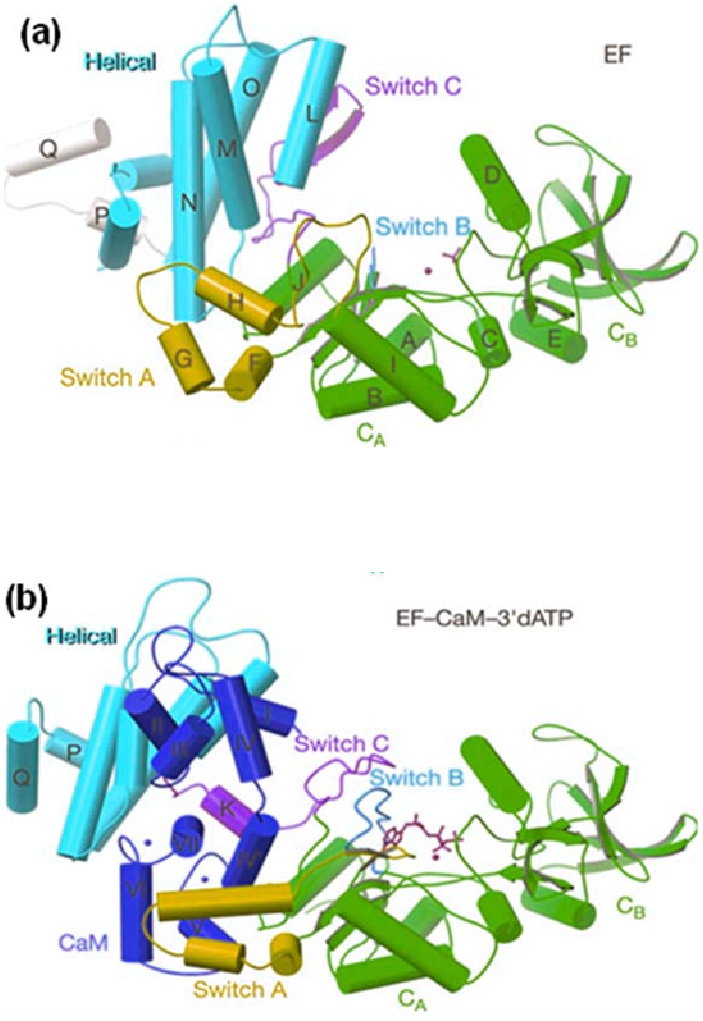

1.2.1.6 Catalytic mechanism of EF

Following activation of EF by CaM, EF catalyzes conversion of ATP to cAMP. Several crystal structures of EF with bound CaM and nucleotide/inhibitor have been solved that greatly helped to improve our understanding of the ATP binding and catalysis processes. The first crystal structure of EF with bound CaM and 3'-d-ATP published by Drum et al., (2002) indicates a single metal ion-mediated catalytic mechanism (Fig. 8, **A**) unlike the mammalian ACs where two-metal-ion-catalysis is observed. Drum et al., (2002) observed that the single metal ion is coordinated by a pair of aspartate residues (D491 and D493) and interacts with the oxygens of the α and β phosphates of the substrate analog 3'-d-ATP. Furthermore, H351 serves as a catalytic base and is thought to interact with the 3'-OH of the substrate to promote nucleophilic attack (25). In support of this hypothesis, Gupta et al., (2005) have shown in their kinetic studies that when H351 was mutated to alanine, aspargine or phenyl alanine, AC activity was reduced several-fold, indicating the importance of histidine 351 in catalysis by EF (119, 120).

A major difference of two-metal-ion catalysis from the proposed mechanism of EF by Drum and co-workers is the presence of additional metal ion, instead of histidine, to facilitate the deprotonation of the 3'-OH. One key feature for enzymes that use two-metal–ion catalysis utilizes two closely spaced aspartate residues to coordinate the catalytic metal ions. Interestingly, EF also has the same setup, raising the possibility that EF may also use two-metal–ion catalysis. Shen et al., (2005) refined the first model and found that EF contains two metal ions similar to mammalian ACs and DNA polymerases. Metal ion A is coordinated by the conserved aspartate residues and H577. Metal ion B is coordinated by D493 and the non-bridging oxygens of all three phosphates of ATP. Furthermore, it was shown that H351 does not act as a catalytic base because it was at least 6 Å away from the 3'-OH of the substrate making it unlikely to be able to accept a proton from the 3'-OH during the cyclization reaction. Site directed mutagenesis studies have shown that when H351 was mutated to lysine, there was no change in AC activity or the pH optimum, further confirming that H351 is not the catalytic base but may act to stabilize the 3'-OH group.

To promote the ATP cyclization reaction, EF needs to bind ATP, facilitate the deprotonation of 3'-OH, stabilize pentacoordinated phosphorane intermediate, and

effectively release cAMP and PPi. It is proposed that EF uses N583 to restrain the rotational freedom of ribose, thus holding 3'-OH in place for its nucleophilic attack during the catalysis (Fig. 8, **D**). The protonated histidine 351 is used to stabilize the OH ion near the 3'-OH group. A variant of this mechanism is that EF uses neutral histidine 351 to deprotonate a neutral water molecule. This OH ion in turn facilitates the deprotonation of 3'-OH of ATP. A suitable catalytic metal ion, Mg_A, near the 3'-OH of ATP is coordinated by D491, D493 and H577 residues. This metal can also facilitate the deprotonation of 3'-OH by stabilizing the negative charge on the resulting 30-oxyanion. The action of Mg_A ion and histidine 351 can be additive (117).

Using the energy term, the free energy cost (ΔG) associated with the proton transfer of 3'-OH is proportional to the difference between pKa of the 3'-OH group and local pH of the solution. The catalytic role of H351 is to increase local pH, whereas the role of the catalytic metal is to decrease the pKa component to make ΔG small or even negative. In addition, this metal ion, Mg_A, also stabilize the reaction intermediate by moving towards the nonbridging oxygen of α-phosphate during the nucleophilic attack step of the catalytic reaction (117).

A second metal ion, Mg_B, is coordinated by D493 and nonbridging oxygens of all three phosphates of ATP. This metal ion can facilitate the bond breakage between α and β-phosphates by stabilizing the developing negative charges. Several positive residues (R329, K353, K372 and K346) are also involved in stabilizing the reaction intermediate and the departure of PP_i. The side chain of N583 forms hydrogen bond with the ribose ring and holds the 3'-OH group in place for nucleophilic attack (117).

Shen et al (2004) have also demonstrated an alternate binding mode of ATP to the catalytic core of EF. They showed that AMPCPP (adenosine 5'-(α, β-methylene)-triphosphate) binds to EF differently compared to 3'-d-ATP and 2'd-3'-ANT-ATP. The ribose ring of AMPCPP is rotated 105˚ and the adenine ring is rotated by 180˚ in the catalytic site of EF (65, 121).

Fig. 8: Catalytic mechanism of EF

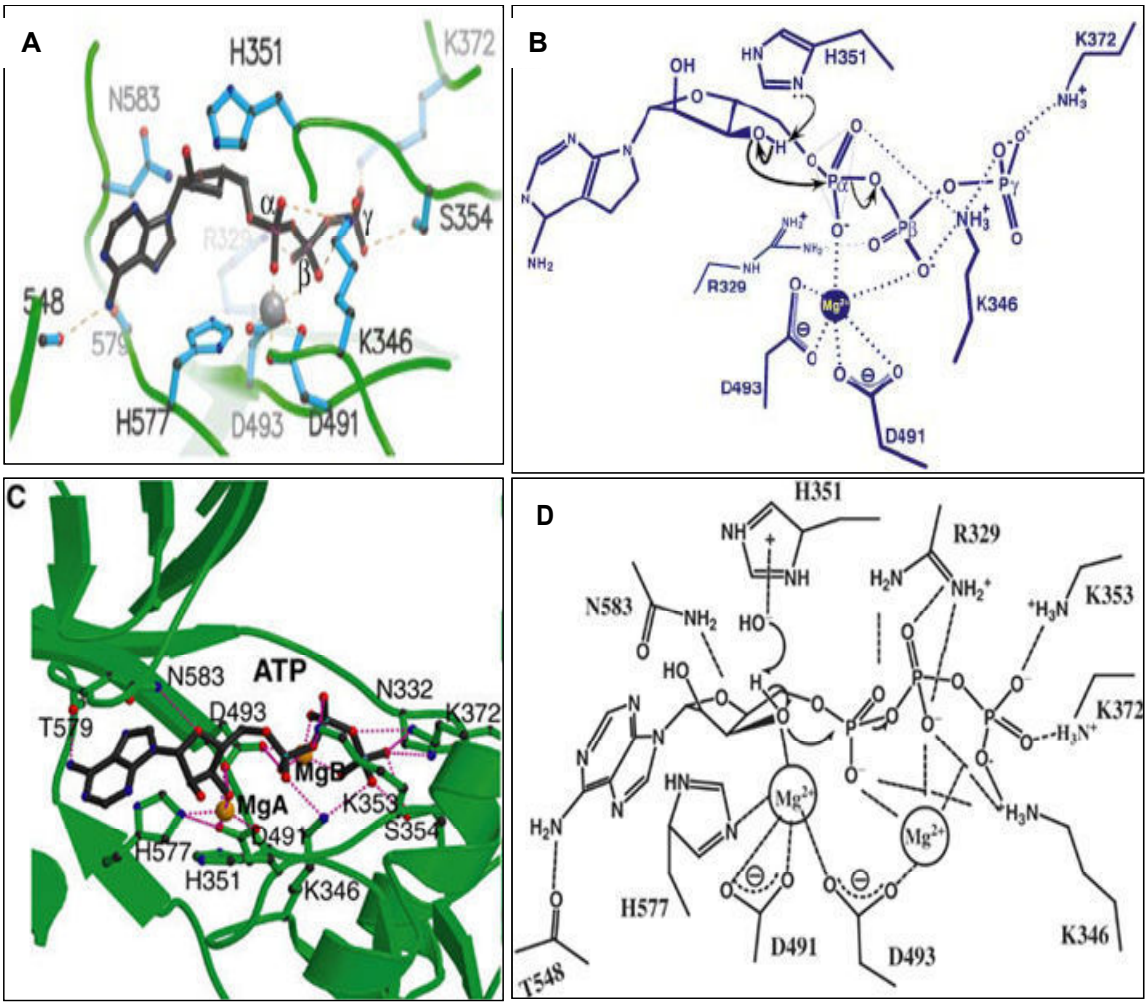

Catalytic mechanism of EF (**A**) A ball and stick model of the EF active site. EF is shown in *green*, side chains of important residues in *blue* and ligand in *black* (25); (**B**) Proposed catalytic mechanism of EF. Single metal ion-mediated catalysis is shown. (25); (**C**) Simulated model based on the EF-CaM-3'-d-ATP catalytic site. EF is in *green*, ligand in *black* and Mg ions are shown in *orange* (117); (**D**) Proposed two metal ion catalytic mechanism of EF (117).

1.2.1.7 Challenges, limitations and future directions of anthrax research with special focus on EF

With a better understanding of the detrimental effects of anthrax, it will become possible to develop highly specific control measures to prevent and treat anthrax infections. The efficacy of the AVA vaccine currently used is a cause for major concern since adverse side effects have been reported in some cases. Another disadvantage of AVA vaccine is that it is available only for military personnel. Antibiotic treatment is effective only against the cutaneous forms of anthrax. Therefore, there is a need for better vaccinations, drugs and other therapeutics to prevent anthrax infection not only in military personnel but also in humans and animals that are at a higher risk of contracting the infection.

With recent evidence that LF binds to monomeric PA, the question arises as to whether monomeric PA could translocate LF and EF into the cytosol. To this end, it has been shown that LF binds to monomeric PA with low affinity and would probably require PA heptamer for its translocation. Another important challenge faced by researchers is the lack of crystal structure of PA heptamer since it is a transmembrane protein. Solving the crystal structure of the PA heptamer would substantially improve our understanding of the PA prepore formation, binding of LF and EF, and help develop PA-based inhibitors. With the current model of the PA heptamer, it is known that the Φ clamp formed by the PA heptamer facilitates the translocation of EF and LF; however, it is not clear how these proteins unfold and refold in the cytosol.

Using various approaches to study the anthrax toxins, several steps in the intoxication mechanism can be blocked and studied for future rational drug design. For example, the binding sites of EF on PA have been mapped, so it would be interesting to study inhibitors that would block protein-protein interaction, EF-PA interaction, thus preventing entry of EF into the cytosol. Once inside the cell, inhibitors can be developed to block two important processes of EF. One is CaM-dependent activation of EF, the second is the catalytic activity of EF. The crystal structure of EF-CaM shows that EF makes extensive contacts with CaM and CaM changes the conformation of EF from a closed to an open conformation, thus exposing the substrate binding site. An important challenge here is to understand the specificity of this interaction, since CaM is a ubiquitously expressed protein that binds

to several other protein targets. Although several small molecules have been designed to block the catalytic activity of EF both *in vitro* and *in vivo*, there is a critical need for more potent and cell-permeable inhibitors (122, 123).

In summary, early detection, appropriate timely treatment and improved vaccines combined with a better understanding of the molecular basis of the biological action of anthrax toxins are critical for control and prevention of anthrax.

1.3 Nucleotide-analogues as inhibitors for mammalian and bacterial adenylyl cyclases

Substrate analogues can be used as inhibitor for the catalytic activity of mammalian and bacterial ACs (124, 125). The classic adenylyl cyclase (AC) inhibitors are adenine nucleotides with a phosphate or a polyphosphate at the 3'-*O*-ribosyl position (124, 126, 127). These compounds are also referred to as P-site inhibitors. P-site inhibitors are noncompetitive or uncompetitive AC inhibitors that bind to the AC-PP_i conformation (128, 129). P-site inhibitors exhibit a moderate degree of specificity for mammalian AC isoforms (127). EF is highly sensitive to some of P-site inhibitors (61, 125). Furthermore, adefovir diphosphate (PMEApp), the active cellular metabolite of the adefovir dipivoxil, which is approved as a drug for the treatment of chronic hepatitis B virus infection, is also a potent EF and CyaA inhibitor. In addition 2',3'-*N*-methylanthraniloyl (MANT)-, anthraniloyl (ANT)- and 2,4,6-trinitrophenyl (TNP)-substituted nucleotides are environmental sensitive fluorescence probes that show an increase in fluorescence with a hydrophobic environment (Fig. 9) (130). ANT- and MANT-nucleotides have been used successfully to study conformational changes in various nucleotide-binding proteins including G-protein and bacterial AC toxins (131, 132).

Fig. 9: Representative examples of AC inhibitors

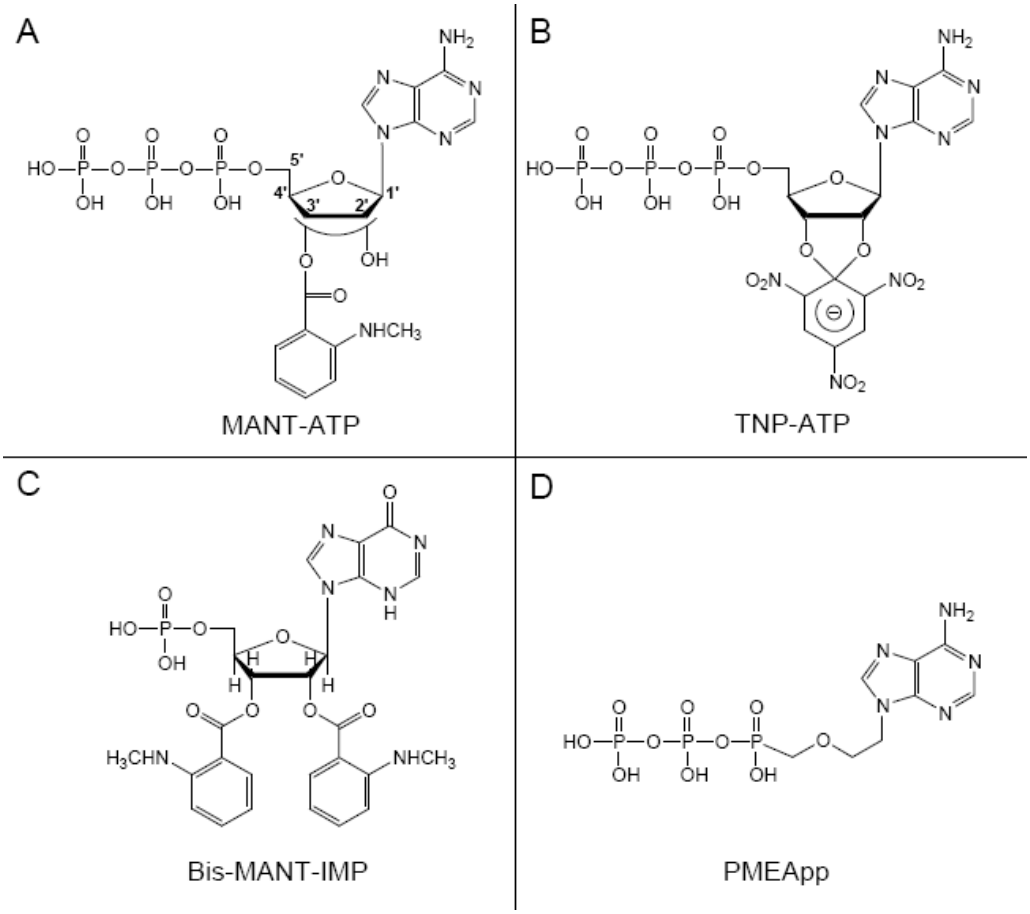

1.3.1 Anthraniloyl-substituted purine and pyrimidine nucleotides

These fluorescent probes possess protein-binding properties similar to those of natural nucleotides that are involved in many metabolic processes (125). The (M)ANT-fluorophore attached to the ribosyl ring (Fig. 10), has a compact nature. Therefore, it is readily accommodated in the substrate binding pocket of several enzymes (125, 130, 133, 134). For this reason, fluorescent nucleotide analogues play an important role in signal transduction research; they can serve as substrate, inhibitor or as regulatory molecules for key enzymes in signaling pathways (61, 135). (M)ANT-nucleotides are extremely valuable for characterization of nucleotide-binding processes. The environmental sensitivity of the (M)ANT-fluorophore often allows the detection of conformational changes of nucleotide-binding proteins, as they are involved in activation of heterotrimeric G-proteins or in activation of the edema factor. Therefore, (M)ANT-fluorophores can serve as a monitor for protein-protein or protein-

ligand interactions (130).

In a project that originally aimed at developing a fluorescence assay for receptor/G-protein coupling by using fluorescent guanine nucleotides (2',3'-O-(N-methylanthraniloyl)-guanosine 5'-[γ-thio]triphosphate (MANT-GTPγS) and 2',3'-O-(N-methylanthraniloyl) guanosine 5'-[β,γ-imido]triphosphate (MANT-GMPPNP)), MANT-nucleotides were serendipitously identified as potent competitive AC inhibitors (133). Now, they serve as a pharmacophor to develop optimized inhibitors with high selectivity for mammalian and bacterial adenylyl cyclases (130).

Fig. 10: General chemical structure of (M)ANT-substituted nucleotides

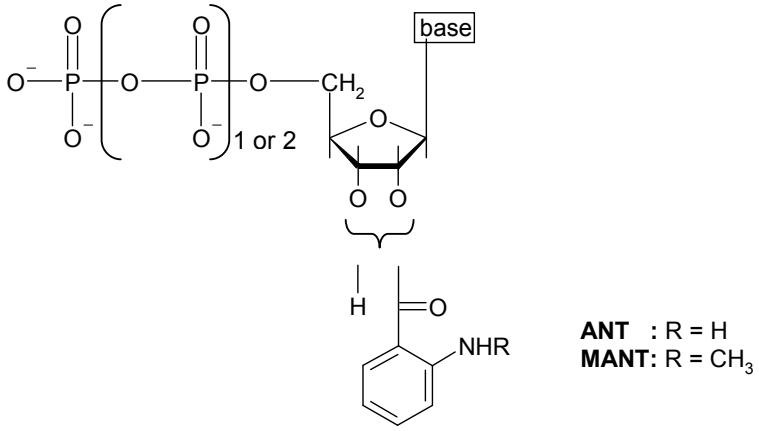

base:

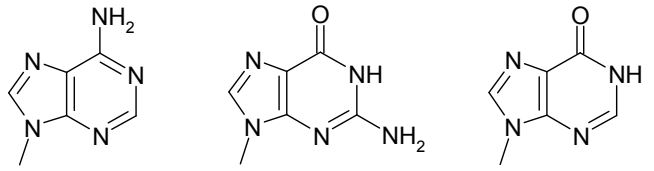

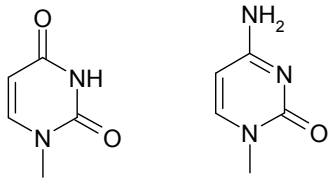

1.4 Fluorescence spectroscopic studies of adenylyl cyclases

Fluorescence spectroscopy is one of the most widely used analytical techniques in the biomedical sciences. Fluorescence has been successfully implemented for various biological applications due to its selectivity and specificity. Various measurement categories like fluorescence intensity, decay time, polarization, FRET, 2-photon excitation, imaging and time gated-analysis broaden the range of possible implementations in experimental science. As a disadvantage, fluorescence is sensitive to quenching, solvent effects, geometry and temperature (136).

One of the most important fluorescence applications is fluorescence resonance energy transfer (FRET). The phenomenon discovered by Theodor Förster in 1946 (137). FRET is a distance-dependent interaction between the electronically excited states of two fluorescent molecules in which excitation is nonradiatively transferred from a donor molecule to an acceptor molecule. This technique is used for studying conformational changes and dynamics of biological molecules that produce changes in molecular proximity. On that account it can be used for determination of molecular distances, binding assays and homogenous competitive assays (137).

MANT-nucleotides are fluorescent and this property was exploited to suggest conformational changes associated with activation in purified catalytic subunits of mammalian ACs (138, 139), and the *Bordetella pertussis* AC toxin Cya A (135). We used FRET to characterize the interaction of the catalytic site of EF with mono- and bis-(M)ANT-nucleotides possesses various purine and pyrimidine bases to better understand the molecular mechanisms of EF inhibition and to provide the basis for the rational development of potent and selective EF inhibitors. At an excitation wavelength of 280 nm, tryptophan and tyrosine residues in proteins are excited, emitting light at 350 nm (137) which can then excite the (M)ANT group of nucleotides (140), provided sufficient proximity between donor and acceptor. Such energy transfer results in increased fluorescence of the MANT-group at 420-450 nm in mAC and CyaA, reflecting the fact that the MANT-group is in a hydrophobic environment (135, 138, 139) (Fig. 11).

Fig. 11: schematic representation of FRET occur from EF to (M)ANT-nucleotides

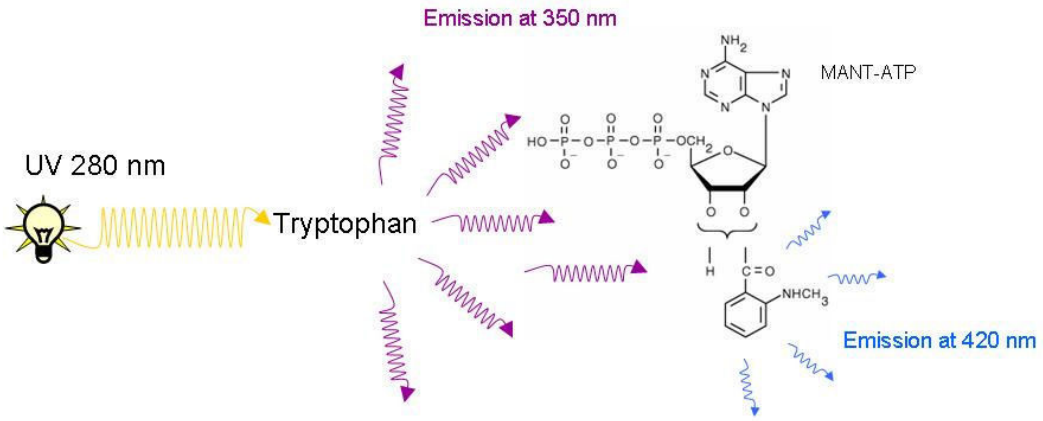

1.5 The aim of this thesis

The primary goal of this thesis was to systematically study the interactions of natural purine and pyrimidine nucleotides and several mono- and bis-(propyl)(M)ANT-substituted analogues with EF in terms of catalysis, fluorescence changes and molecular modeling. We determined the inhibitory potencies of those nucleotide analogues on EF/CaM to better understand the molecular mechanisms of EF inhibition and to provide the basis for the rational development of potent and selective EF inhibitors. The effect of calcium and CaM on the V_{max} and K_m of EF and on the inhibitory potencies of MANT-nucleotides at EF was also examined. Potent and selective EF inhibitors could be useful compounds to treat EF toxemia and antibiotic-resistant *Bacillus anthracis* strains.

2. References

1. Hurley JH. The adenylyl and guanylyl cyclase superfamily. *Curr Opin Struct Biol* 1998; **8**:770-7.

2. Ishikawa Y, Homcy CJ. The adenylyl cyclases as integrators of transmembrane signal transduction. *Circ Res* 1997; **80**:297-304.

3. Tang WJ, Hurley JH. Catalytic mechanism and regulation of mammalian adenylyl cyclases. *Mol Pharmacol* 1998; **54**:231-40.

4. Tang WJ, Yan S, Drum CL. Class III adenylyl cyclases: regulation and underlying mechanisms. *Adv Second Messenger Phosphoprotein Res* 1998; **32**:137-51.

5. Dumont JE, Jauniaux JC, Roger PP. The cyclic AMP-mediated stimulation of cell proliferation. *Trends Biochem Sci* 1989; **14**:67-71.

6. Robison GA, Butcher RW, Sutherland EW. Cyclic AMP. *Annu Rev Biochem* 1968; **37**:149-74.

7. Rodbell M. The role of hormone receptors and GTP-regulatory proteins in membrane transduction. *Nature* 1980; **284**:17-22.

8. de Rooij J, Zwartkruis FJ, Verheijen MH, Cool RH, Nijman SM, Wittinghofer A, Bos JL. Epac is a Rap1 guanine-nucleotide-exchange factor directly activated by cyclic AMP. *Nature* 1998; **396**:474-7.

9. Kawasaki H, Springett GM, Mochizuki N, Toki S, Nakaya M, Matsuda M, Housman DE, Graybiel AM. A family of cAMP-binding proteins that directly activate Rap1. *Science* 1998; **282**:2275-9.

10. Cooper DM, Mons N, Karpen JW. Adenylyl cyclases and the interaction between calcium and cAMP signalling. *Nature* 1995; **374**:421-4.

11. Defer N, Best-Belpomme M, Hanoune J. Tissue specificity and physiological relevance of various isoforms of adenylyl cyclase. *Am J Physiol Renal Physiol* 2000; **279**:F400-16.

12. Alousi AA, Jasper JR, Insel PA, Motulsky HJ. Stoichiometry of receptor-Gs-adenylate cyclase interactions. *FASEB J* 1991; **5**:2300-3.

13. Post SR, Hilal-Dandan R, Urasawa K, Brunton LL, Insel PA. Quantification of signalling components and amplification in the beta-adrenergic-receptor-adenylate cyclase pathway in isolated adult rat ventricular myocytes. *Biochem J* 1995; **311**:75-80.

14. Gao M, Ping P, Post S, Insel PA, Tang R, Hammond HK. Increased expression of adenylylcyclase type VI proportionately increases beta-adrenergic receptor-stimulated production of cAMP in neonatal rat cardiac myocytes. *Proc Natl Acad Sci USA* 1998; **95**:1038-43.

15. MacEwan DJ, Kim GD, Milligan G. Agonist regulation of adenylate cyclase activity in neuroblastoma x glioma hybrid NG108-15 cells transfected to co-express adenylate cyclase type II and the beta 2-adrenoceptor. Evidence that adenylate cyclase is the limiting component for receptor-mediated stimulation of adenylate cyclase activity. *Biochem J* 1996; **318**:1033-9.

16. Iyengar R. Molecular and functional diversity of mammalian Gs-stimulated adenylyl cyclases. *FASEB J* 1993; **7**:768-75.

17. Iyengar R. Gating by cyclic AMP: expanded role for an old signaling pathway. *Science* 1996; **271**:461-3.

18. Buck J, Sinclair ML, Schapal L, Cann MJ, Levin LR. Cytosolic adenylyl cyclase defines a unique signaling molecule in mammals. *Proc Natl Acad Sci USA* 1999; **96**:79-84.

19. Hanoune J, Defer N. Regulation and role of adenylyl cyclase isoforms. *Annu Rev Pharmacol Toxicol* 2001; **41**:145-74.

20. Sunahara RK, Taussig R. Isoforms of mammalian adenylyl cyclase: multiplicities of signaling. *Mol Interv* 2002; **2**:168-84.

21. Seigel R, Wolson AH. The radiographic manifestations of chronic Pneumocystis carinii pneumonia. *AJR Am J Roentgenol* 1977; **128**:150-2.

22. Wolff J, Cook GH, Goldhammer AR, Berkowitz SA. Calmodulin activates prokaryotic adenylate cyclase. *Proc Natl Acad Sci USA* 1980; **77**:3841-4.

23. Leppla SH. Anthrax toxin edema factor: a bacterial adenylate cyclase that increases cyclic AMP concentrations of eukaryotic cells. *Proc Natl Acad Sci USA* 1982; **79**:3162-6.

24. O'Brien J, Friedlander A, Dreier T, Ezzell J, Leppla S. Effects of anthrax toxin components on human neutrophils. *Infect Immun* 1985; **47**:306-10.

25. Drum CL, Yan SZ, Bard J, Shen YQ, Lu D, Soelaiman S, Grabarek Z, Bohm A, Tang WJ. Structural basis for the activation of anthrax adenylyl cyclase exotoxin by calmodulin. *Nature* 2002; **415**:396-402.

26. Bhatnagar R, Batra S. Anthrax toxin. *Crit Rev Microbiol* 2001; **27**:167-200.

27. Sirisanthana T, Nelson KE, Ezzell JW, Abshire TG. Serological studies of patients with cutaneous and oral-oropharyngeal anthrax from northern Thailand. *Am J Trop Med Hyg* 1988; **39**:575-81.

28. Fouet A, Smith KL, Keys C, Vaissaire J, Le Doujet C, Lévy M, Mock M, Keim P. Diversity among French *Bacillus anthracis* isolates. *J Clin Microbiol* 2002; **40**:4732-4.

29. Mourez M, Lacy DB, Cunningham K, Legmann R, Sellman BR, Mogridge J, Collier RJ. 2001: a year of major advances in anthrax toxin research. *Trends Microbiol* 2002; **10**:287-93.

30. Hugh-Jones ME, Hussaini SN. An anthrax outbreak in Berkshire. *Vet Rec* 1974; **94**:228-32.

31. Scorpio A, Blank TE, Day WA, Chabot DJ. Anthrax vaccines: Pasteur to the present. *Cell Mol Life Sci* 2006; **63**:2237-48.

32. Oncu S, Sakarya S. Anthrax--an overview. *Med Sci Monit* 2003; **9**:RA276-83.

33. Hughes JM, Gerberding JL. Anthrax bioterrorism: lessons learned and future directions. *Emerg Infect Dis* 2002; **8**:1013-4.

34. Watson A, Keir D. Information on which to base assessments of risk from environments contaminated with anthrax spores. *Epidemiol Infect* 1994; **113**:479-90.

35. Kawana R. [Human anthrax outbreak due to cow anthrax in Iwate Prefecture]. *Kansenshogaku Zasshi* 2002; **76**:1-8.

36. Datta KK, Singh J. Anthrax. *Indian J Pediatr* 2002; **69**:49-56.

37. http://en.wikipedia.org/wiki/Anthrax.

38. www.bact.wisc.edu/themicrobialworld/anthrax.html).

39. Holgate JA, Holman RA. Diagnosis and treatment of cutaneous anthrax. *Br Med J* 1949; **2**:575-9.

40. Brey RN. Molecular basis for improved anthrax vaccines. *Adv Drug Deliv Rev* 2005; **57**:1266-92.

41. Oncul O, Ozsoy MF, Gul HC, Kocak N, Cavuslu S, Pahsa A. Cutaneous anthrax in Turkey: a review of 32 cases. *Scand J Infect Dis* 2002; **34**:413-6.

42. Henry L. Inhalational anthrax: threat, clinical presentation, and treatment. *J Am Acad Nurse Pract* 2001; **13**:164-8; quiz 9-70.

43. Ascenzi P, Visca P, Ippolito G, Spallarossa A, Bolognesi M, Montecucco C. Anthrax toxin: a tripartite lethal combination. *FEBS Lett* 2002; **531**:384-8.

44. http://www.cdc.gov/mmwr/preview/mmwrhtml/mm5510a4.htm).

45. Helou E. Clinical aspects of intestinal anthrax and its surgical and medical treatment. *Rev Med Moyen Orient* 1967; **24**:64-7.

46. (http://www.bchealthguide.org/kbase/topic/special/ty6357/sec1.htm).

47. http://www.cdc.gov/ncidod/dbmd/diseaseinfo/anthrax_g.htm.

48. http://www.pathguy.com/lectures/anthrax.jpg.

49. http://microbes.historique.net/anthracis.html.

50. http://www.acponline.org/clinical_information/resources/bioterrorism/chest_xray.html.

51. Scorpio A, Tobery SA, Ribot WJ, Friedlander AM. Treatment of experimental anthrax with recombinant capsule depolymerase. *Antimicrob Agents Chemother* 2008; **52**:1014-20.

52. Athamna A, Athamna M, Nura A, Shlyakov E, Bast DJ, Farrell D, Rubinstein E. Is in vitro antibiotic combination more effective than single-drug therapy against anthrax? *Antimicrob Agents Chemother* 2005; **49**:1323-5.

53. Gladstone GP. Anthrax protective antigen. *Brit. J. Exp. Path* 1946; **27**:394.

54. **www.google.com/anthrax**.

55. Sarac MS, Peinado JR, Leppla SH, Lindberg I. Protection against anthrax toxemia by hexa-D-arginine in vitro and in vivo. *Infect Immun* 2004; **72**:602-5.

56. Sanderson WT, Stoddard RR, Echt AS, Piacitelli CA, Kim D, Horan J, Davies MM, McCleery RE, Muller P, Schnorr TM, Ward EM, Hales TR. *Bacillus anthracis* contamination and inhalational anthrax in a mail processing and distribution center. *J Appl Microbiol* 2004; **96**:1048-56.

57. Lee YS, Bergson P, He WS, Mrksich M, Tang WJ. Discovery of a small molecule that inhibits the interaction of anthrax edema factor with its cellular activator, calmodulin. *Chem Biol* 2004; **11**:1139-46.

58. Shoop WL, Xiong Y, Wiltsie J, Woods A, Guo J, Pivnichny JV, Felcetto T, Michael BF, Bansal A, Cummings RT, Cunningham BR, Friedlander AM, Douglas CM, Patel SB, Wisniewski D, Scapin G, Salowe SP, Zaller DM, Chapman KT, Scolnick EM, Schmatz DM, Bartizal K, MacCoss M, Hermes JD. Anthrax lethal factor inhibition. *Proc Natl Acad Sci USA* 2005; **102**:7958-63.

59. Splino M, Patocka J, Prymula R, Chlibek R. Anthrax vaccines. *Ann Saudi Med* 2005; **25**:143-9.

60. Smith H. Discovery of the anthrax toxin: the beginning of in vivo studies on pathogenic bacteria. *Trends Microbiol* 2000; **8**:199-200.

61. Taha HM, Schmidt J, Gottle M, Suryanarayana S, Shen Y, Tang WJ, Gille A, Geduhn J, König B, Dove S, Seifert R. Molecular analysis of the interaction of anthrax adenylyl cyclase toxin, edema factor, with 2'(3')-O-(N-(methyl)anthraniloyl)-substituted purine and pyrimidine nucleotides. *Mol Pharmacol* 2009; **75**:693-703.

62. Richter S, Anderson VJ, Garufi G, Lu L, Budzik JM, Joachimiak A, He C, Schneewind O, Missiakas D. Capsule anchoring in *Bacillus anthracis* occurs by a transpeptidation reaction that is inhibited by capsidin. *Mol Microbiol* 2009; **71**:404-20.

63. Niu MT, Ball R, Woo EJ, Burwen DR, Knippen M, Braun MM. Adverse events after anthrax vaccination reported to the Vaccine Adverse Event Reporting System (VAERS), 1990-2007. *Vaccine* 2009; **27**:290-7.

64. Stubbs MT. Anthrax X-rayed: new opportunities for biodefence. *Trends Pharmacol Sci* 2002; **23**:539-41.

65. Shen Y, Zhukovskaya NL, Zimmer MI, Soelaiman S, Bergson P, Wang CR, Gibbs CS, Tang WJ. Selective inhibition of anthrax edema factor by adefovir, a drug for chronic hepatitis B virus infection. *Proc Natl Acad Sci USA* 2004; **101**:3242-7.

66. Witkowski JA, Parish LC. The story of anthrax from antiquity to the present: a biological weapon of nature and humans. *Clin Dermatol* 2002; **20**:336-42.

67. Tasota FJ, Henker RA, Hoffman LA. Anthrax as a biological weapon: an old disease that poses a new threat. *Crit Care Nurse* 2002; **22**:21-32, 4; quiz 5-6.

68. Szafraniec S, Grzesiowski P, Hryniewicz W. [Anthrax as a bioweapon]. *Przegl Lek* 2004; **61**:177-80.

69. (http://www.defencejournal.com/dec98/anthrax.htm).

70. Manchee RJ, Broster MG, Henstridge RM, Stagg AJ, Melling J. Anthrax island. *Nature* 1982; **296**:598.

71. Meselson M, Guillemin J, Hugh-Jones M, Langmuir A, Popova I, Shelokov A, Yampolskaya O. The Sverdlovsk anthrax outbreak of 1979. *Science* 1994; **266**:1202-8.

72. Keim P, Kalif A, Schupp J, Hill K, Travis SE, Richmond K, Adair DM, Hugh-Jones M, Kuske CR, Jackson P. Molecular evolution and diversity in *Bacillus anthracis* as detected by amplified fragment length polymorphism markers. *J Bacteriol* 1997; **179**:818-24.

73. Keim P, Klevytska AM, Price LB, Schupp JM, Zinser G, Smith KL, Hugh-Jones ME, Okinaka R, Hill KK, Jackson PJ. Molecular diversity in *Bacillus anthracis*. *J Appl Microbiol* 1999; **87**:215-7.

74. Keim P, Smith KL, Keys C, Takahashi H, Kurata T, Kaufmann A. Molecular investigation of the Aum Shinrikyo anthrax release in Kameido, Japan. *J Clin Microbiol* 2001; **39**:4566-7.

75. Heap B. Scientists against biological weapons. *Science* 2001; **294**:1417.

76. Trull MC, du Laney TV, Dibner MD. Turning biodefense dollars into products. *Nat Biotechnol* 2007; **25**:179-84.

77. Rao GR, Padmaja J, Lalitha MK, Rao PV, Kumar HK, Gopal KV, Jaideep M, Mohanraj P. Cutaneous anthrax in a remote tribal area--Araku Valley, Visakhapatnam district, Andhra Pradesh, southern India. *Int J Dermatol* 2007; **46**:55-8.

78. Mock M, Fouet A. Anthrax. *Annu Rev Microbiol* 2001; **55**:647-71.

79. Lacy DB, Mourez M, Fouassier A, Collier RJ. Mapping the anthrax protective antigen binding site on the lethal and edema factors. *J Biol Chem* 2002; **277**:3006-10.

80. Mogridge J, Cunningham K, Lacy DB, Mourez M, Collier RJ. The lethal and edema factors of anthrax toxin bind only to oligomeric forms of the protective antigen. *Proc Natl Acad Sci USA* 2002; **99**:7045-8.

81. Bradley KA, Young JA. Anthrax toxin receptor proteins. *Biochem Pharmacol* 2003; **65**:309-14.

82. Bradley PJ, Ferlito A, Brandwein MS, Benninger MS, Rinaldo A. Anthrax: what should the otolaryngologist know? *Acta Otolaryngol* 2002; **122**:580-5.

83. Bradley KA, Mogridge J, Mourez M, Collier RJ, Young JA. Identification of the cellular receptor for anthrax toxin. *Nature* 2001; **414**:225-9.

84. Nanda A, Buckhaults P, Seaman S, Agrawal N, Boutin P, Shankara S, Nacht M, Teicher B, Stampfl J, Singh S, Vogelstein B, Kinzler KW, St Croix B. Identification of a binding partner for the endothelial cell surface proteins TEM7 and TEM7R. *Cancer Res* 2004; **64**:8507-11.

85. Nanda A, Carson-Walter EB, Seaman S, Barber TD, Stampfl J, Singh S, Vogelstein B, Kinzler KW, St Croix B. TEM8 interacts with the cleaved C5 domain of collagen alpha 3(VI). *Cancer Res* 2004; **64**:817-20.

86. Scobie HM, Rainey GJ, Bradley KA, Young JA. Human capillary morphogenesis protein 2 functions as an anthrax toxin receptor. *Proc Natl Acad Sci USA* 2003; **100**:5170-4.

87. Liu S, Leppla SH. Cell surface tumor endothelium marker 8 cytoplasmic tail-independent anthrax toxin binding, proteolytic processing, oligomer formation, and internalization. *J Biol Chem* 2003; **278**:5227-34.

88. Klimpel KR, Molloy SS, Thomas G, Leppla SH. Anthrax toxin protective antigen is activated by a cell surface protease with the sequence specificity and catalytic properties of furin. *Proc Natl Acad Sci USA* 1992; **89**:10277-81.

89. Lacy DB, Lin HC, Melnyk RA, Schueler-Furman O, Reither L, Cunningham K, Baker D, Collier RJ. A model of anthrax toxin lethal factor bound to protective antigen. *Proc Natl Acad Sci USA* 2005; **102**:16409-14.

90. Abrami L, Liu S, Cosson P, Leppla SH, van der Goot FG. Anthrax toxin triggers endocytosis of its receptor via a lipid raft-mediated clathrin-dependent process. *J Cell Biol* 2003; **160**:321-8.

91. Krantz BA, Melnyk RA, Zhang S, Juris SJ, Lacy DB, Wu Z, Finkelstein A, Collier RJ. A phenylalanine clamp catalyzes protein translocation through the anthrax toxin pore. *Science* 2005; **309**:777-81.

92. Petosa C, Collier RJ, Klimpel KR, Leppla SH, Liddington RC. Crystal structure of the anthrax toxin protective antigen. *Nature* 1997; **385**:833-8.

93. Santelli E, Bankston LA, Leppla SH, Liddington RC. Crystal structure of a complex between anthrax toxin and its host cell receptor. *Nature* 2004; **430**:905-8.

94. Mogridge J, Mourez M, Collier RJ. Involvement of domain 3 in oligomerization by the protective antigen moiety of anthrax toxin. *J Bacteriol* 2001; **183**:2111-6.

95. Yacoub B, Collier WS. Duverney fracture: distinguishing scintigraphic features. *Clin Nucl Med* 2007; **32**:538-9.

96. Pannifer AD, Wong TY, Schwarzenbacher R, Renatus M, Petosa C, Bienkowska J, Lacy DB, Collier RJ, Park S, Leppla SH, Hanna P, Liddington RC. Crystal structure of the anthrax lethal factor. *Nature* 2001; **414**:229-33.

97. Tonello F, Ascenzi P, Montecucco C. The metalloproteolytic activity of the anthrax lethal factor is substrate-inhibited. *J Biol Chem* 2003; **278**:40075-8.

98. Chvyrkova I, Zhang XC, Terzyan S. Lethal factor of anthrax toxin binds monomeric form of protective antigen. *Biochem Biophys Res Commun* 2007; **360**:690-5.

99. Christensen KA, Krantz BA, Collier RJ. Assembly and disassembly kinetics of anthrax toxin complexes. *Biochemistry* 2006; **45**:2380-6.

100. Dixon TC, Meselson M, Guillemin J, Hanna PC. Anthrax. *N Engl J Med* 1999; **341**:815-26.

101. Firoved AM, Moayeri M, Wiggins JF, Shen Y, Tang WJ, Leppla SH. Anthrax edema toxin sensitizes DBA/2J mice to lethal toxin. *Infect Immun* 2007; **75**:2120-5.

102. Kammer GM. The adenylate cyclase-cAMP-protein kinase A pathway and regulation of the immune response. *Immunol Today* 1988; **9**:222-9.

103. Kyriakis JM, Avruch J. Mammalian mitogen-activated protein kinase signal transduction pathways activated by stress and inflammation. *Physiol Rev* 2001; **81**:807-69.

104. Crawford MA, Aylott CV, Bourdeau RW, Bokoch GM. *Bacillus anthracis* toxins inhibit human neutrophil NADPH oxidase activity. *J Immunol* 2006; **176**:7557-65.

105. Hong J, Doebele RC, Lingen MW, Quilliam LA, Tang WJ, Rosner MR. Anthrax edema toxin inhibits endothelial cell chemotaxis via Epac and Rap1. *J Biol Chem* 2007; **282**:19781-7.

106. Hong J, Beeler J, Zhukovskaya NL, He W, Tang WJ, Rosner MR. Anthrax edema factor potency depends on mode of cell entry. *Biochem Biophys Res Commun* 2005; **335**:850-7.

107. Alam S, Gupta M, Bhatnagar R. Inhibition of platelet aggregation by anthrax edema toxin. *Biochem Biophys Res Commun* 2006; **339**:107-14.

108. Wu AG, Alibek D, Li YL, Bradburne C, Bailey CL, Alibek K. Anthrax toxin induces hemolysis: an indirect effect through polymorphonuclear cells. *J Infect Dis* 2003; **188**:1138-41.

109. Drum CL, Yan SZ, Sarac R, Mabuchi Y, Beckingham K, Bohm A, Grabarek Z, Tang WJ. An extended conformation of calmodulin induces interactions between the structural domains of adenylyl cyclase from *Bacillus anthracis* to promote catalysis. *J Biol Chem* 2000; **275**:36334-40.

110. Collier RJ, Young JA. Anthrax toxin. *Annu Rev Cell Dev Biol* 2003; **19**:45-70.

111. Deisseroth K, Heist EK, Tsien RW. Translocation of calmodulin to the nucleus supports CREB phosphorylation in hippocampal neurons. *Nature* 1998; **392**:198-202.

112. DeMaria CD, Soong TW, Alseikhan BA, Alvania RS, Yue DT. Calmodulin bifurcates the local Ca^{2+} signal that modulates P/Q-type Ca^{2+} channels. *Nature* 2001; **411**:484-9.

113. Babu YS, Sack JS, Greenhough TJ, Bugg CE, Means AR, Cook WJ. Three-dimensional structure of calmodulin. *Nature* 1985; **315**:37-40.

114. Zhang M, Tanaka T, Ikura M. Calcium-induced conformational transition revealed by the solution structure of apo calmodulin. *Nat Struct Biol* 1995; **2**:758-67.

115. Kuboniwa H**,** Tjandra N, Grzesiek S**,** Ren H, Klee CB**,** Bax A**.** Solution structure of calcium-free calmodulin. *Nat Struct Biol*. 1995 Sep; 2 :768–776.

116. Tabernero L, Taylor DA, Chandross RJ, VanBerkum MF, Means AR, Quiocho FA, Sack JS. The structure of a calmodulin mutant with a deletion in the central helix: implications for molecular recognition and protein binding. *Structure* 1997; **5**:613-22.

117. Shen Y, Zhukovskaya NL, Guo Q, Florian J, Tang WJ. Calcium-independent calmodulin binding and two-metal-ion catalytic mechanism of anthrax edema factor. *EMBO J* 2005; **24**:929-41.

118. Ulmer TS, Soelaiman S, Li S, Klee CB, Tang WJ, Bax A. Calcium dependence of the interaction between calmodulin and anthrax edema factor. *J Biol Chem* 2003; **278**:29261-6.

119. Gupta M, Alam S, Bhatnagar R. Catalytically inactive anthrax toxin(s) are potential prophylactic agents. *Vaccine* 2007; **25**:8410-9.

120. Gupta M, Alam S, Bhatnagar R. Kinetic characterization and ligand binding studies of His351 mutants of *Bacillus anthracis* adenylate cyclase. *Arch Biochem Biophys* 2006; **446**:28-34.

121. Shen Y, Guo Q, Zhukovskaya NL, Drum CL, Bohm A, Tang WJ. Structure of anthrax edema factor-calmodulin-adenosine 5'-(α,β-methylene)-triphosphate complex reveals an alternative mode of ATP binding to the catalytic site. *Biochem Biophys Res Commun* 2004; **317**:309-14.

122. Chen D, Misra M, Sower L, Peterson JW, Kellogg GE, Schein CH. Novel inhibitors of anthrax edema factor. *Bioorg Med Chem* 2008; **16**:7225-33.

123. Pini A, Runci Y, Falciani C, Lelli B, Brunetti J, Pileri S, Fabbrini M, Lozzi L, Ricci C, Bernini A, Tonello F, Dal Molin F, Neri P, Niccolai N, Bracci L. Stable peptide inhibitors prevent binding of lethal and oedema factors to protective antigen and neutralize anthrax toxin in vivo. *Biochem J* 2006; **395**:157-63.

124. Desaubry L, Shoshani I, Johnson RA. Inhibition of adenylyl cyclase by a family of newly synthesized adenine nucleoside 3'-polyphosphates. *J Biol Chem* 1996; **271**:14028-34.

125. Gille A, Seifert R. 2'(3')-O-(N-methylanthraniloyl)-substituted GTP analogs: a novel class of potent competitive adenylyl cyclase inhibitors. *J Biol Chem* 2003; **278**:12672-9.

126. Desaubry L, Shoshani I, Johnson RA. 2',5'-Dideoxyadenosine 3'-polyphosphates are potent inhibitors of adenylyl cyclases. *J Biol Chem* 1996; **271**:2380-2.

127. Desaubry L, Johnson RA. Adenine nucleoside 3'-tetraphosphates are novel and potent inhibitors of adenylyl cyclases. *J Biol Chem* 1998; **273**:24972-7.

128. Tesmer JJ, Dessauer CW, Sunahara RK, Murray LD, Johnson RA, Gilman AG, Sprang SR. Molecular basis for P-site inhibition of adenylyl cyclase. *Biochemistry* 2000; **39**:14464-71.

129. Dessauer CW, Gilman AG. The catalytic mechanism of mammalian adenylyl cyclase. Equilibrium binding and kinetic analysis of P-site inhibition. *J Biol Chem* 1997; **272**:27787-95.

130. Gille A, Lushington GH, Mou TC, Doughty MB, Johnson RA, Seifert R. Differential inhibition of adenylyl cyclase isoforms and soluble guanylyl

cyclase by purine and pyrimidine nucleotides. *J Biol Chem* 2004; **279**:19955-69.

131. Jameson DM, Eccleston JF. Fluorescent nucleotide analogs: synthesis and applications. *Methods Enzymol* 1997; **278**:363-90.

132. Remmers AE, Posner R, Neubig RR. Fluorescent guanine nucleotide analogs and G protein activation. *J Biol Chem* 1994; **269**:13771-8.

133. Gille A, Seifert R. MANT-substituted guanine nucleotides: a novel class of potent adenylyl cyclase inhibitors. *Life Sci* 2003; **74**:271-9.

134. Gille A, Liu HY, Sprang SR, Seifert R. Distinct interactions of GTP, UTP, and CTP with G(s) proteins. *J Biol Chem* 2002; **277**:34434-42.

135. Göttle M, Dove S, Steindel P, Shen Y, Tang WJ, Geduhn J, König B, Seifert R. Molecular analysis of the interaction of *Bordetella pertussis* adenylyl cyclase with fluorescent nucleotides. *Mol Pharmacol* 2007; **72**:526-35.

136. Gruber M, Wetzl B, Oswald B, Enderlein J, Wolfbeis OS. A new fluorescence resonance energy transfer pair and its application to oligonucleotide labeling and fluorescence resonance energy transfer hybridization studies. *J Fluoresc* 2005; **15**:207-14.

137. Lakowicz JR. *Principles of fluorescence spectroscopy*. In: *edition* ^{n}, (ed.). *Principles of fluorescence spectroscopy* Kluwer Academic. 1999

138. Mou TC, Gille A, Suryanarayana S, Richter M, Seifert R, Sprang SR. Broad specificity of mammalian adenylyl cyclase for interaction with 2',3'-substituted purine- and pyrimidine nucleotide inhibitors. *Mol Pharmacol* 2006; **70**:878-86.

139. Mou TC, Gille A, Fancy DA, Seifert R, Sprang SR. Structural basis for the inhibition of mammalian membrane adenylyl cyclase by 2 '(3')-O-(N-methylanthraniloyl)-guanosine 5 '-triphosphate. *J Biol Chem* 2005; **280**:7253-61.

140. Hiratsuka T. New ribose-modified fluorescent analogs of adenine and guanine nucleotides available as substrates for various enzymes. *Biochim Biophys Acta* 1983; **742**:496-508.

Chapter II

II. Purification of recombinant anthrax edema factor from *Escherichia coli* and calmodulin from bovine brain

1. Abstract

Protein purification is a first step of almost all *in vitro* protein studies. High quality of purified protein is critical in respect to activity and crystallization ability. Almost all proteins lose activity during manipulations. A great deal of strategy and consideration are required in choosing the right condition for extraction and purification in order to get the required results. Thus, the investigators need to have an answer prior to extraction and purification for some common questions which help in selecting the appropriate strategy of purification. In the present chapter, we sought to purify recombinant EF, EF3(F586A) from *E. coli* and their corresponding intracellular activator CaM from bovine brain at the maximum possible state of purity, with maintenance of the catalytic activity. The purified proteins were then used for further investigation of enzyme-ligand interactions in terms of catalysis, and fluorescence spectroscopy. The purifications of EF and EF3(F586A) were performed essentially as described in references (14, 15), with important modifications in the purification protocol to obtain more pure protein with a reasonable yield. In conclusion, we successfully purified the recombinant full-length EF and EF3(F586A) from *E. coli* with the best appealing balance between the high purity and high yield of the purified protein together with retention of activity.

2. Introduction

Protein purification is a first step of almost all *in vitro* protein studies. High quality of purified protein is critical in respect to activity and crystallization ability. Almost all proteins lose activity during manipulations. However, even the protein stored at 4°C can lose activity and crystallization ability. That is why it is important to purify protein as quickly as possible (1, 2). A great deal of strategy and consideration are required in choosing the right condition for extraction and purification in order to get the required results. Thus, the investigators need to have an answer prior to extraction and purification for some common questions which help in selecting the appropriate strategy of purification. The first step is to describe the basic scenario for the purification. What is the intended use of the product? What kind of starting material is available and how should it be handled? What are the purity issues in relation to the source material and intended use of the final product? What has to be removed? What must be removed completely? What will be the final scale of purification? If there is a need for scale-up, what consequences will this have on the chosen purification techniques? What are the economical constraints and what resources and equipment are available? One has to determine the purpose for which the protein is required. For example, to carry out a full chemical and physical analysis of a protein may require several hundreds of milligrams of purified material, whereas a kinetic analysis of the reaction catalyzed by an enzyme could perhaps be done with a few milligrams and less than 1 mg would be required to raise a polyclonal antibody (3).

Protein purification involves the separation of one species from perhaps 1000 or more species of essentially the same general characteristics (they are all proteins) in a mixture of which it may constitute a small fraction of 1 % of the total. It is, therefore, necessary to fully exploit those properties in which proteins differ from one another in devising a purification schedule. There are some protein properties that have to be taken into consideration during purification, for example; solubility, charge, size and specific binding (4). Most purification schemes involve some form of chromatography. As a result, chromatography has become an essential tool in every laboratory where protein purification is needed. Different chromatography techniques with different selectivities can form powerful combinations for the purification of any biomolecule. As general, ion-exchange chromatography provides the most general

method for the isolation of proteins with retention of activity unless the protein has special characteristics that offer alternative strategies (5, 6).

The most versatile system used for protein and biomolecule purification is the Fast Protein Liquid Chromatography system (FPLC). FPLC system is a form of liquid chromatography similar to high-performance liquid chromatography that is used to separate or purify proteins from complex mixtures. FPLC system is a complete system for laboratory scale chromatographic separations of proteins and other biomolecules. Liquid Chromatography is a term which refers to all chromatographic method with a liquid mobile phase. The stationary phase may be a liquid or a solid. FPLC is a type of liquid chromatography where the solvent velocity is controlled by pumps to control the constant flow rate of solvents. The solvents are accessed through tubing from an outside reservoir. Depending on the type of separation preferred, various columns are used. FPLC is commonly used in biochemistry and enzymology. The system was developed and marketed by Pharmacia (now GE Healthcare) in 1982 (7).

EF is a bacterial adenylyl cyclase which, upon activation by its eukaryotic cofactor, CaM, causes a rapid increase in the intracellular cAMP levels of host cells (8). Anthrax edema toxin can differentially regulate lipopolysaccharide-induced production of tumour necrosis factor α and interleukin-6 by increasing intracellular cAMP in monocytes (9). The disruption of the cytokine network may contribute to clinical symptoms of anthrax, such as edema formation.

In addition, the genes for PA, LF, and EF (called *pagA*, *lef*, and *cya*, respectively) reside on a 185-kb plasmid, pXO1, of *B. anthracis*. Strains lacking pXO1 do not produce toxin and are essentially avirulent. All three genes have been cloned and sequenced (4, 5, 21, 26). Efforts have been made to express and purify PA and LF from other expression hosts, such as *Bacillus subtilis* and *Escherichia coli* (10). Large amounts of biologically active PA and LF can now be obtained from *E. coli* with relative ease (10, 11).

Calmodulin is a low molecular weight Ca^{2+}-binding protein which serve to mediate numerous Ca^{2+}-regulated enzyme systems and cellular processes (11). Norman, (1980) noted a correlation between octanol:water partition coefficients of

antipsychotic phenothiazine drugs and their ability to inhibit calmodulin activation of cyclic nucleotide phosphodiesterase, and suggested that these drugs probably bind to calmodulin through hydrophobic interaction (12). This was supported by the demonstration of a Ca^{2+} -induced hydrophobic region on calmodulin in experiments using a fluorescent probe for hydrophobic sites (13). Based on this information, the rapid purification of calmodulin to homogeneity, and high yield, can be achieved in a single step using this hydrophobic interaction chromatography (11).

In the present chapter, we sought to purify recombinant EF, EF3 (F586A) from *E. coli* and their corresponding intracellular activator CaM from bovine brain at the maximum possible state of purity, with maintenance of the catalytic activity. The purified proteins were then used for further investigation of enzyme-ligand interactions in terms of catalysis, and fluorescence spectroscopy. The purifications of EF and EF3(F586A) were performed essentially as described in references (14, 15), with important modifications in the purification protocol to obtain more pure protein with a reasonable yield.

3. Materials and Methods

3.1 Materials:

The plasmids pProExH6-EF and pProExH6-EF3F586A for the expression of N-terminally hexahistidine-tagged (EF and EF3(F586A) mutant) were kindly donated by Dr. W.J.Tang (Ben-May institute for Cancer Research, University of Chicago, Chicago, IL, USA). Ampicillin, kanamycin, lysozyme enzyme, β-mercaptoethanol, Tris base, Tris-HCl, Mes buffer (low moisture content) and dithiothreitol (for molecular biology) were purchased from Sigma-Aldrich, Steinheim, Germany. Tryptone and yeast were purchased from BD Biosciences (Franklin Lakes, NJ, USA). [α−^{32}P]ATP (800 Ci/mmol) was purchased from PerkinElmer, Rodgau Jügesheim, Germany. Aluminum oxide 90 active, (neutral, activity 1, particle size 0.06 - 0.2 mm) was purchased from Biomedicals (Eschwege, Germany). Bovine serum albumin (fraction V, highest quality) was bought from Sigma-Aldrich, Steinheim, Germany. Imidazole highest quality), $CaCl_2$, $MnCl_2$ tetrahydrate and $MgCl_2$ hexahydrate (highest quality) were purchased from Merck. For all experiments double-distilled water was used.

3.2 EF/EF3(F586A) plasmid amplification and protein expression

Plasmids pProExH6-EF and pProExH6-EF3F586A were transformed into *E. coli* BL21(DE3) cells that harbored pUBS520, a plasmid that encoded tRNA^{arg} for the rare arginine AGA and AGG codons. The resulting cells were grown over solid agar media (containing 50 µg/ml Ampicillin and 30 µg/ml kanamycin) for 24 hours at 37°C.

Two freshly grown colonies were picked up. Each of the two colonies was further grown in 6 ml modified Lysogeny-Broth or Luria-Bertani (LB medium) (containing 50 µg/ml Ampicillin and 30 µg/ml kanamycin) at 30°C over night under vigorous agitation (250 rpm). The LB medium consists of the following components to yield the given final concentrations: 20 g/l tryptone, 10 g/l yeast extract and 5 g/l NaCl. At the next day, each of the overnight 6 ml cell cultures was transferred into 2L T7/ampicillin medium, in 5L conical flask, and allowed to grow for 6-8 hour at 30°C, under agitation (250 rpm), until cell density reached OD_{595} = 0.6. Thereafter, expression of recombinant EF/EF3(F586A) in *E. coli* were induced by addition of

isopropyl-1-thio galactopyranoside (IPTG). T7/ampicillin medium containing 16 g/L tryptone, 10 g/L yeast extract, 5 g/L NaCl and 50 µg/ml ampicillin. 19 hour after induction, the 4L *E. coli* culture was centrifuged at 10,000 x g (6800 rpm) at 4°C for 10 minutes. The supernatant was discarded, and the pellets were stored at -80°C for the next day. The freezing at -80°C not only helped in the next step of the cell lysis but also provided a convenient break of the protocol.

3.3 Lysis of *E. coli*

We used both enzymatic and mechanical method for the disruption of the bacterial cell wall. The enzymatic method included lysozyme hydrolysis, which cleaves the glucosidic linkages in the bacterial cell wall. The inner cytoplasmic membrane then was disrupted by sonication.

For preparation of lysis buffer, 4 ml of 1 M Tris-HCl buffer (pH 7.7), 1 ml of 4 M NaCl solution, 200 µl of 0.1 M phenyl methyl sulfonyl fluoride (PMSF) in absolute ethanol and 75 µl of 14.3 M β-mercaptoethanol solution were mixed with 150 ml of double-distilled water and then the volume was completed to 200 ml with water. PMSF was added to the lysis buffer as a last component, because it is unstable in aqueous solution.

The pellets were picked up from -80°C freezer and allowed to thaw, transferred to the crushed ice and re-suspended in lysis buffer. The complete re-suspension of the bacteria is very crucial for the complete lysis of the cells. Therefore, the lysate was passed through a syringe several times to ensure the homogeneity of the cell suspension (neither lysozyme nor sonication is effective against clumps). Two ml of the freshly prepared 10 mg/ml lysozyme solution was added to the cell suspension to yield 0.1 mg/ml final concentration. The cell suspension was decanted into 50 ml Falcon tubes for sonication. The sonication was performed with Bandelin Sonopuls GM 2070 sonicator - KE 76 Tip (Bandelin electronic, Berlin, Germany) with one-second-ON and one-second-OFF cycle using the maximum power of 100%, for a total run time of 12 min. We avoided continuous sonication, because it heated the sample up significantly, even if the sample was placed on ice all the time. After sonication, the lysate was left on ice for one hour, to allow for lysozyme to achieve the complete lysis of the bacterial cell wall. Then, the

cell lysate was centrifuged at 35,000 rpm with a Ti45 rotor (Beckman) for 30 min at 4°C to ensure the complete removal of particulate cell debris and sustain the lifespan of Ni-column. The supernatant (containing the EF/EF3(F586A)) was decanted immediately after the end of centrifugation and the pellet was discarded. Four ml of 0.1 M PMSF stock solution was added to the resultant supernatant immediately to inactivate any proteases.

3.4 Chromatographic purification of EF

Two different chromatographic steps with two different principles were used for purification of EF; the first step was based on the immobilized metal ion-affinity chromatographic (IMAC) technique using Ni^{2+} column (for the purification of hexahistidine-tagged proteins), and the second step was based on ion exchange chromatographic technique using resource-Q column as a strong anion exchange column.

3.4.1 IMAC chromatographic purification using HisTrap fast-flow-rate Ni^{2+} column

Chromatographic purification of the EF was started immediately after the last centrifugation step, because EF is highly sensitive to destruction by proteolytic enzymes even if stored at 4°C.

The HisTrap Fast-flow-rate Ni^{2+} column, 5 ml, (GE Healthcare, Freiburg/Brsg., Germany) was connected to the ÄKTAdesign, FPLC system, (GE Healthcare, Freiburg/Brsg., Germany). Before loading the sample, a blank run was conducted to remove the impurities and other undesirable proteins that could still bind to the column matrix from previous runs. The blank run was applied as follows: the column was washed with 5 column-volumes of water, followed by 5 column-volumes washing with, high-salt buffer B (20 mM Tris-HCl, pH 7.7; 5 mM β-mercaptoethanol; 0.1 mM PMSF; and 500 mM NaCl), 5 column-volumes washing buffer C (20 mM Tris-HCl, pH 7.7; 5 mM β-mercaptoethanol; 0.1 mM PMSF; 100 mM NaCl and 20 mM imidazole), 5 column-volumes elution, low-salt-high-imidazole, buffer D (20 mM Tris-HCl, pH 7.7; 5 mM β-mercaptoethanol; 0.1 mM PMSF; 50 mM NaCl and 200 mM imidazole). Finally, the column was equilibrated with 10-15 column-volumes of equilibration,

imidazole free, buffer A (20 mM Tris-HCl, pH 7.7; 5 mM β-mercaptoethanol; 0.1 mM PMSF; 100 mM NaCl) before sample loading. The flow rate, during the blank run, was adjusted to 5 ml per minute, which is the maximum flow rate of the column.

The protein sample was prepared prior to loading onto Ni^{2+} column by addition of imidazole to the sample to yield 20 mM final concentration (the same imidazole final concentration in the washing buffer C). Then, the sample was diluted with an equal volume of the washing buffer C and filtered through 0.45 µm filter. The imidazole was included in the sample at a concentration equal to that of washing buffer to ensure the best balance of high purity (low binding of unwanted proteins) and high yield (binding of all of the histidine-tagged EF protein). In fact, the ideal imidazole concentration in both the sample and washing buffer is protein-dependent. Thus, imidazole final concentration in both sample and washing buffer was optimized based on both our previous trial experiments, and as previously described by Shen et al., 2002.

Thereafter, the sample was loaded onto the Ni^{2+} column, with a flow rate of 3 ml per minute, followed by two washing steps of the column with 5 column-volumes of buffer B and buffer C respectively, with a flow rate of 5 ml per minute. Then, the EF was eluted from the column by elution with high-imidazole buffer D with a flow rate of 4 ml per minute. The eluate was collected in 8 ml plastic tubes, 4 ml of the eluate per each tube. The 200 mM imidazole final concentration of the elution buffer was the ideal for elution of EF. This imidazole concentration was determined based on this fact, that the concentration of imidazole that gave ideal purification results was slightly higher for the column matrix we used (Ni-sepharose high performance) and our previous trial experiments (fractions collection during the gradient imidazole elution from 50 to 500 mM). The fractions of the area under the peak were collected and EF was identified by sodium dodecyl sulfate; polyacrylamide gel electrophoresis (SDS-PAGE).

3.4.2 Anion exchange chromatographic purification of EF

Resource Q (quaternary ammonium salt) strong anion exchange column, (6 ml), (GE Healthcare, Freiburg, Germany) was used. The media of this column are based on a hydrophilic matrix made from monodispersed, rigid, polystyrene/divinyl benzene and substituted with quaternary ammonium groups. This combination

confers extreme chemical and physical stability to media. The small particle sizes allow fast binding and dissociation to facilitate high resolution. The column was washed with 5 column-volumes water to remove the 20% (v/v) ethanol used for column storage. Then, the column was equilibrated with the start (equilibration) buffer $A_{res.Q}$ (20 mM Tris-HCl, pH 8.6; 1 mM ethylenediaminetetraacetic acid (EDTA); 0.1 mM PMSF). The fractions containing EF protein, obtained after Ni^{2+} column, were diluted five-fold with the start buffer $A_{res.Q}$, in order to be adjusted to the starting pH and ionic strength and then loaded onto the column with a flow rate of 3 ml per minute. The column was washed with five column-volumes of equilibration buffer $A_{res.Q}$ pH 8.6 to wash out all unbound materials from the column. The adsorbed EF protein was eluted at 2 ml/min with a linear NaCl gradient (400-450 mM). The NaCl gradient was mixed by using two buffers; salt-free buffer $A_{res.Q}$ (20 mM Tris-HCl, pH 8.6; 1 mM EDTA; 0.1 mM PMSF) and high-salt buffer $B_{res.Q}$ (20 mM Tris-HCl, pH 8.6; 1 mM EDTA; 0.1 mM PMSF; 1 M NaCl). EF eluted by adjusting the gradient to 40% (v/v) buffer $B_{res.Q}$ per 480 ml of both buffer $A_{res.Q}$ and $B_{res.Q}$.

The Resource Q column was then washed with at least 5 column-volumes of high-salt buffer $B_{res.Q}$ to remove the other unwanted proteins adsorbed into the column matrix due to unspecific binding. This procedure was followed by washes with 5 column-volumes of buffer A and finally with 5 column-volumes water before storage in 20% (v/v) ethanol.

The high-salt column wash with 1 M NaCl buffer B at the end of each separation should keep the Resource Q column in good condition. However, we cleaned the column after two separation cycles to improve the performance and increase the life-span of the column. During column cleaning, the flow rate was adjusted to 6 ml/min. and the direction of flow was reversed so that contaminants did not need to pass through the entire length of the column. The cleaning procedures included: washing with two column-volumes of 2 M NaCl followed by 4 column-volumes of 1 M NaOH, 2 column-volumes 2 M NaCl, 2 column-volumes of water, and finally 4 column-volumes of start buffer.

3.5 Chromatographic purification of EF3(F586A) mutant

3.5.1 IMAC chromatographic purification using HisTrap fast-flow-rate Ni^{2+} column

The IMAC chromatographic purification of EF3(F586A) was performed as described previously in EF purification.

3.5.2 Cation exchange chromatographic purification of EF3(F586A)

The HiPrep 16/10 SP XL column (GE Healthcare, Freiburg, Germany) was used in cation exchange chromatography. The media of this column are based on a hydrophilic matrix made from monodispersed, rigid, polystyrene/divinyl benzene and substituted with propyl sulphonyl groups.

The column was washed with 5 column-volumes water to remove the 20% (v/v) ethanol used for column storage. Then, the column was equilibrated with the start (equilibration) buffer (20 mM 2-(N-morpholino)ethanesulfonic acid (MES) buffer, pH 6.5; 1 mM EDTA; 0.1 mM PMSF; 1 mM dithiothreitol, proteases enzymes free, (DTT)). The fractions containing EF3(F586A) protein, obtained after Ni^{2+} column, were diluted five times with the start buffer, in order to be adjusted to the starting pH and ionic strength and then loaded onto the column with 3 ml per minute flow rate. The column was washed with five column-volumes of equilibration buffer, pH 6.5, to wash out all unbound materials from the column. The adsorbed EF3(F586A) was eluted at 2 ml/min with a linear NaCl gradient (500 mM). The NaCl gradient was generated by using two buffers; salt-free buffer (20 mM MES buffer, pH 6.5; 1 mM EDTA; 0.1 mM PMSF: 1 mM DTT) and high-salt buffer (20 mM mM MES buffer, pH 6.5; 1 mM EDTA; 0.1 mM PMSF: 1 mM DTT; 1 M NaCl). EF eluted by adjusting the gradient to 50% of the high-salt buffer per 480 ml of both salt-free buffer and high-salt buffer.

The HiPrep 16/10 SP XL column was then washed with at least 5 column-volumes of high-salt buffer to remove the other unwanted proteins adsorbed to the column matrix due to unspecific binding. This procedure was followed by washes with 5 column-volumes of the start buffer and finally with 5 column-volumes water before storage in 20% (v/v) ethanol.

3.6 Calmodulin purification from bovine brain

Calmodulin was isolated and purified from bovine brain as described previously by Gopalakrishna and Anderson (11). The detailed procedures of isolation and purification will be discussed at this section.

Bovine brains were purchased several weeks in advance, and cleaned of membranes and blood clots. The bovine brain was stored in plastic freezer bags at -20 °C. It was removed from the freezer 8-12 h before the start of purification and allowed to thaw at room temperature.

3.6.1 Extraction of calmodulin from bovine brain tissues

Unless otherwise stated, all procedures were carried out at 4°C and centrifugations were conducted at 15,000 g for 30 min. Approximately 200 g of brain were homogenized by the tissue homogenizer (ULTRA-TURRAX-Typ Tp18 - Germany) with two volumes of buffer A (50 mM Tris-HCl, pH 7.5; 1 mM β-mercaptoethanol; 1 mM EDTA 0.5; mM PMSF) per weight of brain. The homogenate was centrifuged at 15,000 g (9600) rpm at 4°C for 30 min using 4 °C refrigerated centrifuge (Sorvall RC 5B refrigerated centrifuge using GSA rotor). The pellet was discarded and the supernatant was filtered through gauze swabs to get rid of the lipids. The pH was adjusted to 4.3, the isoelecteric point of calmodulin, at which calmodulin precipitates by dropwise addition of 6 M acetic acid.

The slurry was then transferred into the cold room and stirred for about 30 min. After that, the slurry was centrifuged at 15,000 g (9600) rpm at 4°C for 30 min, then the supernatant was discarded and the pellet was resuspended in 100 ml of buffer A, and the pH was adjusted to 7.5 by dropwise addition of Tris base. The slurry was centrifuged again at 15,000 for 30 min. The pellet was discarded and the concentration of $CaCl_2$ in the supernatant was adjusted to 5 mM final concentration (i.e 0.0375/50 ml of final supernatant). 20 µl of the 0.5 M PMSF stock solutions was added to adjust the concentration of the PMSF in the final supernatant into 0.1 mM. The sample was frozen at -20°C for the next day.

3.6.2 Hydrophobic chromatography purification of calmodulin

The solutions were removed from the freezer about 2 hour before starting the procedure. The FPLC refrigerator was also turned off about two hours before the start because the hydrophobic chromatographic procedure should be performed at room temperature and any decrease in temperature during purification steps could interfere with the hydrophobic binding of calmodulin to the Sephadex matrix. Hiprep 16/10 phenyl FF (high sub) (GE Healthcare, Freiburg, Germany) was used. For the first-time use, the column was washed by 5 column-volumes of low-salt start buffer I (50 mM Tris-HCl, pH 7.5; 1 mM β-mercaptoethanol; 0.1 mM $CaCl_2$), followed by five column-volumes of high-salt buffer I (50 mM Tris-HCl, pH 7.5; 1 mM β-mercaptoethanol; 0.1 mM $CaCl_2$; 500 mM NaCl) and equilibration with 10 column-volumes of start buffer I before sample loading. All column preparation and equilibration steps were performed with a flow rate of 5 ml/min. The sample was loaded onto the column with a flow rate of 1.5 ml/min. This was followed by two washing steps with ten column-volumes of start buffer I and high-salt buffer I respectively with 2.5 ml/min flow rate. Finally, the adsorbed calmodulin was eluted from the column with a flow rate of 2.5 ml/min by elution buffer containing 50 mM Tris-HCl, pH 7.5; 1 mM β-mercaptoethanol; and 1 mM ethylene glycol tetraacetic acid (EGTA). The fractions at the area under the peak (containing calmodulin) were collected and further identified with SDS-PAGE depending on the molecular mass.

3.7 Concentration and characterization of the purified proteins

The fractions containing the purified proteins were pooled and the target protein was identified by SDS-PAGE (a 12% (m/v) polyacrylamide gel was used) depending on its molecular mass. The protein sample (7.5 µl) was mixed with 2.5 µl of the Laemmli dye (migration marker dye). Furthermore, the mixture was incubated with shaking at 95°C for 3 min. Samples (9 µl) and 5 µl of the proper protein standard were loaded into the wells and the electric current with a fixed 150 volt was applied for about 35 min. The gel slabs were washed from the loading buffer three times by double distilled water for 10 min, 10 min., and 30 min., respectively, and stained with Coomassie brilliant blue dye for at least one hour. Finally gels were washed with water for 5 min.

The purified proteins were concentrated using Jumbosep centrifugal devices with 60 ml sample reservoir (Pall Life Sciences, MI, USA). For the maximum retention, we selected a Jumbosep membrane insert with a molecular weight cutoff three times smaller than the molecular weight of the molecule to be retained. Thus, 10K, 20K, and 30K cutoff membranes were used for the concentration of CaM, EF3(F586A), and EF respectively. The Jumbosep centrifugal devices were pre-treated to reduce the non-specific adsorption to the device. For the pre-treatment the sample reservoir was filled with 60 ml of the 10% (m/v) glycerine and soaked over night at room temperature, then rinsed with deionised water and finally, filled with deionised water and twice centrifuged for 15 min. at 3,000 g. For the concentration of the protein sample, it was placed into the sample reservoir and centrifuged at 3,000 g for 40- 60 min.

The concentration of the purified protein was estimated using ultraviolet light absorption at 280 nm using Beckman photometer (Beckman Instruments, Munich, Germany)(1 absorption unit = 1.16 mg/ml) and then determined accurately by Bradford protein assay, because it is simple, rapid and free from interference with common reagents except detergents. Seven different dilutions in duplicates of the standard protein (BSA), in a microtiter plate, were prepared for establishment of the standard curve. The protein samples were diluted 1-20-fold with distilled-deionized water. Two different dilutions of each sample were tested in duplicates. Then 50 µl of the Coomassie® Brilliant Blue G-250 dye were added per well and finally, the water was added to adjust the volumes 250 µl/well. After 5 min the absorbance was measured at 595 nm using Bio-Rad microtiter plate reader. The data were calculated and processed in Excel 2003.

Adenylyl cyclase activity assay. For the determination of K_m and V_{max} values, 10 µl of ATP/Mn^{2+} at final concentration from 10 µM to 1 mM were added, and 20 µl of EF or EF3(F586A) (10 pM final concentration) in 75 mM Tris/HCl, pH 7.4, containing 0.1% (m/v) bovine serum albumin. Tubes were preincubated for 2 min at 25°C, and reactions were initiated by the addition of 20 µL of reaction mixture consisting of the following components to yield the given final concentrations; 100 mM KCl, 100 µM free Ca^{2+}, 5 mM free Mn^{2+}, 100 µM EGTA, 100 µM cAMP, 100 nM CaM. Tubes were incubated for 10 min at 25°C, and reactions were stopped by the addition of 20 µL of 2.2 N HCl.

For the determination of the potency of AC toxin inhibitors, assay tubes contained 10 µl of MANT-ATP at final concentrations from 10 nM to 100 µM as appropriate to obtain saturated inhibition curves plus 20 µl of EF or EF3(F586A) (10 pM final concentration) in 75 mM Tris/HCl, pH 7.4, containing 0.1% (m/v) bovine serum albumin. Tubes were preincubated for 2 min at 25°C, and reactions were initiated by the addition of 20 µL of reaction mixture consisting of the following components to yield the given final concentrations; 100 mM KCl, 100 µM free Ca^{2+}, 5 mM free Mn^{2+}, 100 µM EGTA, 100 µM cAMP, 100 nM CaM. ATP was added as non-labeled substrate at a final concentration of 40 µM and as radioactive tracer [α-^{32}P]ATP (0.2 µCi/tube). Denaturated protein was sedimented by a 1-min centrifugation at 13,000 x g. [^{32}P]cAMP was separated from [α-^{32}P]ATP by transferring the samples to columns containing 1.4 g of neutral alumina. [^{32}P]cAMP was eluted by the addition of 4 ml of 0.1 M ammonium acetate solution, pH 7.0. Blank values were about 0.02% of the total amount of [α-^{32}P]ATP added; substrate turnover was < 3% of the total amount of [α-^{32}P]ATP added. Samples collected in scintillation vials were filled up with 10 ml of double-distilled water and Čerenkov radiation was measured in a PerkinElmer Tricarb 2800TR liquid scintillation counter. V_{max} and K_m values reported in the results section were calculated using the Prism 4.02 software (Graphpad, San Diego, CA, USA). Free concentrations of divalent cations were calculated with WinMaxC (http://www.stanford.edu/~cpatton/maxc.html).

Fluorescence resonance energy transfer (FRET) experiments for monitoring inhibitor binding to EF/EF3(F586A). Fluorescence experiments were performed using quartz UV ultra-microcuvettes from Hellma (Müllheim, Germany, type 105.251- QS, light path length 3 x 3 mm, center 15 mm, total volume 70 µl and type 105.250- QS, light path length 10 x 2 mm, center 15 mm, total volume 150 µl) in a thermostated multicell holder at 25°C in a Varian Cary Eclipse fluorescence spectrometer (Varian, Darmstadt, Germany). In case of 150 µl cuvettes, 140 µl of buffer consisting of 100 mM KCl, 100 µM $CaCl_2$, 10 mM $MnCl_2$ and 25 mM HEPES/NaOH, pH 7.4, was added into the cuvette. Five µl of 10 µM full-length EF/EF3(F586A) (final concentration 300 nM), 5 µl of 10 µM CaM (final concentration 300 nM) and fluorescent 2'-MANT-3'-d-ATP (300 nM each) was added. In case of experiments with 70 µl cuvettes, volumes were

adjusted stoichiometrically. The results obtained with 70 µl- and 150 µl-cuvettes were identical, with the 70 µl-cuvettes offering an opportunity to save EF/EF3(F586A) mutant protein.

Steady-state fluorescence emission spectra of nucleotides were recorded at low speed in the scan mode from λ_{em} 300 nm to 550 nm with λ_{ex} 280 nm. Fluorescence recordings were analyzed with the spectrum package of the Varian Cary Eclipse software version 1.1. Baseline fluorescence (buffer alone) and the baseline-corrected nucleotide-dependent emission of each concentration of the ligand (buffer + nucleotide) were subtracted from the spectra shown in Fig. 10.

4. Results and discussion

4.1 Purification and characterization of the Full length EF

Figs. 1 and 2 show examples of the unsatisfactory Ni^{2+} column and Resource Q column purification results of the initial purification trials that had been performed as described by Shen et al., 2002 without modifications. The resolution, the purity, and the yield After Ni^{2+} column were all very poor. It was clear at SDS-PAGE, that the target protein was strongly contaminated by other unwanted proteins. Unfortunately at the further purification of the sample on the Resource Q column, a multiple peak chromatogram without a characteristic peak was obtained. Also, the EF fractions of Resource Q column as analyzed by SDS-PAGE, were highly contaminated with other proteins. This meant that the purification protocol applied was not ideal and needed further optimization. Hence, the following modifications were performed: The imidazole was included in the sample in a concentration equal to that of washing buffer to ensure the best balance of high purity (low binding of unwanted proteins) and high yield (binding of all of the histidine-tagged EF protein molecules). The imidazole was included in the sample. Imidazole at low concentrations is commonly used in the binding and wash buffer to minimize binding of unwanted host cell proteins and for the same reason, it has to be also included in the sample (4). Moreover, the sample was diluted with the imidazole-containing washing buffer C to adjust the pH and the ionic strength of the sample, also to ensure the balance of the high purity and high yield. In addition, the final concentration of imidazole in elution buffer was increased from 150 mM to 200 mM because the HisTrap Fast-flow-rate Ni^{2+} column used at the EF initial step purification require a higher imidazole concentration in the elution buffer than the other commercially available IMAC columns. Finally, at the anion exchange chromatography step of the purification, the fractions containing EF collected from Ni^{2+} column were pooled and diluted with the start buffer $A_{res.Q}$ before loading to resource Q column. Based on these modifications of the purification protocol ideal chromatograms (with sharp narrow single peak) were obtained during the purification of EF on both Ni^{2+} and resource Q columns as shown in Figs. 3 and 4.

Fig. 1: Initial results of the primary purification step of EF on Ni^{2+} column and SDS-PAGE of the collected fractions (before the important modifications).

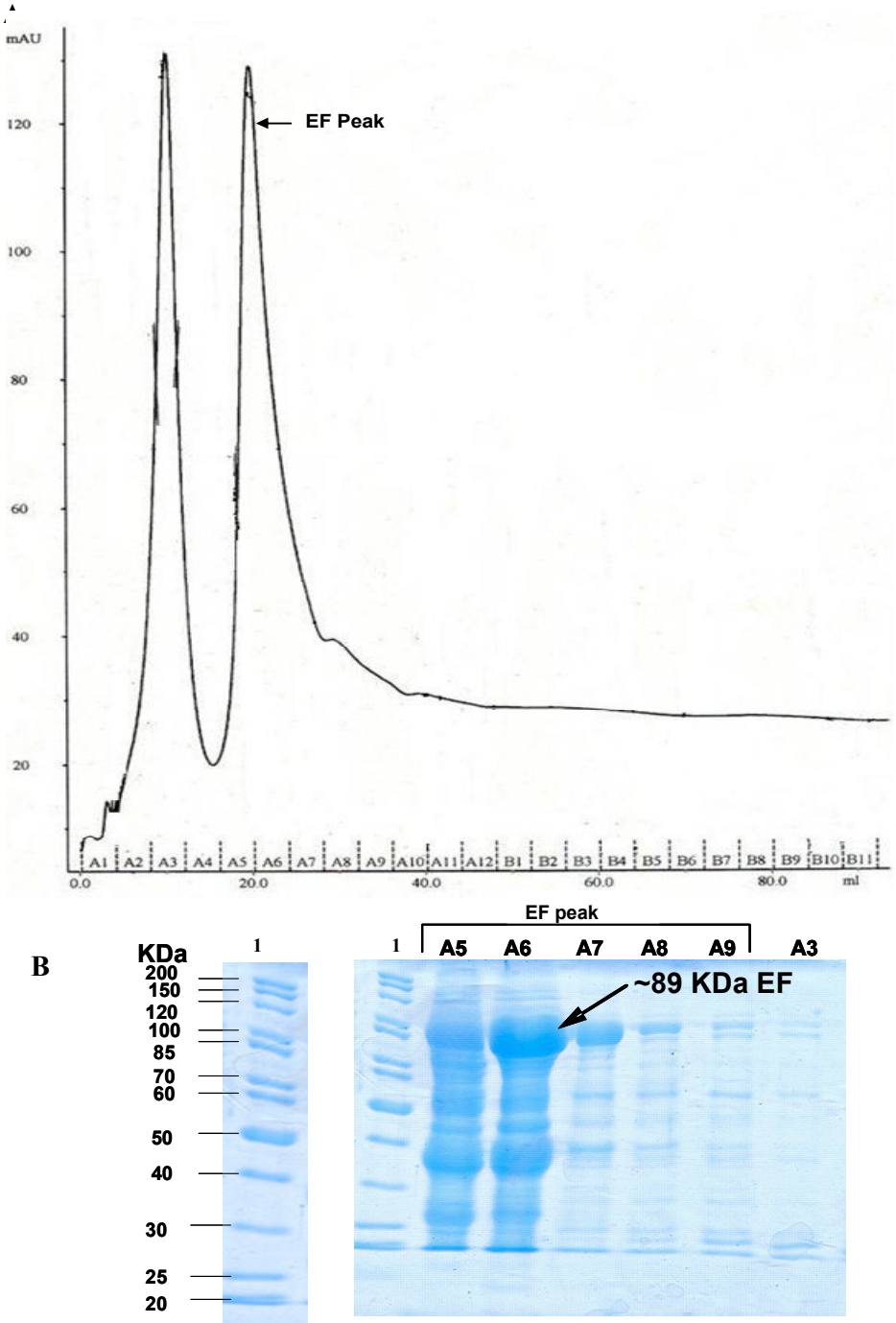

The initial purification step of recombinant EF from *E. coli* on Ni^{2+} column, **A)** the chromatogram obtained during the separation of the sample on Ni^{2+} column. The separation was performed as described by Shen et al., 2002 without modifications **B)** the identification of the EF on 12% (m/v) SDS-PAGE. Lane 1, shows the protein standard (Fermentas, PageRuler protein standard SM0661, Germany), lanes A5-A9, the fractions of the 2nd peak (EF peak), and lane A3 the fraction of 1st peak. SDS-PAGE was performed as described in the Materials and Methods section. As shown, the resolution of the purification process was poor and the protein was heavily contaminated.

Fig. 2: Initial results of secondary purification step of EF on resource Q column and SDS-PAGE of the the collected fractions (before the important modifications).

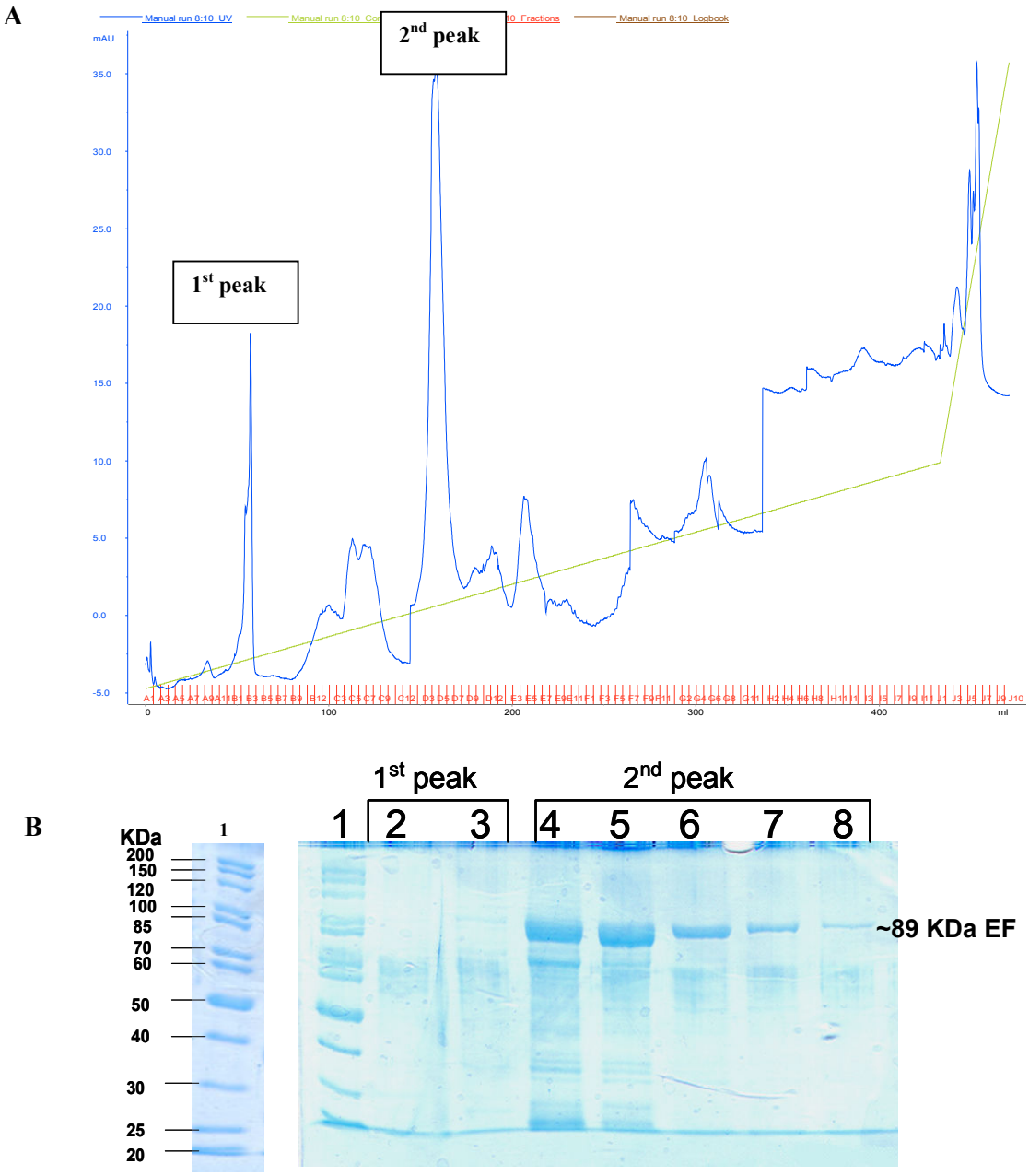

The secondary purification step of recombinant EF from *E. coli* on resource Q column, **A)** the chromatogram obtained during the separation of the sample on Q column. The separation was performed as described by Shen et al., 2002 without modifications. **B)** the identification of the EF on 12% (m/v) SDS-PAGE. Lane 1, shows the protein standard (Fermentas, PageRuler protein standard SM0661, Germany), lanes 2 and 3, the fractions of the 1st peak and lanes 4-8, the fractions of 2nd peak (EF peak). SDS-PAGE was performed as described in the Materials and Methods section. As shown, the resolution of the purification process was poor and the protein was heavily contaminated.

Fig. 3: Final results of primary purification step of EF on Ni^{2+} column and SDS-PAGE of the collected fractions (after the important modifications).

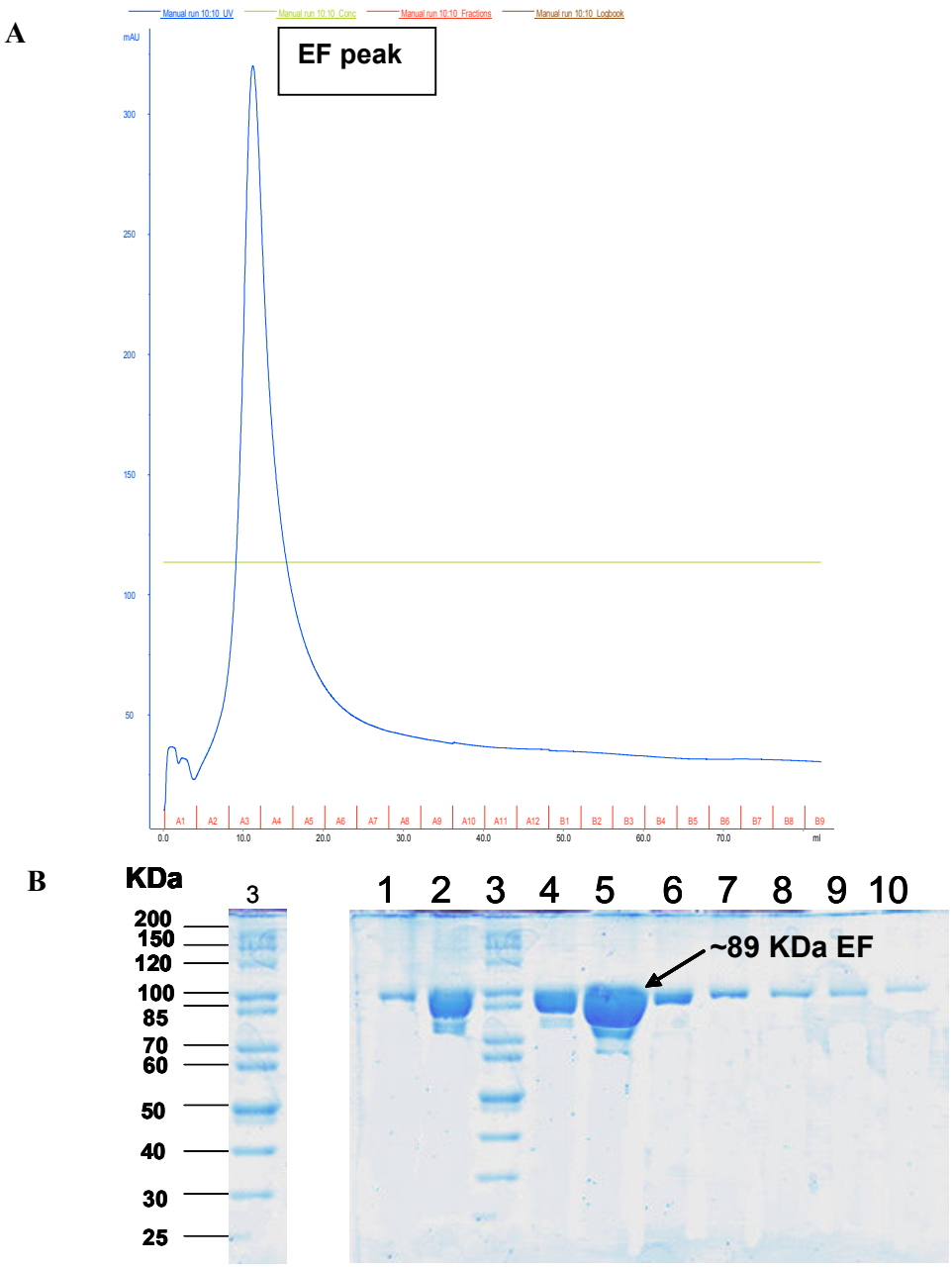

Final results of the primary purification step of recombinant EF from *E. coli* on Ni^{2+} column, **A)** the chromatogram obtained during the separation of the sample on Ni^{2+} column. The separation was performed as described by Shen et al., 2002 with the previously mentioned modifications. **B)** the identification of the EF on 12% (m/v) SDS-PAGE. Lane 3, shows the protein standard (Fermentas, PageRuler protein standard SM0661, Germany), lanes 1, 2, 4-10, the fractions of the EF peak. The SDS-PAGE was performed as described in the Materials and Methods section. As shown, a single sharp peak chromatogram obtained and the protein approximately pure before the second step of purification. These results were reproduced at least 6 times.

Fig. 4: Final results of secondary purification step of EF on resource Q column and SDS-PAGE of the collected fractions (after the important modifications).

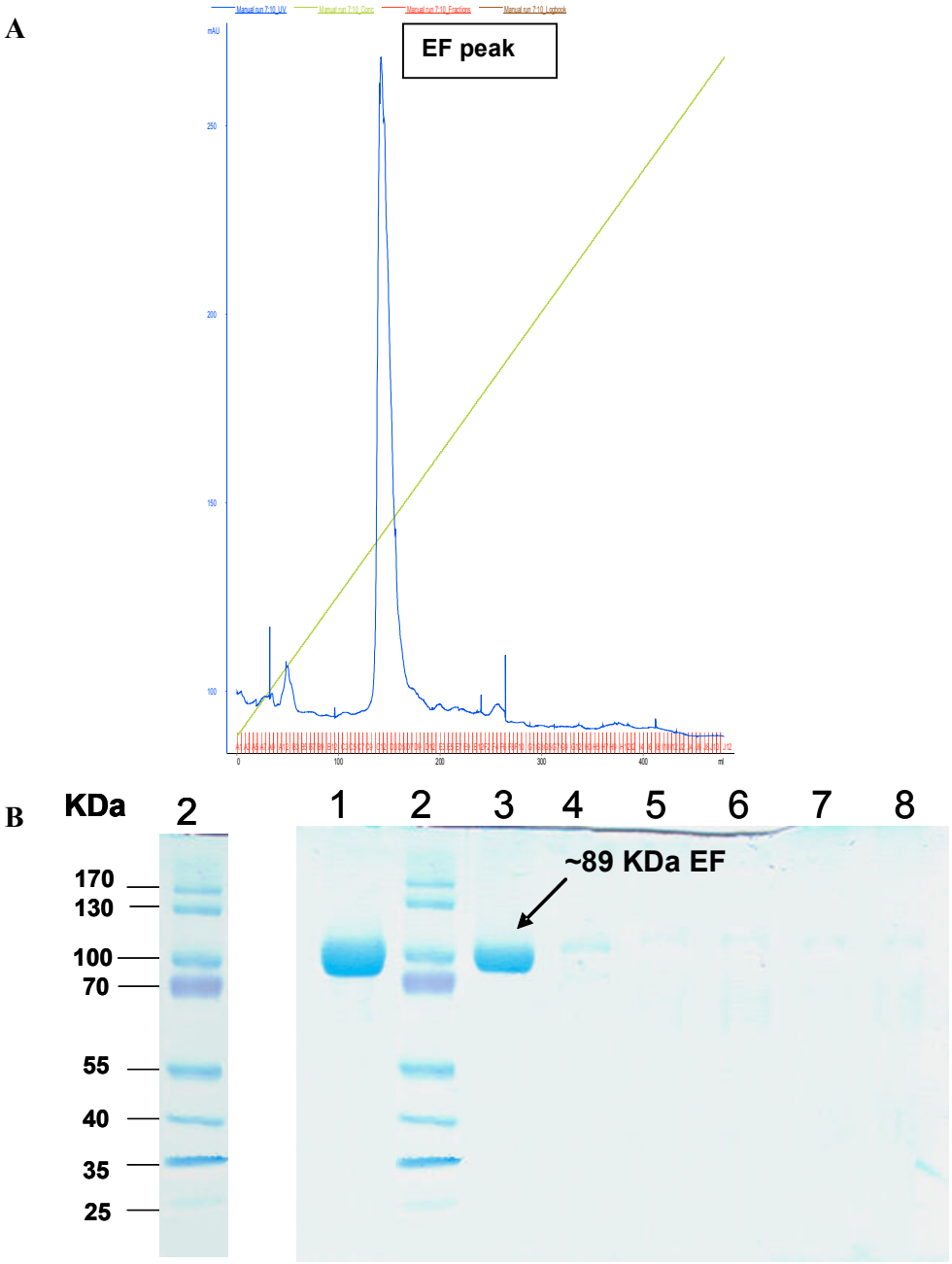

Final results of the secondary purification step of recombinant EF from *E. coli* on resource Q column, **A)** the chromatogram obtained during the separation of the sample on resource Q column. The separation was performed as described by Shen et al., 2002 with the previously mentioned modifications. **B)** the identification of the EF on 12% SDS-PAGE. Lane 2, shows the protein standard (Fermentas, PageRuler prestained protein standard SM0671, Germany), lanes 1, 3, 4, the fractions of the EF peak. Lanes 5-8, the fractions collected during the cleaning steps of the column. SDS-PAGE was performed as described in the Materials and Methods section. As shown, a single sharp peak chromatogram obtained and the protein approximately 98% pure. These results were reproduced at least 6 times.

Furthermore, the yield was increased > 25 mg EF protein/L *E. coli* culture with a

highest purity > 98% as represented by 12% (m/v) SDS-PAGE (Fig. 3 and 4). Fig. 5 shows kinetic analysis of the catalytic activity of EF in the presence of Ca^{2+} and its intracellular activator CaM by ATP/Mn^{2+} saturation assay. The V_{max} and K_m values of EF are 232 ± 34 and 84.5 ± 8.3 respectively. Those values were obtained by nonlinear regression analysis of substrate-saturation experiment and are the means ± standard deviation of at least three independent experiments performed in triplicates

Fig. 5: Substrate saturation experiments of full length EF

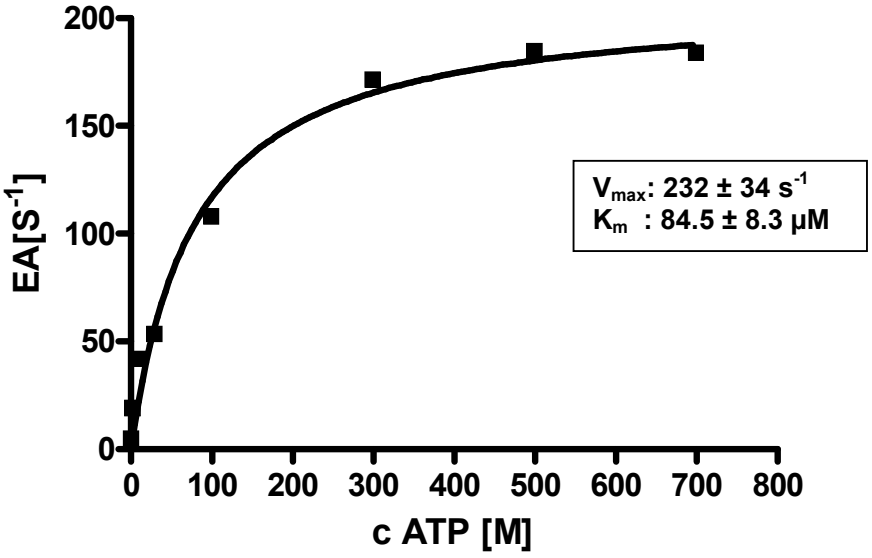

The assay was performed as described under Materials and Methods section. K_m and V_{max} values were obtained by non-linear regression analysis of substrate-saturation experiments and are the means ± SD of at least 3 independent experiments performed in triplicates. For the determination of the V_{max} and K_m of EF, reaction mixtures contained 100 µM free Ca^{2+}, 5 mM free Mn^{2+}, 100 µM EGTA, 0.2-1.0 µCi/tube [α-^{32}P]ATP, 100 µM cAMP, 100 nM calmodulin and 10 pM enzyme in 75 mM Tris-HCl, pH 7.0. The unlabeled ATP/Mn^{2+} concentrations ranged from 100 nM to 700 µM as appropriate to obtain saturated curves.

4.2 Purification and characterization of EF3(F586A)

EF3 is the truncated form of edema factor and is the CaM-sensitive adenylyl cyclase domain. EF3(F586A), in the slightly acidic MES buffer, pH 6.5, acquires a positive charge and hence could be easily purified on the strong cationic exchange column. EF3(F586A) mutant has been effectively purified using HisTrap Fast-flow-rate Ni^{2+} column and HiPrep 16/10 SP XL column, resulting in > 98% pure protein as judged by SDS-PAGE as shown in Figs. 6 and 7. This preparation yields approximately 40 mg EF3(F586A) mutant/L *E. coli* culture. The mutant was expressed and purified essentially as described (Shen et al., 2002) with minor modifications as in the purification of full-length EF. Specifically, the imidazole concentration in the elution buffer for the Ni^{2+} column was 200 mM, and imidazole (20 mM) was included in the sample. The HisTrap fast flow rate affinity Ni column (5 ml) was used for immobilized matrix-affinity chromatography and the HiPrep 16/10 SP XL column (GE Healthcare) was used for cation exchange chromatography.

Fig. 8 shows kinetic analysis of the catalytic activity of EF3(F586A) in the presence of Ca^{2+} and its intracellular activator CaM by ATP/Mn^{2+} saturation assay. The V_{max} and K_m values of EF3(F586A) are 128 ± 5 and 92.0 ± 14.7 respectively. The V_{max} value of that mutant was about half of that of wild-type EF, but the K_m was not changed significantly. Those values were obtained by nonlinear regression analysis of substrate-saturation experiments and are the means ± standard deviation of at least three independent experiments performed in triplicates

Fig. 6: Separation of the recombinant EF3(F586A) from *E. coli* on Ni^{2+} column and SDS-PAGE of the collected fractions

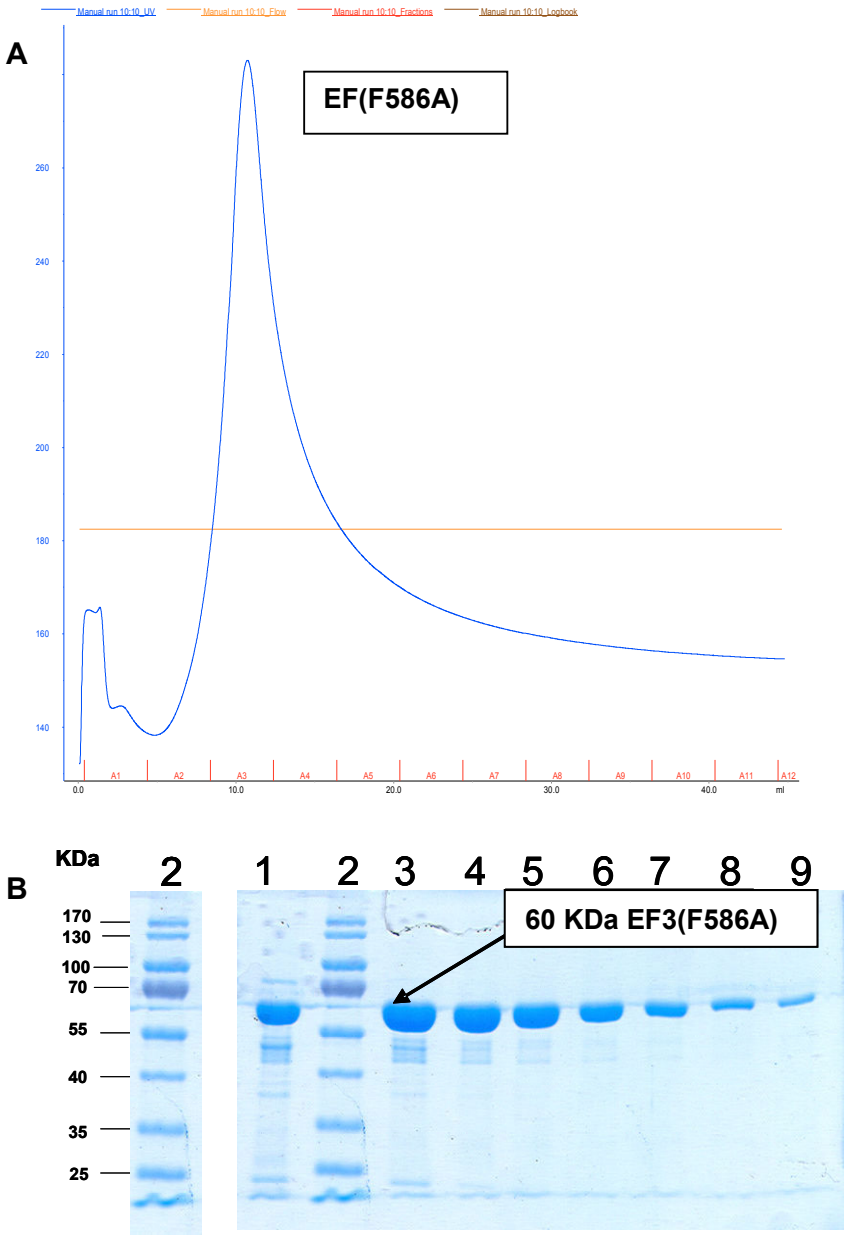

The results of the primary purification step of recombinant EF3(F586A) from *E. coli* on Ni^{2+} column, **A)** the chromatogram obtained during the separation of the sample on Ni^{2+} column. The separation was performed as described by Shen et al., 2002 with the previously mentioned modifications. **B)** the identification of the EF3(F586A) on 12% (m/v) SDS-PAGE. Lane 2, shows the protein standard (Fermentas, PageRuler prestained protein standard SM0671, Germany), lanes 1, 3, 4-9, the fractions of the EF3(F586A) peak. The SDS-PAGE was performed as described in the Materials and Methods section. As shown, a single sharp peak chromatogram obtained and the protein was already almost pure before the second step of purification. These results were reproduced at least 5 times.

Fig. 7: Separation of the recombinant EF3(F586A) from *E. coli* on HiPrep 16/10 SP XL and SDS-PAGE of the collected fractions

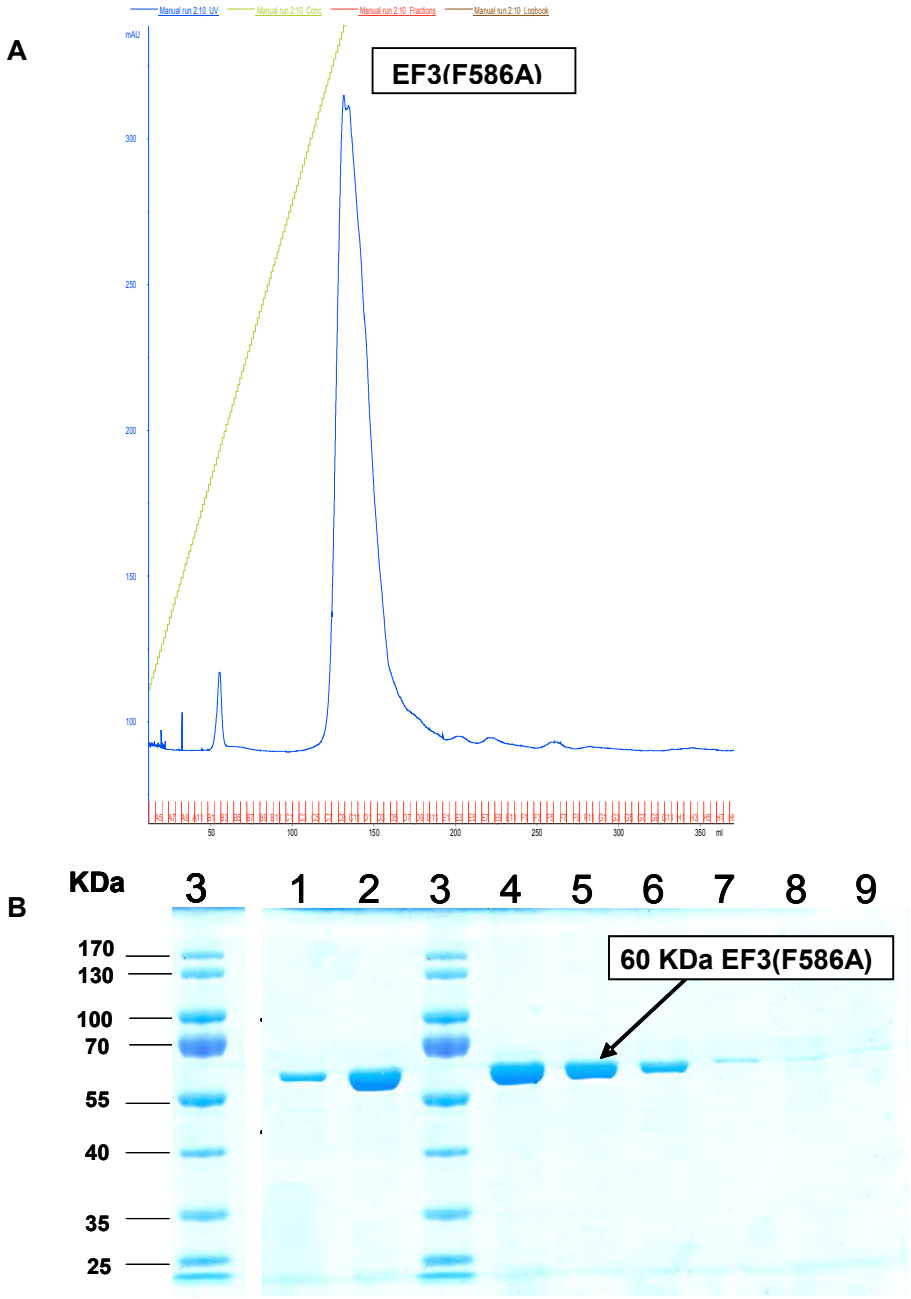

The results of the secondary purification step of recombinant EF3(F586A) from *E. coli* on HiPrep 16/10 SP XL column, **A)** chromatogram obtained during the separation of the sample on Ni^{2+} column. The separation was performed as described by Shen et al., 2002 with the previously mentioned modifications. **B)** identification of the EF3(F586A) on 12% (m/v) SDS-PAGE. Lane 3, shows the protein standard (Fermentas, PageRuler prestained protein standard SM0671, Germany), lanes 1, 2, 4-9, the fractions of the EF3(F586A) peak. The SDS-PAGE was performed as described in the Materials and Methods section. As shown, a single sharp peak chromatogram obtained and the protein purity was > 98%. These results were reproduced at least 5 times.

Fig. 8: Substrate saturation experiments of EF3(F586A) mutant

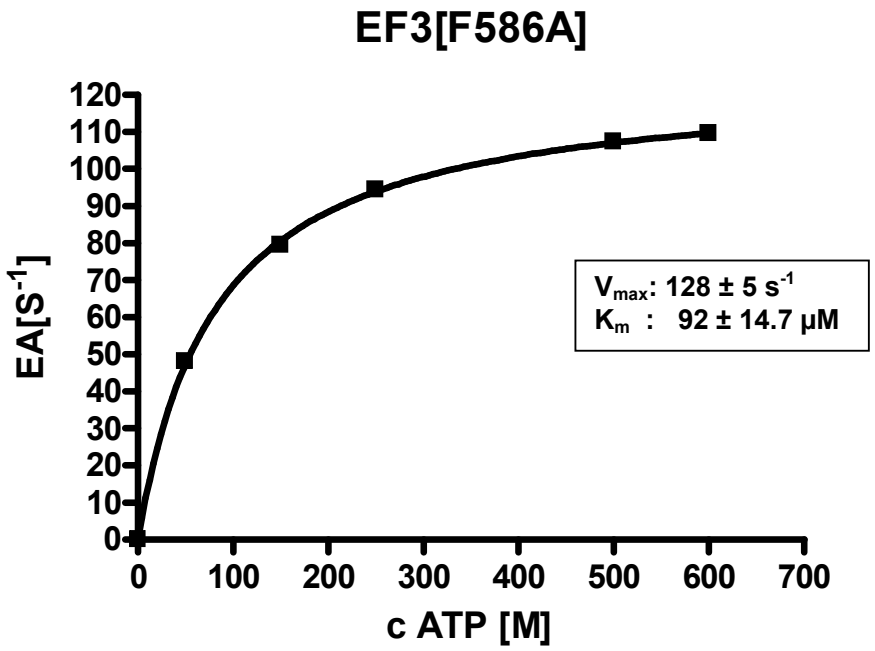

The assay was performed as described under Materials and Methods section. K_m and V_{max} values were obtained by non-linear regression analysis of substrate-saturation experiments and are the means ± SD of at least 3 independent experiments performed in triplicates. For the determination of the V_{max} and K_m of EF3(F586A), reaction mixtures contained 100 µM free Ca^{2+}, 5 mM free Mn^{2+}, 100 µM EGTA, 0.2-1.0 µCi/tube [α–^{32}P]ATP, 100 µM cAMP, 100 nM calmodulin and 10 pM enzyme in 75 mM Tris-HCl, pH 7.0. The unlabeled ATP/Mn^{2+} concentrations ranged from 100 nM to 700 µM as appropriate to obtain saturated curves.

4.3 Purification of calmodulin from bovine brain

This purification of CaM from bovine brain extract on phenyl-sepharose after isoelecteric precipitation is considered as a very good and easy method to obtain CaM in a high yield and purity. The yield was about 35 mg CaM per 200 g of bovine brain with a purity > 95% as judged by the 12% (m/v) SDS-PAGE as shown in Fig. 9. The biological activity of the purified CaM was very good, when tested with the purified EF and EF3(F586A) mutant as shown in Figs. 5 and 8. The purified CaM exhibited the same activity as the commercially available CaM.

Fig. 9: Purification of calmodulin from bovine brain extract on Hiprep 16/10 phenyl FF and SDS-PAGE of the collected fractions

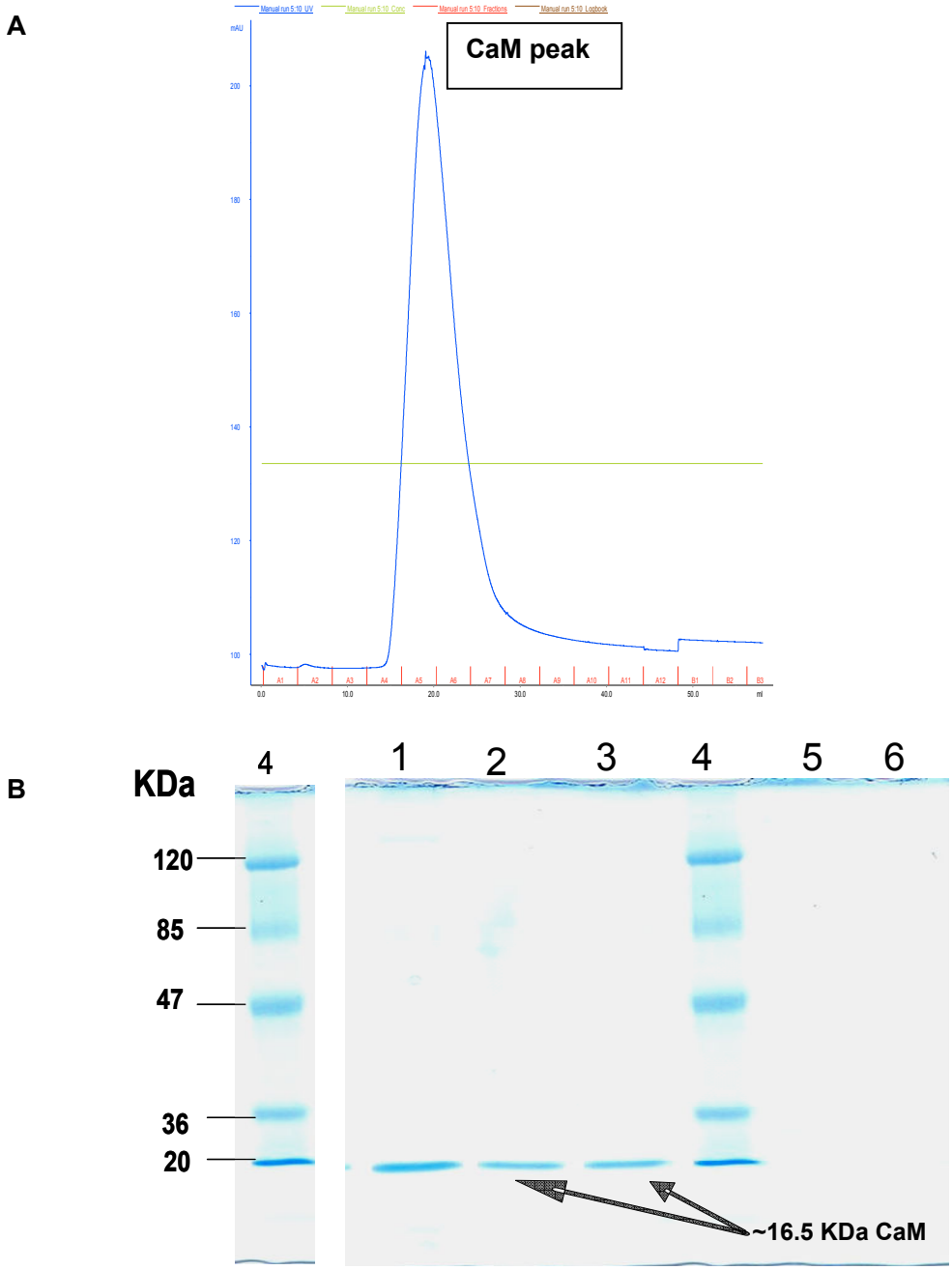

The results of the CaM purification from bovine brain extract on HiPrep 16/10 phenyl FF column, **A)** the chromatogram obtained during the separation of the sample on HiPrep 16/10 phenyl FF column. **B)** the identification of the CaM on 12% SDS-PAGE. Lane 4, shows the protein standard (Fermentas, PageRuler prestained protein standard SM0441, Germany), lanes 1-3, the fractions of the CaM peak. Lanes 5 and 6, the fractions collected during cleaning of the column. The separation and SDS-PAGE was performed as described in the Materials and Methods section. As shown, a single sharp peak chromatogram obtained and the protein approximately pure. These results reproduced at least 5 times.

Fig. 10: Analysis of MANT-nucleotide binding to the catalytic site of EF3 and EF3(F586A) using FRET

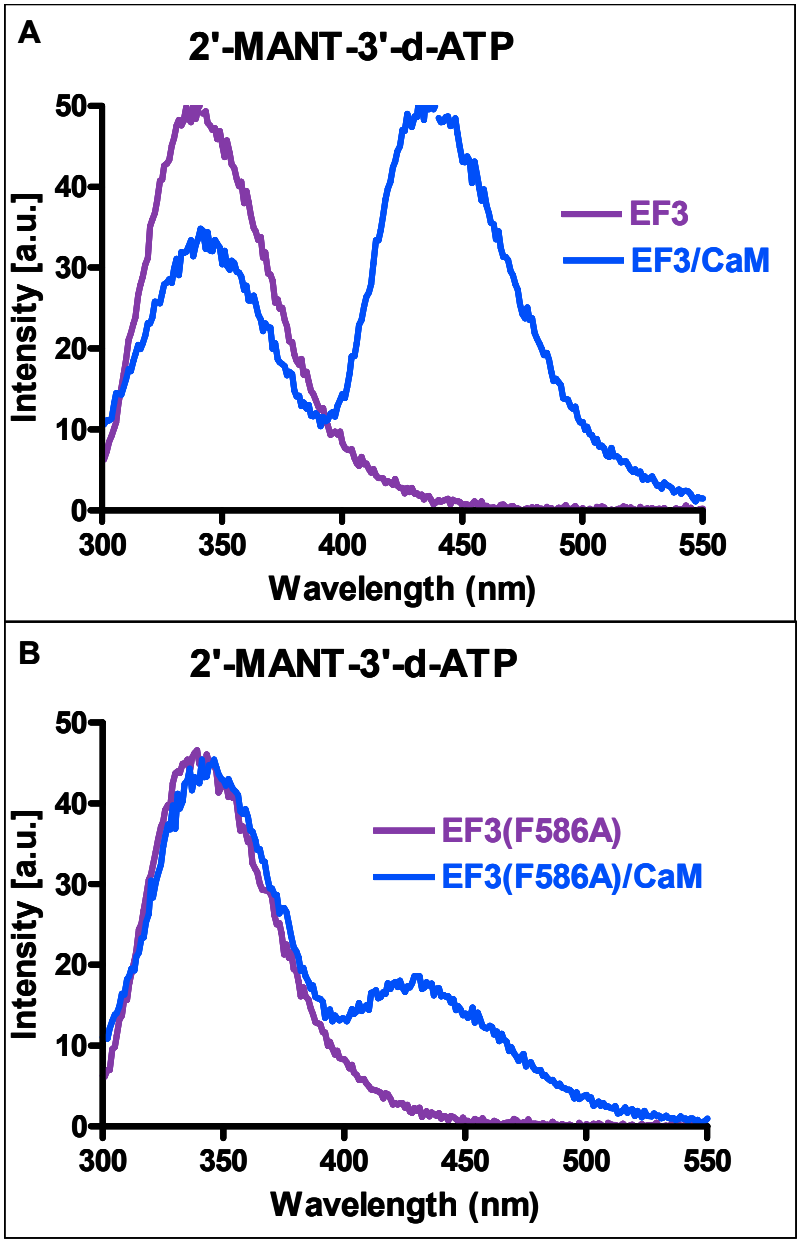

FRET experiments were performed as described under "Materials and Methods". The assay buffer consisted of 75 mM HEPES/NaOH, 100 μM $CaCl_2$, 100 mM KCl and 5 mM $MnCl_2$, pH 7.4. Nucleotide was added to the buffer to yield 300 nM final concentrations. EF3/EF3(F586A) (300 nM final concentration) was added followed by the addition of CaM (1 μM final concentration). Emission was scanned at an excitation wavelength of 280 nm after each addition. The buffer and the MANT-nucleotide basal fluorescence was subtracted from the fluorescence after addition of EF3/EF3(F586A) (*purple* line) and CaM (*blue* line). Shown are superimposed recordings of a representative experiment. Similar data were obtained in 5 independent experiments. a.u., arbitrary unit

4.4 Analysis of the interaction of MANT-nucleotides with EF3 in FRET experiments

At an excitation wavelength of 280 nm, tryptophan and tyrosine residues in proteins are excited, emitting light at 350 nm (16) which can then excite the (M)ANT group of nucleotides (17), provided sufficient proximity between donor and acceptor. Such energy transfer results in increased fluorescence of the MANT-group at 420-450 nm in mAC and CyaA, reflecting the fact that the MANT-group is in a hydrophobic environment (18-20). Previous studies with mAC showed that in the presence of Mn^{2+}, FRET signals were much larger than in the presence of Mg^{2+} (19). Preliminary studies with EF3 showed that the Mn^{2+}-preference also applies to the toxin (data not shown). Therefore, all subsequent FRET studies with EF3 were conducted in the presence of Mn^{2+} (see Materials and Methods).

In the absence of CaM, EF3 exhibits a strong emission peak at 350 nm when excited at 280 nm under steady-state conditions (Fig. 10**A**). Upon addition of the EF activator CaM, an additional prominent fluorescence peak with an emission maximum at 440 nm appeared with MANT-ATP (Fig. 10**A**), reflecting FRET from tryptophan and tyrosine residues to the MANT-group. In EF3(F586A), the endogenous tryptophan and tyrosine fluorescence was similar as in EF3, but the FRET signal (difference in fluorescence at an emission wavelength of 440 nm in the presence and absence of calmodulin) was reduced by 64% (Fig. 10**B**).

5. Summary and conclusion

We successfully purified the recombinant full length EF and EF3(F586A) from *E. coli* with a very good balance between the high purity and high yield of the purified protein together with retention of activity. These results were obtained based on the modifications that were applied to the EF purification protocol of Shen et al., 2002.

6. References

1. http://proteincrystallography.org/protein-purification/.
2. Asenjo JAaP, I. large-scale protein purification. In: Harris ELVaA,. protein purification applications :A Practcal Approach. *Second Edition*, *IRL, Oxford*. 1990.
3. Bristow AF. purification of protein for therapeutic use In: Harris ELVaA,. protein purification applications :A Practcal Approach. *Second Edition*, *IRL, Oxford*. 1990.
4. Doonan S, Cutler, P. General strategies. In:. Methods in Molecular Biology, Protein purification Protocols. *Second Edition*. Humana, Totowa, NJ. 2004.
5. Levison PR, Hopkins AK, Hathi P. Influence of column design on process-scale ion-exchange chromatography. *J Chromatogr A* 1999; **865**:3-12.
6. Lightfoot EN. The invention and development of process chromatography: Interaction of mass transfer and fluid mechanics. *American Laboratory* 1999; **31**:13-8.
7. Sheehan D. Fast Protein Liquid Chromatography. Fast Protein Liquid Chromatography.*First Edition* . 2003. 244-253
8. Leppla SH. Anthrax toxin edema factor: a bacterial adenylate cyclase that increases cyclic AMP concentrations of eukaryotic cells. *Proc Natl Acad Sci USA* 1982; **79**:3162-6.
9. Hoover DL, Friedlander AM, Rogers LC, Yoon IK, Warren RL, Cross AS. Anthrax edema toxin differentially regulates lipopolysaccharide-induced monocyte production of tumor necrosis factor alpha and interleukin-6 by increasing intracellular cyclic AMP. *Infect Immun* 1994; **62**:4432-9.
10. Ivins BE, Ezzell JW, Jr., Jemski J, Hedlund KW, Ristroph JD, Leppla SH. Immunization studies with attenuated strains of *Bacillus anthracis*. *Infect Immun* 1986; **52**:454-8.
11. Gopalakrishna R, Anderson WB. Ca^{2+}-induced hydrophobic site on calmodulin: application for purification of calmodulin by phenyl-Sepharose affinity chromatography. *Biochem Biophys Res Commun* 1982; **104**:830-6.

12. Norman JA. Neuroleptic drugs are nonstereospecific inhibitors of calmodulin-stimulated phosphodiesterase activity. *Ann N Y Acad Sci* 1980; **356**:415-6.

13. Tanaka T, Hidaka H. Hydrophobic regions function in calmodulin-enzyme(s) interactions. *J Biol Chem* 1980; **255**:11078-80.

14. Shen Y, Lee YS, Soelaiman S, Bergson P, Lu D, Chen A, Beckinghan K, Grabarek Z, Marksich M, Tang WJ. Physiological calcium concentrations regulate calmodulin binding and catalysis of adenylyl cyclase exotoxins. *EMBO J* 2002; **21**:6721-32.

15. Drum CL, Yan SZ, Sarac R, Shen YQ, Lu D, Soelaiman S, Grabarek Z, Bohm A, Tang WJ. An extended conformation of calmodulin induces interactions between the structural domains of adenylyl cyclase from *Bacillus anthracis* to promote catalysis. *J Biol Chem* 2000; **275**:36334-40.

16. Lakowizc R J., Principles of fluorescence spectroscopy. Principles of fluorescence spectroscopy. *Second Edition ,* Kluwer Academic. 1999

17. Hiratsuka T. New ribose-modified fluorescent analogs of adenine and guanine nucleotides available as substrates for various enzymes. *Biochim Biophys Acta* 1983; **742**:496-508.

18. Göttle M, Dove S, Steindel P, Shen Y, Tang WJ, Geduhn J, König B, Seifert R. Molecular analysis of the interaction of *Bordetella pertussis* adenylyl cyclase with fluorescent nucleotides. *Mol Pharmacol* 2007; **72**:526-35.

19. Mou TC, Gille A, Fancy DA, Seifert R, Sprang SR. Structural basis for the inhibition of mammalian membrane adenylyl cyclase by 2'(3')-O-(N-methylanthraniloyl)-guanosine 5 '-triphosphate. *J Biol Chem* 2005; **280**:7253-61.

20. Mou TC, Gille A, Suryanarayana S, Richter M, Seifert R, Sprang SR. Broad specificity of mammalian adenylyl cyclase for interaction with 2',3'-substituted purine- and pyrimidine nucleotide inhibitors. *Mol Pharmacol* 2006; **70**:878-86.

Chapter III

III. Molecular Analysis of the Interaction of Anthrax Adenylyl Cyclase Toxin, Edema Factor, with 2'(3')-*O*-(N- (methyl)anthraniloyl)-Substituted Purine and Pyrimidine Nucleotides

1. Abstract

Bacillus anthracis causes anthrax disease and exerts its deleterious effects by the release of three exotoxins, i.e. lethal factor, protective antigen and edema factor EF), a highly active calmodulin-dependent adenylyl cyclase (AC). However, conventional antibiotic treatment is ineffective against either toxemia or antibiotic- resistant strains. Thus, more effective drugs for anthrax treatment are needed. Previous studies from our laboratory showed that mammalian membranous AC (mAC) exhibits broad specificity for purine and pyrimidine nucleotides (Mou et al., *Mol Pharmacol* **70**: 878 (2006)). Here, we investigated structural requirements for EF inhibition by natural purine and pyrimidine nucleotides and nucleotides modified with N-methylanthraniloyl (MANT)- or anthraniloyl groups at the 2'(3')-*O*-ribosyl position. MANT-CTP was the most potent EF inhibitor (K_i, 100 nM) among 16 compounds studied. MANT-nucleotides inhibited EF competitively. Activation of EF by calmodulin resulted in effective fluorescence resonance energy transfer (FRET) from tryptophan and tyrosine residues located in the vicinity of the catalytic site to MANT-ATP, but FRET to MANT-CTP was only small. Mutagenesis studies revealed that F586 is crucial for FRET to MANT-ATP and MANT-CTP and that the mutations N583Q, K353A and K353R differentially alter the inhibitory potencies of MANT-ATP and MANT-CTP. Docking approaches relying on crystal structures of EF indicate similar binding modes of the MANT nucleotides with subtle differences in the region of the nucleobases. In conclusion, like mAC, EF accommodates both purine and pyrimidine nucleotides. The unique preference of EF for the base cytosine offers an excellent starting point for the development of potent and selective EF inhibitors.

2. Introduction

The spore-forming bacterium *Bacillus anthracis* exerts its deleterious effects by production of three major exotoxins, i.e. EF, protective antigen, and lethal factor (1). EF and lethal factor enter host cells *via* a complex with membrane-associated protective antigen, which acts as a pH-dependent protein transporter. Lethal factor, a specific zinc-metalloprotease, inactivates mitogen-activated protein kinase (2). EF possesses ~800 amino acid residues and an apparent molecular weight of ~89 kDa and is a CaM-dependent AC (3). After entering host cells, EF forms a complex with CaM, a mammalian regulatory protein that mediates many aspects of calcium-regulated signaling (4). The binding of CaM induces a major conformational change in the catalytic domain of EF (3). This rearrangement renders EF highly efficient at catalyzing the conversion of ATP into cAMP, disrupting intracellular signaling pathways through excessive activation of cAMP-dependent signaling pathways (5).

We resolved several crystal structures of nucleotide-EF-CaM complexes and characterized the amino acids that are important for binding of the substrate ATP and catalysis (3-5). Additionally, we showed that mAC and bacterial AC toxins are potently inhibited by MANT-substituted nucleoside 5'-triphosphates (6-9). MANT-nucleotides are fluorescent, and we exploited this property to suggest conformational changes associated with activation in purified catalytic subunits of mAC (7, 8) and the Bordetella pertussis AC toxin, CyaA (9). In addition, by combining crystallographic and molecular modeling approaches, we developed a three-site pharmacophore model for mAC and CyaA, with binding domains for the base, the MANT-group and the polyphosphate chain (8-11). Those studies revealed that the catalytic sites of mAC and CyaA exhibit substantial conformational flexibility, accommodating both purine and pyrimidine nucleotides. Despite this flexibility, the structure/activity relationships of MANT-nucleotides at mAC and CyaA are quite different, offering the opportunity to design potent and isoform-selective AC inhibitors.

In contrast to mAC (6-8, 10) and CyaA (9), a detailed analysis of MANT-nucleotide/EF interactions has not yet been presented. Therefore, in the present study, we systematically examined the interactions of natural purine and pyrimidine nucleotides and several (M)ANT-substituted analogs with EF in terms of catalysis,

fluorescence changes and molecular modeling.

3. Materials and Methods

3.1 Materials:

MANT-GTP, ANT-GTP, MANT-ATP and MANT-ADP were purchased from Jena Bioscience, Germany. PMEApp was supplied by Gilead Sciences, Foster City, CA. GTP, UTP and CTP were purchased from Roche, Mannheim, Germany. ITP, ampicillin, kanamycin, lysozyme enzyme, β- mercaptoethanol, Mes buffer (low moisture content) and dithiothreitol (for molecular biology) were purchased from Sigma-Aldrich, Steinheim, Germany. Tryptone and yeast were purchased from BD Biosciences (Franklin Lakes, NJ). [α–^{32}P]ATP (800 Ci/mmol) was purchased from PerkinElmer, Rodgau Jügesheim, Germany. Aluminum oxide 90 active, (neutral, activity 1, particle size 0.06 - 0.2 mm) was purchased from Biomedicals (Eschwege, Germany). Bovine serum albumin (fraction V, highest quality) was bought from Sigma-Aldrich, Steinheim, Germany. Imidazole (highest quality), $CaCl_2$, $MnCl_2$ tetrahydrate and $MgCl_2$ hexahydrate (highest quality) were purchased from Merck. For all experiments double-distilled water was used.

3.2 (M)ANT-nucleotides synthesis and analysis

3.2.1 (M)ANT-nucleotides synthesis: general procedure

MANT-CTP, MANT- CDP, MANT-UTP, MANT-UDP, MANT-ITP, MANT-IDP, ANT-ATP and ANT-ADP were synthesized according to Hiratsuka (1983) with modifications. The nucleotide (0.33 mmol, 1 eq) was propounded in a small two-neck round flask and dissolved in a minimum amount of water (3 ml). Under continuous stirring a crystalline preparation of (methyl)isatoic anhydride (0.5 mmol, 1.5 eq) was added. After heating to 38°C the pH-value was adjusted to 8.6 and maintained by titration of 1 N NaOH solution for 2 hours. The reaction mixture was extracted three times with chloroform (3 x 20 ml; only for MANT-nucleotides, not for ANT-nucleotides). The aqueous phase was dry- frozen. The received foam showed white to brown color and was applied to a Sephadex® LH-20 column (85 x 2 cm)

and subsequently eluted with double-distilled water. The desired product could be detected directly by its blue fluorescence in the collection tubes at λ_{ex} of 366 nm and by TLC. For further purification, reversed-phase preparative HPLC was used to separate (M)ANT-NTP from (M)ANT-NDP. After final dry-freezing white solid compounds (purity >99%) were obtained.

3.2.2 HPLC analysis of (M)ANT-nucleotides

The samples were filtered using a PTFE filter (Chromafil, O-20/15, organic, pore size 0.2 mm; Machery-Nagel, Düren, Germany). A 10 µl sample was analyzed using a HPLC model 1100 (Agilent Technologies, Waldbronn, Germany) fitted with a C18 analytical column (Phenomenex Luna, particle size 3 µm, 150 x 4.60 mm, Aschaffenburg, Germany) and DAD. Data were analyzed using a HPLC-3D ChemStation Rev. A.10.01 [1635]. Gradient elution was performed with 0.05 M ammonium acetate (solvent A) and acetonitrile (solvent B) at a constant flow rate of 1.0 ml/min. A gradient profile with the following proportions of solvent B was applied [t (min), % B]: [0, 5], [10, 5], [30, 45]. [40, 80]. The chromatograms were monitored at UV absorption at 220 and 254 nm. In addition, a fluorescence detector was used for the analysis of the fluorescent anthraniloylic compounds at λ_{ex} of 350 nm and λ_{em} of 450 nm.

3.2.3 LC/MS online coupling

All samples were filtered using a PTFE filter and injected into a HPLC model 1100 (Hewlett- Packard, Waldbronn, Germany). The compound to be analyzed was separated by a C18 column (Phenomenex luna, particle size 3 µm, 150 x 2 mm, Aschaffenburg, Germany). A binary eluent mixture consisting of water (10 mM ammonium acetate) (eluent A) and acetonitrile (eluent B) was pumped with a constant flow of 0.3 ml/min. The following gradient profile was used t [min], % B: [0, 5], [10, 5], [30, 45]. [40, 80]. The injected volume was 3 µl. Using a triple stage mass spectrometer (TSQ 7000, Thermoquest Finnigan, Toronto, Canada) the mass of the respective compound was determined.

3.2.4 Preparative HPLC

Compound mixtures were dissolved in water (concentration: 30-50 mg/ml) and filtered using a PTFE filter. Compounds were separated using a HPLC model 1100 (Agilent Technologies, Waldbronn, Germany) fitted with a C18 preparative column (phenomenex Luna, particle size) 10 µm 21.2 mm). Gradient elution was performed with 0.05 M ammonium acetate (solvent A) and acetonitrile (solvent B) at a constant flow rate of 21 ml/min. The chromatograms were monitored by UV absorption at 220 and 254 nm.

3.2.5 Synthesized nucleotides:

MANT-UTP (*N*-methyl-2'(3')-*O*-anthraniloyl-uridine-5'-triphospate) or [(2R,3S,4R,5R)-5-(2,4-dioxopyrimidin-1-yl)-4(3)-hydroxy-2-[[hydroxy-(hydroxy-phosphonooxyphosphoryl)oxyphosphoryl]oxymethyl]oxolan-3(4)-yl]2-methylaminobenzoate.

182 mg of introduced disodium salt of UTP yielded over all purification steps 32 mg (52 µmol, 15%) pure product. R_f = 0.21 (1-propanol:H_2O:NH_3 (32%) = 2:1:1). HPLC (analytic): R_t = 18.78 min, 19.15 min; k = 12.49, 12.75; LC/MS (ESI, H_2O/CH_3CN): m/z = 635.2 [$M+NH_4^+$] (R_t = 19.69 min, 19.88 min, 100 %), 652.2 [$M-H+2NH_4^+$] (R_t = 20.15 min, 100%); (-ESI, H_2O/CH_3CN): m/z = 616.2 [$M-H^-$] (R_t:19.53 min, 20.01 min, 100 %); HPLC (preparative), gradient (t [min], % B: [0, 14], [20, 14], [30, 80]): R_t = 6.07 min, 6.79 min; empirical formula: $_{17}H_{22}N_3O_{16}P_3$; MW = 617.29.

MANT-UDP (*N*-methyl-2'(3')-*O*-anthraniloyl-uridine-5'-diphospate) or [(2R,3S,4R,5R)-5-(2,4-dioxopyrimidin-1-yl)-4(3)-hydroxy-2-[(hydroxy-phosphonooxyphosphoryl)oxymethyl]oxolan-3(4)-yl]2-methylaminobenzoate.

182 mg of introduced disodium salt of UDP yielded over all purification steps 8 mg (15 µmol, 3.8%) pure product. R_f = 0.25 (1-propanol:H_2O:NH_3 (32 %) = 2:1:1). HPLC (analytic): R_t = 19.75 min, 19.93 min; k = 13.19, 13.32; LC/MS (ESI, H_2O/CH_3CN): m/z = 555.2 [$M + NH_4^+$] (R_t = 20.64 min, 20.94 min, 100%), 572.2 [$M-H + 2NH_4^+$] (R_t = 20.64 min, 20.94 min, 40 %); (-ESI, H_2O/CH_3CN): m/z = 536.2 [M-

H^-] (R_t: 20.50 min, 20.78 min, 100%); HPLC (preparative), gradient (t [min], % B: [0, 14], [20, 14], [30, 80]): R_t = 8.79 min, 9.49 min; empirical formula: $C_{17}H_{21}N_3O_{13}P_2$; MW = 537.31.

MANT-CTP (*N*-methyl-2'(3')-*O*-anthraniloyl-cytosine-5'-triphospate) or [(2R,3S,4R,5R)-5-(4-amino-2-oxopyrimidin-1-yl)-4(3)-hydroxy-2-[[hydroxy-(hydroxy-phosphonooxyphosphoryl)oxyphosphoryl]oxymethyl]oxolan-3(4)-yl]2-methylaminobenzoate.

200 mg of introduced trisodium salt of CTP yielded over all purification steps 30 mg (48 μmol, 14%) pure product. R_f = 0.24 (1- propanol:H_2O:NH_3 (32%) = 2:1:1). HPLC (analytic): R_t = 16.86 min, 17.60 min; k = 11.17, 11.70; LC/MS (ESI, H_2O/CH_3CN): m/z = 634.2 [$M+NH_4^+$] (R_t = 12.98 min, 16.98 min, 100%); (-ESI, H_2O/CH_3CN): m/z = 615.2[$M-H^-$] (R_t:13.75 min, 17.24 min, 100%); HPLC (preparative), gradient (t [min], % B: [0, 14], [20, 14], [30, 80]): R_t = 4.08 min, 4.61 min; empirical formula: $C_{17}H_{23}N_4O_{15}P_3$; MW = 616.30.

MANT-CDP (*N*-methyl-2'(3')-*O*-anthraniloyl-cytosine-5'-diphospate) or [(2R,3S,4R,5R)-5-(4-amino-2-oxopyrimidin-1-yl)-4(3)-hydroxy-2-[(hydroxy-phosphonooxyphosphoryl)oxymethyl]oxolan-3(4)-yl]2-methylaminobenzoate.

200 mg of introduced disodium salt of CDP yielded over all purification steps 2 mg (3.7 μmol, 1%) pure product. R_f = 0.28 (1-propanol:H_2O:NH_3 (32%) = 2:1:1). HPLC (analytic): R_t =18.38 min; k = 12.27; LC/MS (ESI, H_2O/CH_3CN): m/z = 554.2 [$M+NH_4^+$] (R_t = 18.55 min, 100%); (-ESI, H_2O/CH_3CN): m/z = 535.2 [$M-H^-$] (R_t:18.66 min, 100%); HPLC (preparative), gradient (t [min], % B: [0, 14], [20, 14], [30, 80]): R_t = 5.80 min; empirical formula: $C_{17}H_{22}N_4O_{12}P_2$; MW = 536.32.

MANT-ITP (*N*-methyl-2'(3')-*O*-anthraniloyl-inosine-5'-triphospate) or [(2R,3S,4R,5R)-5-(6-oxo-1H-purin-9-yl)-4(3)-hydroxy-2-[[hydroxy-(hydroxy-phosphonooxyphosphoryl)oxyphosphoryl]oxymethyl]oxolan-3(4)-yl]2-methylaminobenzoate.

189 mg of introduced trisodium salt of ITP yielded over all purification steps 39 mg (61 μmol, 18%) pure product. R_f = 0.31 (1-propanol:H_2O:NH_3 (32%) = 2:1:1).

HPLC (analytic): R_t = 19.74 min, 19.86 min; k = 12.65, 12.73; LC/MS (ESI, H_2O/CH_3CN): m/z = 676.2 [M-H+2NH_4^+] (R_t = 20.92 min, 100 %), 659.2 [M+NH_4^+] (R_t = 20.92 min, 80%); (-ESI, H_2O/CH_3CN): m/z = 640.2 [M-H^-] (R_t:20.92 min, 100%); HPLC (preparative), gradient (t [min], % B: [0, 14], [20, 14], [30, 80]): R_t = 8.03 min, 8.23 min; empirical formula: $C_{18}H_{22}N_5O_{15}P_3$; MW = 641.31.

MANT-IDP (*N*-methyl-2'(3')-*O*-anthraniloyl-inosine-5'-diphospate) or [(2R,3S,4R,5R)-5-(6-oxo-1H-purin-9-yl)-4(3)-hydroxy-2-[(hydroxy-phosphonooxyphosphoryl)oxymethyl]oxolan-3(4)-yl]2-methylaminobenzoate.

189 mg of introduced disodium salt of IDP yielded over all purification steps 15 mg (27 μmol, 7%) pure product. R_f = 0.35 (1-propanol:H_2O:NH_3 (32%) = 2:1:1). HPLC (analytic): R_t = 20.34 min, 20.58 min; k = 13.07, 13.23; LC/MS (ESI, H_2O/CH_3CN): m/z = 596.3 [M-H+2NH_4^+] (R_t = 21.38 min, 100%), 579.3 [M+NH_4^+] (R_t = 21.38 min, 70%); (-ESI, H_2O/CH_3CN): m/z = 560.2[M-H^-] (R_t: 21.39 min, 21.55 min, 100%); HPLC (preparative), gradient (t [min], % B: [0, 14], [20, 14], [30, 80]): R_t = 10.62 min, 11.36 min; empirical formula: $C_{18}H_{21}N_5O_{12}P_2$; MW = 561.33.

ANT-ATP (2'(3')-*O*-anthraniloyl-adenosine-5'-triphospate) or [(2R,3S,4R,5R)-5-(6-aminopurin-9-yl)-4(3)-hydroxy-2-[[hydroxy-(hydroxy-phosphonooxyphosphoryl)oxyphosphoryl]oxymethyl]oxolan-3(4)-yl]2-aminobenzoate.

189 mg introduced disodium salt of ATP yielded over all purification steps 59 mg (94 μmol, 26%) pure product. R_f = 0.24 (1-propanol:H_2O:NH_3 (32%) = 2:1:1). HPLC (analytic): R_t = 17.44 min; k = 10.07; LC/MS (ESI, H_2O/CH_3CN): m/z = 661.3 [M-H+2NH_4^+] (R_t = 18.12 min, 18.32 min, 100%), 644.2 [M+NH_4^+] (R_t = 18.12 min, 18.32 min, 80%); (-ESI, H_2O/CH_3CN): m/z = 625.2 [M-H^-] (R_t = 18.12 min, 18.33 min, 100%); HPLC (preparative), gradient (t [min], % B: [0, 11], [9, 11], [19, 80]): R_t = 7.07 min, 7.51 min; empirical formula: $C_{17}H_{21}N_6O_{14}P_3$; MW = 626.30.

ANT-ADP (2'(3')-*O*-anthraniloyl-adenosine-5'-diphospate) or [(2R,3S,4R,5R)-5-(6-aminopurin-9-yl)-4(3)-hydroxy-2-[(hydroxy-phosphonooxyphosphoryl)oxymethyl]oxolan-3(4)-yl]2-aminobenzoate.

200 mg introduced disodium salt of ADP yielded over all purification steps 8 mg (15 μmol, 4%) pure product. R_f = 0.27 (1-propanol:H_2O:NH_3 (32%) = 2:1:1). HPLC (analytic): R_t = 18.09 min; k = 10.73; LC/MS (ESI, H_2O/CH_3CN): m/z = 564.3 [M+NH_4^+] (R_t = 18.81 min, 19.04 min, 100%); (-ESI, H_2O/CH_3CN): m/z = 545.2 [M-H^-] (R_t = 18.81 min, 19.04 min, 100%); HPLC (preparative), gradient (t [min], % B: [0, 11], [9, 11], [19, 80]): R_t = 8.99 min; empirical formula: $C_{17}H_{20}N_6O_{11}P_2$; MW = 546.32.

3.3 Expression and purification of EF and EF3(F586A)

The plasmids pProExH6-EF and pProExH6-EF3F586A were prepared as described and amplified in *E. coli* BL21 (DE3)/pUBS520 cells (3-5, 12). The EF3 mutants (H577A, N583A, N583Q, N583H, K353A and K353R) were purified as described in references (3-5, 12).

Expression and purification of EF was essentially performed as described in reference (4) with minor modifications. Specifically, the imidazole concentration in the elution buffer for the HisTrap fast flow rate Ni column was increased to 200 mM. Moreover, imidazole (20 mM) was added into the sample, thus yielding the same imidazole concentration as in the second wash buffer of the Ni column. The following columns were used for EF protein purification; HisTrap fast flow rate affinity Ni column (5 ml) and resource Q (quaternary ammonium salt) strong anionic exchange column (6 ml) (GE Healthcare, Freiburg/Brsg., Germany). EF3(F586A) mutant was expressed and purified essentially as described in reference (4) with minor modifications. Specifically, the imidazole concentration in the elution buffer for the Ni column was 200 mM, and imidazole (20 mM) was included in the sample. The HisTrap fast flow rate affinity Ni column (5 ml) was used for immobilized matrix affinity chromatography and the HiPrep 16/10 SP XL column (GE Healthcare) was used in cation exchange chromatography. CaM was extracted and purified from bovine brain as described in reference (13). The HiPrep 16/10phenyl FF (high sub) column (GE Healthcare) was used in hydrophobic chromatography purification of CaM.

3.4 AC activity assay

For the determination of the potency of AC toxin inhibitors, assay tubes contained 10 µl of MANT-nucleotides at final concentrations from 10 nM to 100 µM as appropriate to obtain saturated inhibition curves and 20 µl of EF, EF3 or EF3(F586A) (10 pM final concentration) in 75 mM Tris/HCl, pH 7.4, containing 0.1% (m/v) bovine serum albumin. Tubes were preincubated for 2 min at 25°C, and reactions were initiated by the addition of 20 µL of reaction mixture consisting of the following components to yield the given final concentrations; 100 mM KCl, 100 µM free Ca^{2+}, 5 mM free Mn^{2+} or Mg^{2+}, 100 µM EGTA, 100 µM cAMP, 100 nM CaM. ATP was added as non-labeled substrate at a final concentration of 40 µM and as radioactive tracer [α–^{32}P]ATP (0.2 µCi/tube). For the determination of K_m and V_{max} values, 10 µM to 1 mM ATP/Mn^{2+} or ATP/Mg^{2+} were added, plus 5 mM of free Mn^{2+} or Mg^{2+}, respectively. Tubes were incubated for 10 min at 25°C, and reactions were stopped by the addition of 20 µL of 2.2 N HCl. Denaturated protein was sedimented by a 1-min centrifugation at 13,000 x g. [^{32}P]cAMP was separated from [α–^{32}P]ATP by transferring the samples to columns containing 1.4 g of neutral alumina. [^{32}P]cAMP was eluted by the addition of 4 ml of 0.1 M ammonium acetate solution, pH 7.0. Blank values were about 0.02% of the total amount of [α–^{32}P]ATP added; substrate turnover was < 3% of the total amount of [α–^{32}P]ATP added. Samples collected in scintillation vials were filled up with 10 ml of double-distilled water and Čerenkov radiation was measured in a PerkinElmer Tricarb 2800TR liquid scintillation counter. Free concentrations of divalent cations were calculated with WinMaxC (http://www.stanford.edu/~cpatton/maxc.html). V_{max} and K_m values reported in Table 1 and K_i values reported in Tables 2 and 3 were calculated using the Prism 4.02 software (Graphpad, San Diego, CA, USA).

For determination of the potency of AC toxin inhibitors at various EF3 mutants (H577A, N583A, N583Q, N583H, K353A and K353R), the experiments were essentially performed as described for EF and EF3 with some modifications. Specifically, the final enzyme concentrations were increased up to 2 nM in order to account for the lower catalytic activity of the mutants. Moreover, the reaction time was prolonged to 20 min at 30°C. For the determination of V_{max} and K_m, the ATP/Mn^{2+} concentration ranged from 100 µM to 4 mM. The higher substrate concentrations compared to EF were essential in order to obtain saturated enzyme

kinetics.

For determination of the potency of AC toxin inhibitors at EF3 in absence of both CaM and Ca^{2+}, experiments were performed as described for standard experiments with some modifications in order to increase assay sensitivity. Specifically, the final enzyme concentration was increased up to 5 nM, and the reaction was stopped after 30 min incubation at 30°C. Moreover, in competition experiments, the concentration of unlabeled ATP was decreased to 20 μM and [α–^{32}P]ATP was used at a high amount (1.0 μCi/tube). For the determination of V_{max} and K_m, the same modifications were performed, except that the ATP/Mn^{2+} concentration was varied.

For studying of the inhibition mechanism of the EF3 by MANT-nucleotides, enzyme saturation experiments were performed in the presence of various inhibitor concentrations as shown in Fig. 1. Assay tubes contained MANT-nucleotides at final concentrations from 0.5 μM to 20 μM as appropriate according to the potency of the inhibitor. For the basal saturation curve 5 µl of double-distilled water was added instead of the inhibitor. Next, 5 µl of 50 µM to 600 µM ATP/Mn^{2+}, plus 20 µl of 10 pM EF3 in 75 mM Tris/HCl, pH 7.4, containing 0.1% (m/v) bovine serum albumin were added. Tubes were preincubated for 2 min at 25°C, and reactions were initiated by the addition of 20 µL of reaction mixture consisting of the following components to yield the given final concentrations; 100 mM KCl, 100 µM free Ca^{2+}, 5 mM free Mn^{2+}, 100 µM EGTA, 100 µM cAMP, 100 nM CaM, and [α–^{32}P]ATP (0.2 µCi/tube).

3.5 Fluorescence resonance energy transfer (FRET) experiments for monitoring inhibitor binding to EF

Fluorescence experiments were performed using quartz UV ultra-microcuvettes from Hellma (Müllheim, Germany, type 105.251- QS, light path length 3 x 3 mm, center 15 mm, total volume 70 μl and type 105.250- QS, light path length 10 x 2 mm, center 15 mm, total volume 150 μl) in a thermostated multicell holder at 25°C in a Varian Cary Eclipse fluorescence spectrometer (Varian, Darmstadt, Germany). In case of 150 μl cuvettes, 140 μl of buffer consisting of 100 mM KCl, 100 μM $CaCl_2$, 10 mM $MnCl_2$ and 25 mM HEPES/NaOH, pH 7.4, was added into the cuvette. Five μl of 10 μM full-length EF

(final concentration 300 nM), 5 µl of 10 µM CaM (final concentration 300 nM) and MANT-ATP or MANT-CTP (300 nM each) were added. In case of experiments with 70 µl cuvettes, volumes were adjusted stoichiometrically. The results obtained with 70 µl- and 150 µl-cuvettes were identical, with the 70 µl-cuvettes offering an opportunity to save EF/EF3 mutant protein.

Steady-state fluorescence emission spectra of nucleotides were recorded at low speed in the scan mode from λ_{em} 300 nm to 550 nm with λ_{ex} 280 nm. Fluorescence recordings were analyzed with the spectrum package of the Varian Cary Eclipse software version 1.1. Baseline fluorescence (buffer alone) and the baseline-corrected nucleotide-dependent emission of each concentration of the ligand (buffer + nucleotide) were subtracted from the spectra shown in Fig. 2. In the competition experiments shown in Fig. 3, MANT-nucleotides were displaced from the EF catalytic site using PMEApp. In some experiments, we also directly excited MANT-nucleotides at λ_{ex} 350 nm and monitored fluorescence emission from 400-500 nm.

3.6 Modeling of the nucleotide binding mode to EF-CaM

Docking studies were performed with the molecular modeling package SYBYL 7.3 (Tripos International, St. Louis, MO) on a Silicon Graphics Octane workstation. An initial computer model was generated from the crystal structure of EF-CaM in complex with 2'-deoxy-3'ANT-ATP, PDB 1lvc, chain C (4). Yb^{2+} was replaced by Mg^{2+}. Water molecules were added from the crystal structure of EF-CaM in complex with 3'-deoxy-ATP, PDB 1k90 (3). Hydrogens were added and AMBER_FF99 charges assigned to the protein and the water. 2'-Deoxy-3'ANT-ATP was provided with Gasteiger-Hueckel-charges. The model was then pre-optimized with the AMBER_FF99 force field (14) (ligand and Mg^{2+} fixed, distant dependent dielectric constant ε = 4, 25 cycles steepest descent, followed by Powell conjugate gradient, end gradient of 0.1 kcal $mole^{-1}$ $Å^{-1}$) were performed.

Initial docking positions of 2'-MANT-CTP, 3'-MANT-CTP and 3'-MANT-ATP were based on the localization and conformation of 2'-deoxy-3'-ANT-ATP in this model, allowing the modification of rotatable bonds. Each complex was refined in a stepwise approach. Firstly, ~25 minimization cycles with fixed ligand

(AMBER_FF99 force field, steepest descent, ε = 4), secondly, minimization of the ligand and the surrounding protein residues (distance up to 6 Å) with the Tripos force field (15), (Powell conjugate gradient, ε = 1, end gradient of 0.05 kcal $mole^{-1}$ $Å^{-1}$), and, thirdly, final refinement with fixed ligand (AMBER_FF99 force field, Powell conjugate gradient, ε = 4, end gradient of 0.01 kcal $mole^{-1}$ $Å^{-1}$). The RMS deviation between the three minimized models amounts to 0.2 – 0.25 Å if all atoms of the protein are considered.

4. Results

4.1 Kinetic analysis of the catalytic activities of EF, EF3 and various EF3 mutants

In Table 1, the V_{max} and K_m values of EF, EF3 and various EF3 mutants in the presence of Ca^{2+}/CaM and Mn^{2+} are summarized. The difference between EF and EF3 is that EF3 does not contain the binding domain for protective antigen (3, 5). The V_{max} and K_m values were very similar for EF and EF3. In EF3(F586A), V_{max} decreased by about 50% compared to EF3 with little change in K_m. The H577A mutation dramatically reduced V_{max} and moderately decreased K_m. Substitution of N583 with other hydrogen-bond-forming residues such as Q583 or H583 significantly reduced V_{max} together with a 10-50-fold increase in K_m. Mutation of K353 into A353 reduced V_{max} 55-fold and increased K_m 10-fold. EF(K353R) exhibited about 5-fold reduced V_{max} and similar K_m compared to the EF3. There are some differences in the kinetic parameters of EF3 and EF3 mutants in the presence of Mg^{2+} (3) and Mn^{2+} (Table 1), supporting the view that these divalent cations interact differentially with ACs (6-9). Since the FRET signals presented below were much smaller in the presence of Mg^{2+} than Mn^{2+} (data not shown), we decided to conduct all enzymatic studies in the presence of Mn^{2+} as well.

We also determined the kinetic parameters of EF3 in the presence of Mn^{2+} but in the absence of Ca^{2+}/CaM. By removing both CaM and Ca^{2+} from the reaction mixture, V_{max} was reduced about 2000-fold, but there was no effect on K_m.

Table 1: K_m and V_{max} values of EF, EF3 and various EF3 mutants

Toxin	Ca^{2+}/CaM	V_{max} (s^{-1})	K_m (µM)
EF	**+**	**232 ± 34**	**84.5 ± 8.3**
EF3	**+**	**223 ± 12**	**82.6 ± 8.2**
EF3(F586A)	**+**	**128 ± 5.0**	**92.0 ± 14.7**
EF3(H577A)	**+**	**0.013 ± 0.003**	**34.5 ± 9.7**
EF3(N583A)	**+**	**15.4 ± 0.13**	**224 ± 7.3**
EF3(N583Q)	**+**	**18.4 ± 0.08**	**855 ± 39**
EF3(N583H)	**+**	**59.7 ± 10.4**	**3,890 ± 1,220**
EF3(K353A)	**+**	**3.93 ± 0.02**	**804 ± 137**
EF3(K353R)	**+**	**32.3 ± 0.06**	**75.4 ± 1.35**
EF3	**-**	**0.11 ± 0.007**	**60.0 ± 0.89**

AC toxin activities were determined as described under “Materials and Methods”. K_m and V_{max} values were obtained by non-linear regression analysis of substrate-saturation experiments and are the means ± SD of at least 3 independent experiments performed in triplicates. For the determination of the V_{max} and K_m of EF, EF3 and EF3(F586A), reaction mixtures contained 100 µM free Ca^{2+}, 5 mM free Mn^{2+}, 100 µM EGTA, 0.2 µCi/tube [α–^{32}P]ATP, 100 µM cAMP, 100 nM calmodulin and 10 pM enzyme in 75 mM Tris/HCl, pH 7.4. In case of the other EF3 mutants, reaction mixtures contained 0.4 µCi [α–^{32}P]ATP per tube and 2 nM enzyme. For determination of V_{max} and K_m without CaM and Ca^{2+}, the enzyme concentration was 5 nM. The unlabeled ATP/Mn^{2+} concentrations ranged from 100 nM to 4 mM as appropriate to obtain saturated curves.

4.2 Inhibition of the catalytic activity of EF, EF3 and various EF3 mutants by (M)ANT-nucleotides

Table 2 summarizes the K_i values of MANT-ATP and MANT- CTP at EF, EF3 and EF3 mutants in the presence of Mn^{2+}. At EF and EF3, MANT- CTP was a 5-10-fold more potent inhibitor than MANT-ATP. The F586A mutation reduced the inhibitory potencies of MANT-ATP and MANT-CTP by 5-6-fold, whereas the H577A mutation did not decrease inhibitor potency. The N583A mutation decreased nucleotide-potency by 90-100-fold. The N583Q substitution reduced the potency of MANT-ATP by 70-fold and the potency of MANT-CTP by 2,500-fold. For the N583H mutant, a 200-300-fold decrease in potency of MANT-ATP and MANT-CTP was observed. The K353A substitution reduced the potency of MANT-ATP by less than 20-fold, whereas the potency of MANT-CTP was reduced by more than 500-fold. The K_i value of MANT-ATP at EF3(K353R) increased just 3-fold, while the K_i value of MANT-CTP increased by 65-fold. The omission of Ca^{2+}/CaM had only little effect on the K_i values of both MANT-ATP and MANT-CTP at EF3.

Table 2: Inhibitory potencies of MANT-ATP and MANT-CTP at EF, EF3 and EF3 mutants in the presence of Mn^{2+}

Toxin	Ca^{2+}/CaM	MANT-ATP K_i (µM)	MANT-ATP rel. pot.	MANT-CTP K_i (µM)	MANT-CTP rel. pot.
EF	+	0.58 ± 0.13	169	0.11 ± 0.04	91
EF3	+	0.98 ± 0.08	100	0.10 ± 0.008	100
E3(F586A)	+	4.54 ± 1.15	22	0.61 ± 0.11	16
EF3(H577A)	+	0.52 ± 0.05	189	0.11 ± 0.017	91
EF3(N583A)	+	91.7 ± 2.5	1.1	10.4 ± 0.02	1.0
EF3(N583Q)	+	67.4 ± 4.8	1.5	248 ± 23	0.04
EF3(N583H)	+	308 ± 89	0.3	22 ± 5.4	0.5
EF3(K353A)	+	17.4 ± 4.0	5.6	54.8 ± 0.83	0.2
EF3(K353R)	+	3.27 ± 0.08	30	6.53 ± 0.26	1.5
EF3	-	1.07 ± 0.04	92	0.16	63

Inhibitory potencies of MANT-ATP and MANT-CTP at EF, EF3 and various EF3 mutants were determined as described under "Materials and Methods". K_i-values are given in µM and are the means ± SD of 3 experiments performed in triplicates. The relative potencies (rel. pot.) of MANT-ATP and MANT-CTP are given, too, EF3 being the reference. For determination of the inhibitory potencies of MANT-ATP and MANT-CTP at EF, EF3 and EF3(F586A), reaction mixtures contained100 µM free Ca^{2+}, 5 mM free Mn^{2+}, 100 µM EGTA, 40 µM ATP, 0.2 µCi/tube [α-^{32}P]ATP, 100 µM cAMP, 100 nM CaM and 10 pM enzyme in 75 mM Tris/HCl, pH 7.4. For other EF3 mutants, reaction mixtures contained 0.4 µCi [α-^{32}P]ATP per tube. The enzyme concentration was 2 nM. For the determination of K_i-values of MANT-ATP and MANT-CTP without CaM and Ca^{2+}, the ATP/Mn^{2+} concentration was 20 µM and the enzyme concentration was 5 nM. Nucleotides were added at different concentrations as appropriate to obtain saturated concentration-response curves. Inhibition curves were analyzed by non-linear regression using the Prism 4.02 software.

Fig. 1 shows the double-reciprocal analysis of EF3 inhibition kinetics by MANT-ATP and MANT-CTP according to Lineweaver-Burk. The linear regression lines intersected at the y-axis, i.e. V_{max} remained constant, whereas K_m increased with increasing inhibitor concentration.

Table 3 summarizes the K_i values of various natural purine and pyrimidine nucleotides and various (M)ANT-NDPs and -NTPs at EF in the presence of Mn^{2+} and Mg^{2+}. In general, inhibitor potencies were higher with Mn^{2+} than with Mg^{2+}, but the impact of the cation varied with the nucleotide studied. For example, ANT-ATP, MANT-CTP and MANT-CDP were about 10-fold more potent in the presence of Mn^{2+} than in the presence of Mg^{2+}, whereas for MANT-GTP, the affinity difference was less than 2-fold. A differential impact of Mg^{2+} and Mn^{2+} on MANT-nucleotide-affinity was also noted for mAC and CyaA (6-9).

All natural nucleoside 5'-triphosphates studied inhibited the catalytic activity of EF with CTP being the most potent inhibitor. Substitution of the 2'(3')-*O*-ribosyl group with a (M)ANT group substantially increased inhibitor potency. For example, in the presence of Mn^{2+}, MANT-CTP showed about 60-fold higher potency at EF than the unmodified nucleotide. The potency-increasing effect of the (M)ANT-group depended on the specific nucleotide examined. For example, in the presence of Mn^{2+}, the potency of MANT-GTP was just 3.5-fold higher than the potency of GTP. (M)ANT- NDPs were less potent EF inhibitors than the corresponding (M)ANT-NTPs. In the presence of Mn^{2+}, MANT-ATP and ANT-ATP were similarly potent EF inhibitors, whereas in the presence of Mg^{2+}, MANT-ATP was about 4-fold more potent than ANT-ATP. MANT-GTP was up to 2.5-fold more potent than ANT-GTP.

Table 3: Inhibitory potencies of NTPs and (M)ANT-nucleotides at EF in the presence of Mn^{2+} and Mg^{2+}

Nucleotide	K_i (µM)	
	Mn^{2+}	Mg^{2+}
GTP	9.2 ± 0.79	73.6 ± 6.02
ITP	45.4 ± 3.60	233 ± 15.8
UTP	63.9 ± 9.21	138 ± 2.53
CTP	5.10 ± 0.38	45.2 ± 9.18
MANT-ATP	0.58 ± 0.09	1.36 ± 0.57
MANT-ADP	3.26 ± 0.50	34.7 ± 3.34
ANT-ATP	0.44 ± 0.09	5.15 ± 2.12
ANT-ADP	3.85 ± 1.25	57.9 ± 25.1
MANT-GTP	2.49 ± 0.08	4.70 ± 0.32
ANT-GTP	4.10 ± 1.09	13.0 ± 1.86
MANT-ITP	4.06 ± 0.06	10.6 ± 3.29
MANT-IDP	11.0 ± 1.89	48.5 ± 3.16
MANT-UTP	3.67 ± 0.08	32.2 ± 0.82
MANT-UDP	38.7 ± 0.48	107 ± 20.6
MANT-CTP	0.10 ± 0.01	1.26 ± 0.09
MANT-CDP	1.30 ± 0.12	13.8 ± 0.06

Inhibitory potencies of various purine and pyrimidine nucleotides at EF were determined as described under “Materials and Methods”. K_i values are given in µM and are the means ± SEM of 3-4 independent experiments performed in triplicates. The K_m value of EF for ATP in the presence of Mg^{2+} was 120 ± 6.5 µM. Reaction mixtures contained 5 mM $MnCl_2$ or 5 mM $MgCl_2$, 100 mM KCl, 100 µM $CaCl_2$, 40 µM ATP, [α–^{32}P]ATP (0.2-0.4 µCi/tube), 100 µM cAMP and 100 nM CaM. Nucleotides were added at different concentrations as appropriate to construct saturated concentration-response curves. Inhibition curves were analyzed by non-linear regression using the Prism 4.02 software.

Fig. 1: Lineweaver-Burk analysis of the inhibition of EF3 AC activity by MANT-ATP and MANT-CTP.

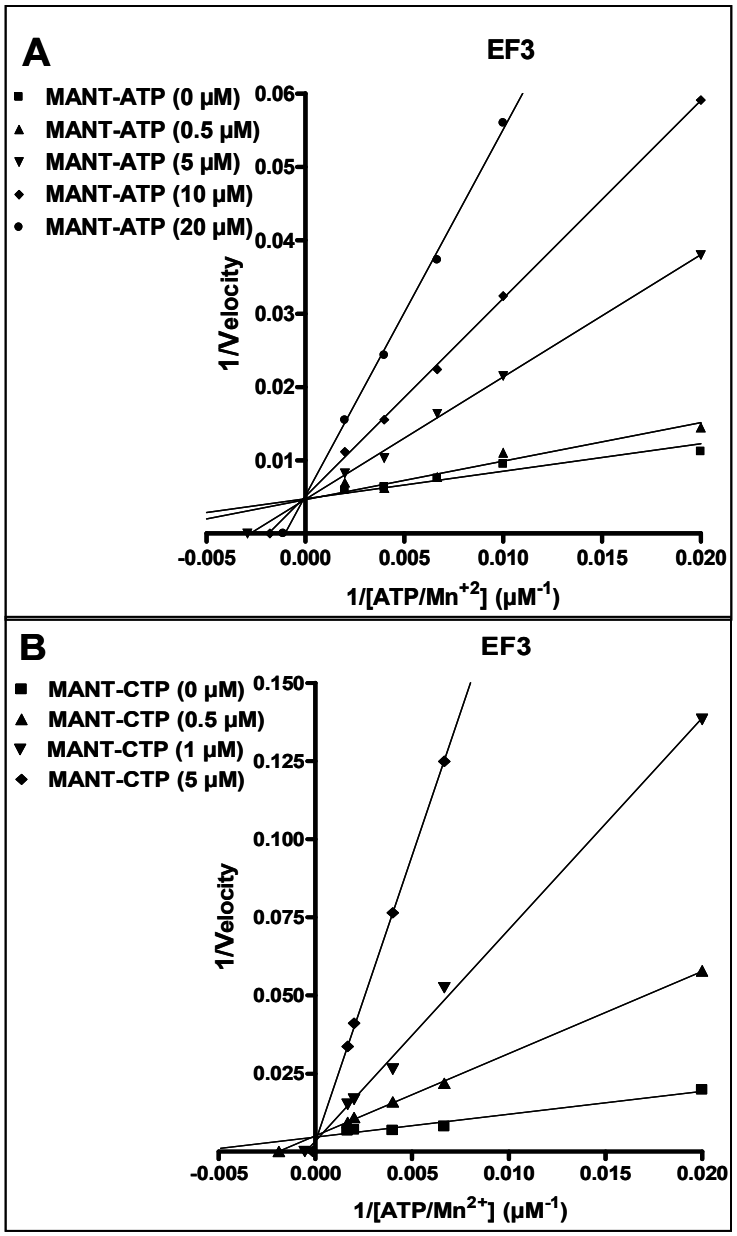

AC activities were determined as described under "Materials and Methods" with the indicated concentrations of MANT-ATP (0 µM, 0.5 µM, 5 µM, 10 µM and 20 µM) (**A**) and MANT-CTP (0 µM, 0.5 µM, 1 µM and 5 µM) (**B**). Reaction mixtures contained 10 pM EF3, 100 mM KCl, 100 µM free Ca^{2+}, 5 mM free Mn^{2+}, 100 µM EGTA, 100 µM cAMP, 100 nM calmodulin, 0.2 µCi/tube [α-^{32}P]ATP and unlabeled ATP/Mn^{2+} concentrations indicated in the graph. Data were plotted reciprocally and analyzed by linear regression according to Lineweaver- Burk. Shown are the results of a representative experiment performed in triplicates. Similar results were obtained in two independent experiments.

4.3 Analysis of the interaction of MANT-nucleotides with EF3 in FRET experiments

At an excitation wavelength of 280 nm, tryptophan and tyrosine residues in proteins are excited, emitting light at 350 nm (16) which can then excite the (M)ANT group of nucleotides (17), provided sufficient proximity between donor and acceptor. Such energy transfer results in increased fluorescence of the MANT-group at 420-450 nm in mAC and CyaA, reflecting the fact that the MANT-group is in a hydrophobic environment (7-9). Previous studies with mAC showed that in the presence of Mn^{2+}, FRET signals were much larger than in the presence of Mg^{2+} (7). Preliminary studies with EF3 showed that the Mn^{2+}-preference also applies to the toxin (data not shown). Therefore, all subsequent FRET studies with EF3 were conducted in the presence of Mn^{2+} (see Materials and Methods).

In the absence of CaM, EF3 exhibits a strong emission peak at 350 nm when excited at 280 nm under steady-state conditions (Figs. 2**A** and 2**C**). Upon addition of the EF activator CaM, an additional prominent fluorescence peak with an emission maximum at 440 nm appeared with MANT-ATP (Fig. 2**A**), reflecting FRET from tryptophan and tyrosine residues to the MANT-group. In EF(F586A), the endogenous tryptophan and tyrosine fluorescence was similar as in EF3, but the FRET signal (difference in fluorescence at an emission wavelength of 440 nm in the presence and absence of calmodulin) was reduced by 55% (Fig. 2**B**). With MANT-CTP, only a small FRET signal was apparent with EF3 upon addition of CaM (Fig. 2**C**). Even an increase of the final CaM concentration to 3 μM, yielding a 10-fold molar excess of CaM relative to EF3, did not increase FRET with MANT-CTP (data not shown). The small FRET signal with MANT-CTP was reduced by 43% in EF(F586A) (Fig. 2**D**). Analysis of the EF mutants H577A, N583A, N583Q, N583H and K353A with MANT- ATP and MANT-CTP revealed no FRET at all (data not shown). With CaM and MANT-nucleotides alone, i.e. in the absence of EF3, no FRET signal was observed (data not shown).

Fig. 2: Analysis of MANT-nucleotide binding to the catalytic site of EF3 and EF3(F586A) using FRET

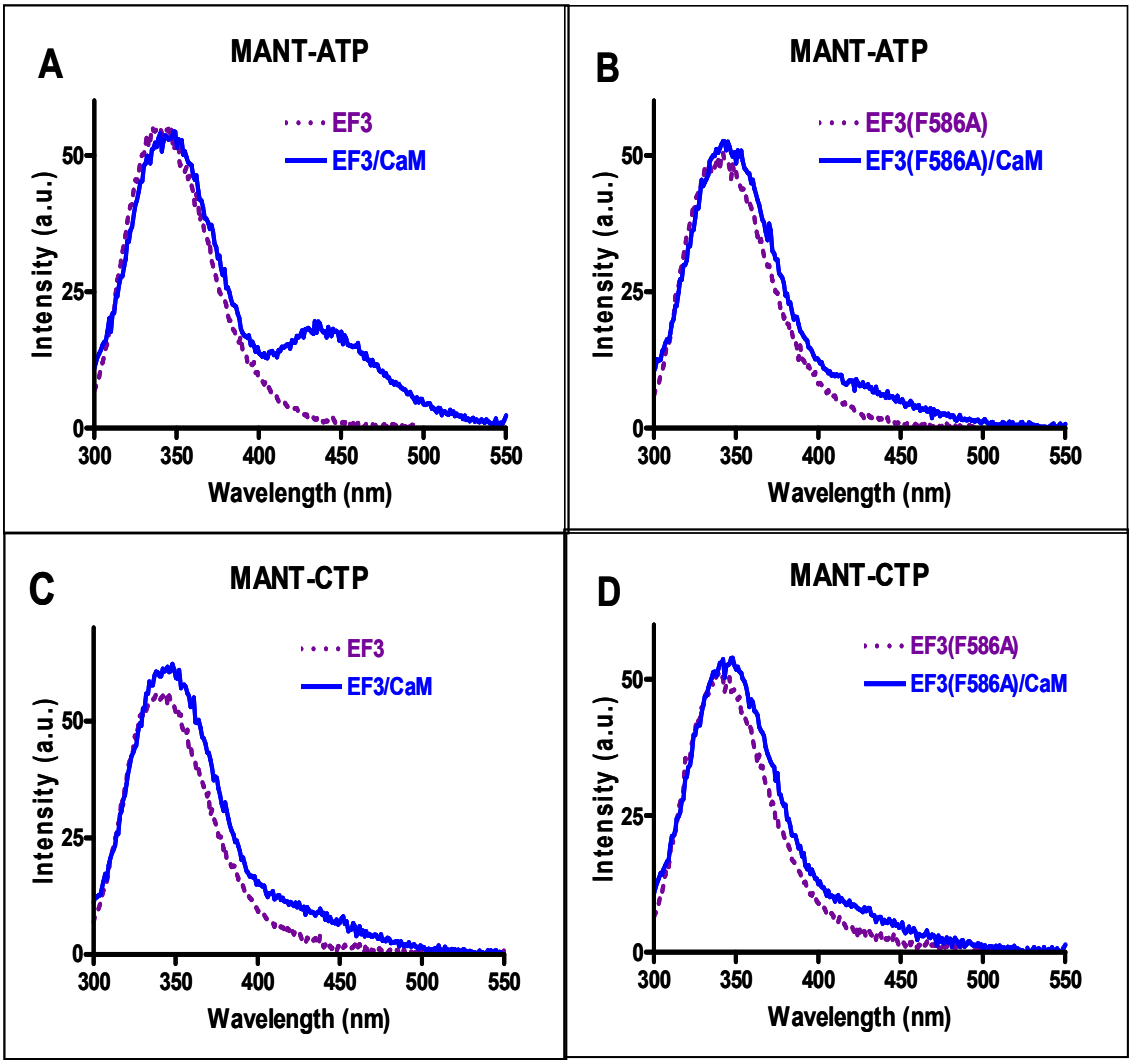

FRET experiments were performed as described under "Materials and Methods". The assay buffer consisted of 75 mM HEPES/NaOH, 100 μM $CaCl_2$, 100 mM KCl and 5 mM $MnCl_2$, pH 7.4. Nucleotides were added to the buffer to yield 300 nM final concentrations. EF3/EF3(F586A) (300 nM final concentration) was added followed by the addition of CaM (1 μM final concentration). Emission was scanned at an excitation wavelength of 280 nm after each addition. The buffer and the MANT-nucleotide basal fluorescence was subtracted from the fluorescence after addition of EF3/EF3(F586A) (*dotted purple* line) and CaM (*solid blue* line). Shown are superimposed recordings of a representative experiment. Similar data were obtained in 5 independent experiments. a.u., arbitrary unit.

In FRET experiments, the appearance of the new fluorescence peak at λ_{em} 440 nm would have been expected to be accompanied by a decrease in fluorescence at λ_{em} 350 nm as was the case for mAC (7, 8) and CyaA (9). Rather, a small increase in EF3 fluorescence upon CaM addition was observed (Fig. 2). An explanation for these findings could be that the endogenous tyrosine and tryptophan fluorescence of EF3 is quenched by surrounding polar amino acids such as aspartate, glutamate and histidine (16). Upon addition of CaM, a large conformational change occurs in EF3 (3, 4), abrogating the quenching effects of polar amino acids and, thereby, masking the expected decrease in fluorescence at λ_{em} 350 nm.

Control experiments with dimethyl sulfoxide ranging from 0-100% (v/v) (17) revealed that MANT-ATP and MANT-CTP possess similar relative increases in fluorescence upon exposure to a hydrophobic environment (λ_{ex} 350 nm; λ_{em} 400-500 nm) (data not shown). Thus, differences in biophysical properties of nucleotides do not account for the different FRET responses observed with MANT-ATP and MANT-CTP upon interaction with EF. We also studied the interaction of EF with MANT-nucleotides by exciting nucleotides directly at λ_{em} 350 nm. As was true in the FRET experiments (Fig. 2), the response observed with MANT-ATP at λ_{em} 450 nm was greater than with MANT-CTP (data not shown).

Fig. 3 shows the kinetics of FRET experiments with MANT-ATP and MANT-CTP at a fixed emission wavelength of 440 nm. Sequential addition of EF3 and CaM resulted only in small fluorescence increases, reflecting the far end of the tryptophan/tyrosine emission spectrum (see Fig. 2). Addition of MANT-nucleotides to cuvettes instantaneously resulted in substantial fluorescence increases, reflecting FRET. Addition of the high-affinity EF inhibitor and non-fluorescent nucleotide analog PMEApp (1 μM) (18) to cuvettes reduced the fluorescence signals with both MANT-nucleotides (300 nM each), but the inhibitory effect of PMEApp was more pronounced and more rapid in onset with MANT-ATP than with MANT-CTP.

Fig. 3: Kinetic analysis of the interaction of EF3 with MANT-nucleotides and CaM in FRET experiments

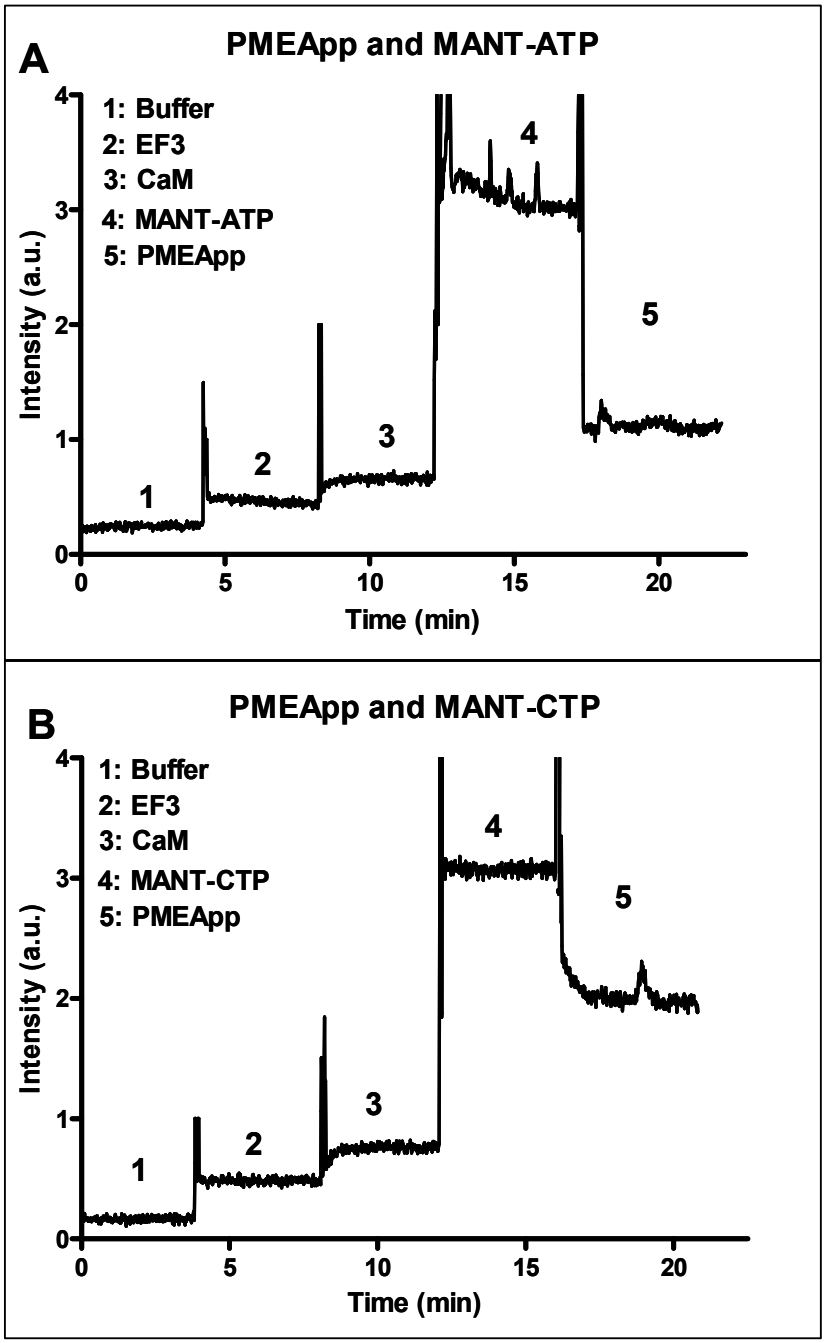

Kinetic experiments were performed as described in "Materials and Methods". The excitation wavelength was 280 nm and emission was detected at 430 nm over time. Successively, buffer (**1**), 300 nM EF3 (**2**), 1 µM CaM (**3**), nucleotide (**A**: MANT-ATP, **B**: MANT-CTP, 300 nM each) (**4**) and PMEApp (1 µM) (**5**) were added. A recording of a representative experiment is shown. Similar data were obtained in 4 independent experiments. a.u., arbitrary unit.

4.4 Modeling of the binding modes of MANT-nucleotides to EF-CaM.

The crystal structure of EF in complex with CaM and 2'-deoxy-3'-ANT-ATP (PDB 1lvc, (4)) served as basis for the docking of MANT-CTP and MANT-ATP. Fig. 4**A** shows that the nucleotide binding site of EF is a spacious cavity located at the interface of two structural domains, C_A (D294 – N349, A490 – K622) and C_B (V350 – T489). Three switches, A (Q507 – L549), B (G578 – N591), and C (R630 – T659), which strongly change their conformation and position on the transition from EF alone to EF-CaM (3, 4) cover the catalytic site in the EF-CaM state. A metal cation (Yb^{2+} in the template, replaced by Mg^{2+} in the models) is involved in ionic interactions with D491, D493 and the α-phosphate of the nucleotides. The MANT group is aligned in parallel with the phenyl ring of F586. Thus, hydrophobic interactions account for the generally higher potency of the ANT- and MANT-derivatives compared to their natural parent nucleotides (Table 3).

The docking approaches were performed to suggest possible reasons why MANT-CTP inhibits EF-CaM more potently than MANT-ATP. Fig. 4**B** and 4**D** compare the putative binding mode of 3'-MANT-CTP and 3'-MANT-ATP in more detail. The common structures of both molecules interact with EF-CaM in the same manner. In the minimized models, the ribosyl rings adopt a 3'-exo conformation like the ribosyl moiety of 3'-MANT-ATP in complex with mAC (8). The triphosphate moieties fit into a deep polar pocket forming ionic interactions with the lysines 346, 353 and 372 as well as an H bond with S354 (γ-phosphate). These interactions account for the higher inhibitory potencies of the triphosphates compared to the diphosphate analogs in Table 3. The ring oxygens of the ribosyl moieties are hydrogen-bonded to the amide NH_2 of N583. The 2'-OH groups approach the side chain of L348. Additionally to the parallel fit to F586, the 3'-MANT Substituents interact via their amino function with H351.

The nucleobases show both shared and different interactions. Most striking is the flat alignment with the side chain of N583. In the case of 3'-MANT-CTP, such type of interaction is more favorable since the oxygen in 2'-position of the base may align with the positive pole of the amide dipole. However, this difference

cannot be the only reason for the higher potency compared to MANT-ATP, because also on the N583A mutant, MANT-CTP is more potent than its ATP analog (Table 3).

Considering the farther environment of the cytosine oxygen, additional reasons can be suggested. In the minimized model, it is in a 3.3 Å distance from the guanidino group of R329. Moreover, a water molecule can be placed in an ideal position into the EF-MANT-CTP model where it forms three H bonds, bridging the cytosine oxygen with the side chains of R329 and E580. The NH_2 groups of the cytosine and adenine moieties interact similarly with EF-CaM via H bonds to backbone oxygens (3'-MANT- CTP to G578 and/or T579, 3'MANT-ATP to T548 and T579). The signifinace of these interactions is confirmed by the lower potency of MANT-UTP and MANT-GTP (Table 3). Interestingly, the N583H mutant disproportionately reduces the potency of MANT- ATP, whereas on the N583Q species, MANT-CTP is even less potent than its ATP analog. In the former case, an alignment of the heterocycles should be still possible. However, the larger glutamine side chain in N583Q restricts the binding cavity for the nucleobases so that the mode of interaction changes. As suggested for MANT-CTP, also the affinity of the other nucleotides to EF3 and EF mutants may be affected by a specific arrangement of water molecules.

The MANT nucleotides used in the assays are mixtures of 2'-MANT and 3'-MANT isomers, and there is spontaneous isomerization between the two species under physiological conditions (17, 19, 20). So far, only the putative binding mode of 3'-MANT-isomers has been considered. The question arises whether the MANT group may fit to the same EF- CaM site in both isomers as shown for the binding of MANT-nucleotides to CyaA (9). Fig. 4**C** indicates that 2'-MANT-CTP may indeed interact with EF-CaM in a very similar position like its 3'-MANT analog. The main difference is a 3'- endo conformation of the ribosyl moiety, present also in the complex of 3'-deoxy-ATP with EF-CaM (3). This geometry implies an axial position of the 2'- MANT group which may then project to the space between H351 and F586. Additionally, an intramolecular H bond between the 3'-hydroxy group and the proximal α-phosphate oxygen is possible. Fig. 4**E**, showing the alignment of 2'-MANT-CTP, 3'-MANT-CTP and 3'-MANT-ATP in the docked poses, indicates a

close fit of the 2'-MANT and 3'-MANT isomers. Only the positions of the MANT groups themselves are slightly different (variability of the triphosphate conformation is due to the individual minimization courses).

Fig. 4: Docking of MANT- CTP and MANT-ATP on EF-CaM.

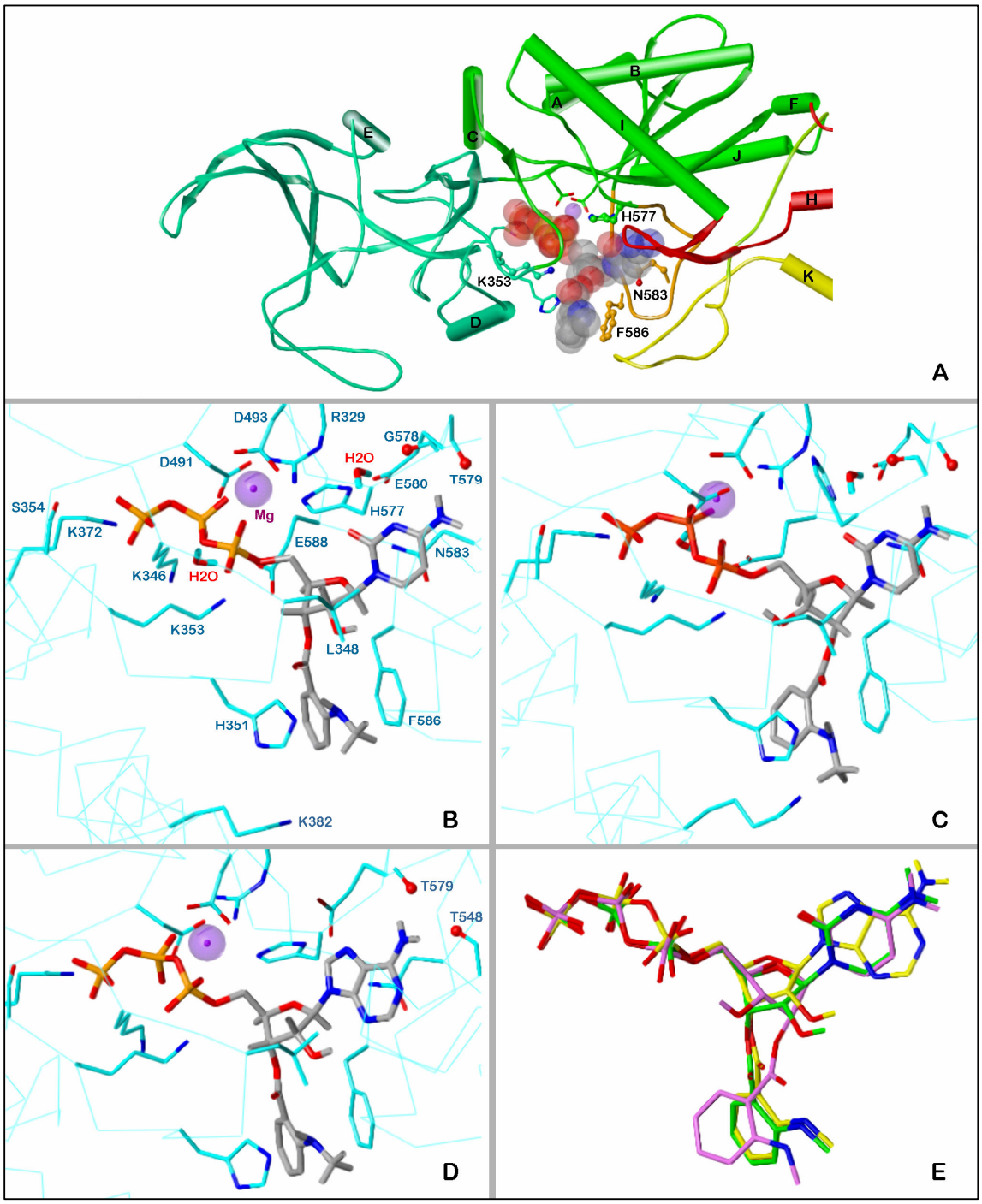

The minimized models are based on the crystal structure of EF-CaM-3'ANT-2'deoxy-ATP, PDB 1lvt (Shen et al., 2002). Colors of atoms, unless otherwise indicated: P – *orange*, O – *red*, N – *blue*, C, H –*grey,* Mg^{2+} – *purple* spheres. **A**, topology diagram of the EF domains surrounding the binding site with docked 3'-MANT-CTP (represented as transparent CPK model). Domains C_A – *green*, C_B – *greenblue*, switch A – *red*, switch B – *orange*, switch C – *yellow*. Amino acids subjected to mutation – balls and sticks models. **B-D**, detailed representation of interactions of MANT-nucleotides with EF-CaM. The side chains of amino acids within a sphere of 3 Å around the ligand and Mg^{2+} are drawn as sticks (C atoms – cyan) and labeled. For clarity, repeating labels are omitted in panels C and D

(see panel B). Cα-trace – *cyan* line. **B**, docking of 3´-MANT-CTP. **C**, docking of 2´-MANT-CTP. **D**, docking of 3´-MANT-ATP. **E**, superposition of the docked MANT nucleotides based on alignment of the three EF models (all heavy protein atoms considered). Colors of C and essential H atoms: 3´-MANT-CTP – *green,* 2´-MANT-CTP – *purple*, 3´-MANT-ATP – *yellow*.

5. Discussion

The major goal of the present study was to characterize the interaction of the catalytic site of EF with (M)ANT-nucleotides possessing various purine and pyrimidine bases in order to better understand the molecular mechanisms of EF inhibition and to provide the basis for the rational development of potent and selective EF inhibitors. Such EF inhibitors could be useful compounds to treat EF toxinemia and antibiotic-resistant *Bacillus anthracis* strains (1).

In previous studies, we developed a three-site pharmacophore model for mAC and CyaA toxin with binding regions for the base, the MANT-group and the polyphosphate chain (8-11). Those studies revealed that the MANT-group and the polyphosphate chain are the major determinants of inhibitor potency, whereas the base plays a relatively small role in this respect. This is reflected by the fact that the catalytic sites of mAC and CyaA are conformationally flexible and accommodate both purine and pyrimidine nucleotides.

Likewise, in EF, the (M)ANT-group and the length of the polyphosphate chain have a substantial impact on inhibitor potency, and EF accommodates various purine and pyrimidine bases (Table 3). These data indicate that the three-site binding model developed for mAC and CyaA can also be extended to EF. The structure/activity relationships of (MANT)-nucleotides at EF, CyaA and mAC are different, indicating that in principle, the development of potent and AC isoform-specific inhibitors is feasible. Most strikingly, CTP inhibited EF more than 400-fold more potently than mAC (Table 3)(10). Substitution of the 2'(3')-*O*-ribosyl position of CTP with a MANT group decreased the K_i value from 5 μM to 100 nM, yielding an EF inhibitor that is even 5-10-fold more potent than MANT-ATP in the presence of Mn^{2+} (Tables 2 and 3).

The highly unexpected preference of EF for the base cytosine prompted us to analyze EF inhibition by MANT-CTP and MANT-ATP in more detail. The analysis of enzyme inhibition kinetics revealed that both MANT-CTP and MANT-ATP are competitive EF inhibitors; i.e., they bind to the same site as, and freely compete with, the substrate ATP (Fig. 1). These data ruled out the existence of a hitherto unidentified cytosine base-preferring nucleotide-binding site in the

structurally very complex EF protein (Fig. 4**A**) (3, 4). Kinetic FRET competition experiments with the non-fluorescent ATP analog PMEApp revealed that both MANT- ATP and MANT-CTP reversibly bind to the catalytic site (Fig. 3), corroborating the competitive inhibition mode and the existence of a single nucleotide-binding site in EF. The faster displacement of MANT-ATP from EF by PMEApp compared to the displacement of MANT-CTP is explained by the higher affinity of EF for MANT-CTP.

To dissect possible differences in the binding modes of MANT-ATP and MANT-CTP to EF, we studied their interaction with several EF mutants in terms of enzyme inhibition and fluorescence spectroscopy. A previous study had shown that F586 mediates π-stacking interactions with 2'-deoxy-3'-ANT-ATP, resulting in a fluorescence increase upon excitation of the ANT-group (4). In agreement with those data, mutation of F586 reduced the potency of MANT-ATP and largely reduced the CaM-dependent FRET of MANT-ATP (Table 2 and Fig. 2). F586 is also important for the interaction with MANT-CTP as is revealed by the 6-fold reduction in potency. However, compared to MANT-ATP, the FRET signal with MANT-CTP in EF was much smaller, and the F586A mutation had a smaller inhibitory effect on the FRET. This difference in FRET cannot be explained by a lower CaM-affinity of EF bound to MANT-CTP compared to the protein complex bound to MANT-ATP since a 10-fold molar excess of CaM relative to EF did not yield a larger FRET with MANT-CTP. The models shown in Fig. 4 suggest a similar binding mode of MANT-CTP and its ATP analog. However, subtle differences due to the nucleobases occur and may account for the higher potency and the small FRET signal of MANT-CTP. In particular, the cytosine moiety may form water-mediated hydrogen bonds with R329 and E580 and favorably fit to the amide dipole of N583. Additionally, the flexibility of the bound cytosine should be greater than in the case of the bulkier adenine ring. Together with the specific charge distribution in the vicinity of the nucleobase, this may lead to absorption and thus attenuation of the FRET energy which is mainly due to tyrosine and tryptophan residues in switch C.

H577 plays a crucial role in catalysis as is reflected by the very low catalytic activity of the H577A mutant (Table 1) (3, 12). Nonetheless, the catalytic activity of the H577A mutant was sufficiently large to determine substrate- and MANT-

nucleotide affinity. Indeed, this mutation does not exert detrimental effect on substrate- and inhibitor binding per se (Tables 1 and 2).

N583 forms a crucial hydrogen bond with the ribosyl moiety of nucleotides bound to the catalytic site of EF (3). Accordingly, replacement of N583 by a non-hydrogen bond-forming amino acid (N583A) or hydrogen bond- forming amino acid with a different spatial arrangement of the bonding partners (N583Q and N383H) substantially decreases catalytic activity of the resulting EF mutants and also increases K_m (Table 1) (3). Thus, it was also not surprising that N583 mutants substantially reduced the potencies of MANT-ATP and MANT-CTP (Table 2). However, whereas the N583A mutation and the N583H mutation affected inhibitor potencies to a similar extent, the potency of MANT-CTP was much more strongly reduced by the N583Q mutation than the potency of MANT- ATP. These findings suggest that the binding of MANT-CTP is severely impaired by the longer side chain of Q as compared to N, indicative for a substantial spatial constraint in this part of the binding pocket.

The carboxyl group of E588 and the amino group of K353 form an ionic bond that locks the base into the catalytic site (3). Disruption of this ionic bond by the K353A mutation largely reduces catalytic activity and lowers substrate affinity (3) (Table 1). The K353R mutation that alters the spatial arrangement of the catalytic site but still allows ionic bridge formation displays less severe impairment of catalysis and no change in K_m (Table 1). Intriguingly, binding of MANT-CTP to the catalytic site is much more sensitive to disruption of ionic bond formation between E588 and K353 and reorientation of the ionic bond than binding of MANT-ATP (Table 2), further corroborating the notion that there are subtle differences in the binding modes of MANT-ATP and MANT-CTP.

The high sensitivity of our AC assay, largely due to very low blank values (see Materials and Methods) allowed us not only to precisely determine the kinetic parameters of EF mutants but also of wild-type EF in the absence of CaM. In fact, the catalytic activity of EF is not absolutely CaM-dependent. Even in the absence of CaM, we could accurately determine kinetic parameters using appropriate experimental conditions, i.e. higher protein and [α-^{32}P]ATP amounts, higher incubation temperature and longer incubation time. The fact that in the absence of

CaM, EF displays unaltered substrate- and inhibitor affinity despite the largely reduced catalytic activity was rather surprising. Even the MANT-CTP/MANT-ATP potency ratio is conserved. Comparing the crystal structures of EF-CaM (PDB 1lvc, (4)) and EF alone (PDB 1k8t, (3)), 13 mutually resolved amino acids of the MANT-nucleotide binding sites (Fig. 4**B**) fit very well (RMSD of the backbone atoms 0.99 Å, only G578 and T579 at the N-terminus of switch B are outliers with distances of greater than 1.5 Å). However, switch B stabilized by switch C in EF-CaM is disordered in the structure of EF alone and contains amino acids involved in substrate- and MANT-nucleotide binding to EF-CaM (T579, E580, N583, F586, E588) or in the stabilization of residues that participate in catalysis (e.g., D590 forming a salt bridge with R329). To explain the unaltered potency of the MANT inhibitors at EF alone, we postulate that the nucleotides stabilize switch B in a conformation like that in EF-CaM. The substrate may act similarly in terms of affinity, but the resulting switch B conformation is insufficient for high catalytic activity. Experiments with membrane-permeable CaM inhibitors (21) will have to answer the question whether the CaM-independent catalytic activity of EF is of pathophysiological relevance.

6. Summary and conclusion

In conclusion, through a combination of enzymological, fluorescence spectroscopy, mutagenesis and molecular modeling approaches, we have shown that there are subtle differences in the binding modes of MANT-ATP and MANT-CTP to EF. EF, unlike all other ACs studied so far including mAC and CyaA toxin from *Bordetella pertussis*, exhibits a unique preference for the base cytosine, offering an excellent starting point for the development of EF inhibitors with specificity for the toxin relative to mAC. Finally, our studies also raise the intriguing question whether CTP, exhibiting an unusually high affinity for EF is not only an inhibitor of cAMP synthesis but, perhaps, a substrate itself.

7. References

1. Jedrzejas MJ. The structure and function of novel proteins of *Bacillus anthracis* and other spore-forming bacteria: development of novel prophylactic and therapeutic agents. *Crit Rev Biochem Mol Biol* 2002; **37**:339-73.

2. Hong J, Beeler J, Zhukovskaya NL, He W, Tang WJ, Rosner MR. Anthrax edema factor potency depends on mode of cell entry. *Biochem Biophys Res Commun* 2005; **335**:850-7.

3. Drum CL, Yan SZ, Bard J, Shen YQ, Lu D, Soelaiman S, Grabarek Z, Bohm A, Tang WJ. Structural basis for the activation of anthrax adenylyl cyclase exotoxin by calmodulin. *Nature* 2002; **415**:396-402.

4. Shen Y, Lee YS, Soelaiman S, Bergson P, Lu D, Chen A, Beckingham K, Grabarek Z, Mrksich M, Tang WJ. Physiological calcium concentrations regulate calmodulin binding and catalysis of adenylyl cyclase exotoxins. *EMBO J* 2002; **21**:6721-32.

5. Shen Y, Zhukovskaya NL, Guo Q, Florian J, Tang WJ. Calcium-independent calmodulin binding and two-metal-ion catalytic mechanism of anthrax edema factor. *EMBO J* 2005; **24**:929-41.

6. Gille A, Lushington GH, Mou TC, Doughty MB, Johnson RA, Seifert R. Differential inhibition of adenylyl cyclase isoforms and soluble guanylyl cyclase by purine and pyrimidine nucleotides. *J Biol Chem* 2004; **279**:19955-69.

7. Mou TC, Gille A, Fancy DA, Seifert R, Sprang SR. Structural basis for the inhibition of mammalian membrane adenylyl cyclase by 2 '(3')-O-(N-Methylanthraniloyl)-guanosine 5 '-triphosphate. *J Biol Chem* 2005; **280**:7253-61.

8. Mou TC, Gille A, Suryanarayana S, Richter M, Seifert R, Sprang SR. Broad specificity of mammalian adenylyl cyclase for interaction with 2',3'-substituted purine- and pyrimidine nucleotide inhibitors. *Mol Pharmacol* 2006; **70**:878-86.

9. Göttle M, Dove S, Steindel P, Shen Y, Tang WJ, Geduhn J, König B, Seifert R. Molecular analysis of the interaction of *Bordetella pertussis* adenylyl cyclase with fluorescent nucleotides. *Mol Pharmacol* 2007; **72**:526-35.

10. Gille A, Guo J, Mou TC, Doughty MB, Lushington GH, Seifert R. Differential interactions of G-proteins and adenylyl cyclase with nucleoside 5'-triphosphates, nucleoside 5'-[gamma-thio]triphosphates and nucleoside 5'-[beta,gamma-imido]triphosphates. *Biochem Pharmacol* 2005; **71**:89-97.

11. Wang JL, Guo JX, Zhang QY, Wu JJ, Seifert R, Lushington GH. A conformational transition in the adenylyl cyclase catalytic site yields different binding modes for ribosyl-modified and unmodified nucleotide inhibitors. *Bioorg Med Chem* 2007; **15**:2993-3002.

12. Guo Q, Shen Y, Zhukovskaya NL, Florian J, Tang WJ. Structural and kinetic analyses of the interaction of anthrax adenylyl cyclase toxin with reaction products cAMP and pyrophosphate. *J Biol Chem* 2004; **279**:29427-35.

13. Gopalakrishna R, Anderson WB. Ca^{2+}-induced hydrophobic site on calmodulin: application for purification of calmodulin by phenyl-Sepharose affinity chromatography. *Biochem Biophys Res Commun* 1982; **104**:830-6.

14. Cornell WD CP, Bayly CI, Gould IR, Merz KMJ, Ferguson DM, Spellmeyer DC, Fox T, Caldwell JW, and Kollman PA. A second generation force field for the simulation of proteins and nucleic acids. *J Am Chem* 1995; **117**:5179-97.

15. Clark M CRr, Van Opdenbosh N. Validation of the general purpose Tripose 5.2 force field. *J Comput Chem* 1989; **10**:982-1012.

16. Lakowizc RJ. Principles of fluorescence spectroscopy. *second edition* , *Principles of* fluorescence spectroscopy. *Kluwer Academic.* 1999

17. Hiratsuka T. New ribose-modified fluorescent analogs of adenine and guanine nucleotides available as substrates for various enzymes. *Biochim Biophys Acta* 1983; **742**:496-508.

18. Shen Y, Guo Q, Zhukovskaya NL, Drum CL, Bohm A, Tang WJ. Structure of anthrax edema factor-calmodulin-adenosine 5'-(alpha,beta-methylene)-triphosphate complex reveals an alternative mode of ATP binding to the catalytic site. *Biochem Biophys Res Commun* 2004; **317**:309-14.

19. Hiratsuka T. Fluorescent and colored trinitrophenylated analogs of ATP and GTP. *Eur J Biochem* 2003; **270**:3479-85.

20. Jameson DM, Eccleston JF. Fluorescent nucleotide analogs: synthesis and applications. *Methods Enzymol* 1997; **278**:363-90.

21. Wolberg G, Zimmerman TP. Effects of calmodulin antagonists on immune mouse lymphocytes. *Mol Pharmacol* 1984; **26**:286-92.

Chapter IV

IV. Molecular Analysis of the Interaction of Anthrax Adenylyl Cyclase Toxin, Edema Factor, with Bis-2',3'-*O*-(N- (propyl)/(methyl)anthraniloyl)-Substituted Purine and Pyrimidine Nucleotides

1. Abstract

Bacillus anthracis causes anthrax disease and exerts its deleterious effects by the release of three exotoxins, i.e. lethal factor, protective antigen and edema factor (EF), a highly active calmodulin-dependent adenylyl cyclase (AC). However, conventional antibiotic treatment is ineffective against either toxemia or antibiotic-resistant strains. Thus, more effective drugs for anthrax treatment are needed. The studies reported in Chapter III showed that EF is differentially inhibited by various purine and pyrimidine nucleotides modified with N-methylanthraniloyl (MANT)- or anthraniloyl (ANT) groups at the 2'(3')-*O*-ribosyl position, with the unique preference for the base cytosine. MANT-CTP was the most potent EF inhibitor (K_i, 100 nM) among 16 compounds studied. In this Chapter, we examined the interaction of EF with 2',3'-*O*-bis-(M)ANT-substituted nucleotides. Bis-MANT-ATP and Bis-MANT-CTP were the most potent EF inhibitors among nucleotides studied (K_i, 210 nM for both nucleotides). Bis-MANT-nucleotides inhibited EF competitively. Propyl-ANT-ATP was more potent than Bis-propyl-ANT-ATP and MANT-ATP. Activation of EF by calmodulin resulted in effective fluorescence resonance energy transfer (FRET) from tryptophan and tyrosine residues located in the vicinity of the catalytic site to Bis-MANT-ATP, but FRET to Bis-MANT-CTP was only small. Mutagenesis studies revealed that F586 is crucial for FRET to Bis-MANT-ATP and Bis-MANT-CTP and that the mutations N583Q, K353A and K353R differentially alter the inhibitory potencies of Bis-MANT-ATP and Bis-MANT-CTP. We conclude that the nucleotide binding site of EF is spacious and readily accommodates bulky Bis-(M)ANT-substituted purine and pyrimidine nucleotides. Longer aliphatic chain substitution at N-position of ANT-ATP may increase the potency of EF inhibition. These data provide a solid basis for future structure/activity relationship studies aiming at the development of potent EF inhibitors with high selectivity relative to mammalian ACs.

2. Introduction

The spore-forming *Bacillus anthracis* secretes three major toxins: edema factor (EF), protective antigen (PA), and lethal factor (LF) (1, 2). As an adenylyl cyclase, EF raises the concentration of a second messenger, cyclic AMP (cAMP), inside host cells to supraphysiological levels (3, 4). EF is the key virulence factor for anthrax pathogenesis. An inactivating mutation in EF results in reduced survival of germinated anthrax spores in macrophages, indicating an active role for EF at early stages of anthrax infection (5). Moreover, EF modulates the profile of cytokines such as tumor necrosis factor α (TNF-α) and interleukin 6 (IL-6) produced by human monocytes, which impair cellular antimicrobial responses (6). In addition, a strain of anthrax with a defective EF gene has 100-fold reduced lethality in mice (7).

EF enters host cells via a complex with PA, which is a pH-dependent protein transporter (8). LF, a zinc metalloprotease that inactivates mitogen-activated protein kinase kinase, also enters into host cells by its association with PA (9, 10). LF works coordinately with EF to facilitate bacterial survival in macrophages and to impair host innate immunity (5-7, 11, 12). The combination of toxemia caused by anthrax toxins and bacteremia due to the rapid growth of anthrax bacteria in vital organs can result in sepsis, pulmonary edema, and/or meningitis within few days, making inhalational anthrax a deadly disease.

Natural isolates of *Bacillus anthracis* are sensitive to a broad spectrum of antibiotics; thus antibiotics have been the primary recourse for therapy (13). However, antibiotics are ineffective against either toxemia or antibiotic-resistant strains of anthrax. The antibiotic treatment used for victims of the 2001 bioterrorism-related anthrax attack in the United States resulted in a survival rate of slightly better than 50% for cases of inhalational anthrax. Some survivors have experienced illness with symptoms such as fatigue, shortness of breath, chest pain, and memory loss. This situation highlights an urgent need for a more effective treatment to improve the survival rate and quality of life of Anthrax patients (14).

Previous studies resolved several crystal structures of nucleotide-EF-CaM complexes and characterized the amino acids that are important for binding of the substrate ATP and catalysis (4, 15, 16). Additionally, we showed that mAC and

bacterial AC toxins are potently inhibited by MANT-substituted nucleoside 5'-triphosphates (17-20). Those (M)ANT-nucleotides are environmentally sensitive fluorescence probes that show an increase in fluorescence upon interaction with a hydrophobic environment (21, 22). We exploited this property to suggest conformational changes associated with activation in purified catalytic subunits of mAC (18, 19), the *Bordetella pertussis* AC toxin, CyaA (20) and *Bacillus anthracis* AC toxin EF (23). In addition, by combining crystallographic and molecular modeling approaches, we developed a three-site pharmacophore model for mAC, CyaA, and EF with binding domains for the base, the MANT-group and the polyphosphate chain (19, 20, 24, 25).

In our recent study, we systematically examined the interactions of natural purine and pyrimidine nucleotides and several (M)ANT- substituted analogues with EF in terms of catalysis, fluorescence changes and molecular modeling. This study revealed that the structure/activity relationships of (MANT)-nucleotides at EF, CyaA and mAC are different; indicating that in principle, the development of potent and specific EF-inhibitors is feasible. Additionally, EF exhibited a highly unexpected and unique preference for the base cytosine. MANT-CTP was the most potent EF-inhibitor among the studied nucleotides, 5-10-fold more potent than MANT-ATP (23).

Moreover, we found that MANT-CTP and MANT-ATP are competitive EF inhibitors, i.e. they bind to the same site as, and freely compete with, the substrate ATP. These data ruled out the existence of a hitherto unidentified cytosine base-preferring nucleotide-binding site in the structurally very complex EF protein (4, 15). Kinetic FRET competition experiments with the non-fluorescent ATP analog PMEApp revealed that both MANT- ATP and MANT-CTP reversibly bind to the catalytic site, corroborating the competitive inhibition mode and the existence of a single nucleotide-binding site in EF. Mutagenesis studies revealed that F586 is crucial for FRET to MANT-ATP and MANT-CTP and that the mutations N583Q, K353A and K353R differentially alter the inhibitory potencies of MANT-ATP and MANT-CTP (23).

In our previous studies, we have also shown that the catalytic sites of both CyaA and EF are spacious and readily accommodate a broad variety of 2',3'-substituted nucleotides. The catalytic site of CyaA even accommodates a bis-

substituted MANT-nucleotide. Interestingly, Bis-MANT-IMP exhibited higher potency at CyaA in comparison to the corresponding mono-substituted MANT-nucleotide (23). These data prompted us to study systematically the interactions of several newly synthesised mono- and bis-substituted (M)ANT-nucleotides with EF and several EF mutants in terms of catalysis, fluorescence changes and molecular modeling, Focusing on Bis-MANT-ATP and Bis-MANT-CTP to better dissect the unique preference of EF for the base cytosine. The major goal of the present study was to provide the basis for the rational development of potent and selective EF inhibitors. Such EF inhibitors could be useful compounds to treat EF toxemia and antibiotic-resistant *Bacillus anthracis* strains.

3. Materials and Methods

3.1 Materials:

Expression and purification of EF was performed as described in Chapter II. The following columns were used for EF protein purification; HisTrap fast flow rate affinity Ni column (5 ml) and resource Q (quaternary ammonium salt) strong anionic exchange column (6 ml) (GE Healthcare, Freiburg/Brsg., Germany). EF3(F586A) mutant was expressed and purified as described in Chapter II. The HisTrap fast flow rate affinity Ni column (5 ml) was used for immobilized matrix affinity chromatography and the HiPrep 16/10 SP XL column (GE Healthcare) was used in cation exchange chromatography. CaM was extracted and purified from bovine brain as described in Chapter II. The HiPrep 16/10phenyl FF (high sub) column (GE Healthcare) was used in hydrophobic chromatography purification of CaM. PMEApp was supplied by Gilead Sciences, Foster City, CA. ATP, ITP, CTP, IMP, ampicillin, kanamycin, lysozyme enzyme, β-mercaptoethanol, Mes buffer (low moisture content) and dithiothreitol (for molecular biology) were purchased from Sigma-Aldrich, Steinheim, Germany. Tryptone and yeast were purchased from BD Biosciences (Franklin Lakes, NJ). [α-^{32}P]ATP (800 Ci/mmol) was purchased from PerkinElmer, Rodgau Jügesheim, Germany. Aluminum oxide 90 active, (neutral, activity 1, particle size 0.06 - 0.2 mm) was purchased from Biomedicals (Eschwege, Germany). Bovine serum albumin (fraction V, highest quality) was bought from Sigma-Aldrich, Steinheim, Germany. Imidazole (highest quality), $CaCl_2$, $MnCl_2$ tetrahydrate and $MgCl_2$ hexahydrate (highest quality) were purchased from Merck. For all experiments double-distilled water was used.

3.2 Mono- and bis-(M)ANT-nucleotides synthesis and analysis

3.2.1 General procedure for mono- and bis- (M)ANT-nucleotides synthesis

(M)ANT-nucleotides were synthesized according to Hiratsuka (1983) with modifications. In general, mono- and bis-substituted (M)ANT-nucleotides could be achieved both in an one pot synthesis procedure. The nucleotide (0.33 mmol, 1 eq)

was propounded in a small two-neck round flask and dissolved in a minimum amount of water (3 ml). Under continuous stirring a crystalline preparation of the appropriate isatoic anhydride derivative (0.5 mmol, 1.5 eq) was added. After heating to 38 °C the pH- value was adjusted to 8.6 and maintained by titration of 1 N NaOH solution for 2 hours. The reaction mixture was extracted three times by 20 ml chloroform (only for MANT-nucleotides). The aqueous phase was dry-frozen. The received foam showed white to brown color. The crude reaction mixture was purified by preparative reversed phase high pressure liquid chromatography. Especially for the sensitive separation of mono- and bis-(M)ANT-NTPs from mono- and bis-(M)ANT-NDPs this purification strategy was required. In case of monophosphate derivatives only size-exclusion chromatography with a long Sephadex® LH-20 column (85 x 2 cm) and subsequently elution with double-distilled water was applied. The desired product could be detected directly by its blue fluorescence in the collection tubes at λ_{ex} of 366 nm and by TLC. After final dry-freezing white to brown solid compounds (purity > 98 %) were obtained. For all derivatives yields were determined by analytical HPLC measurements of crude reaction mixtures and correlate with the maximal accessible yield. Because of the time consuming and costly preparative HPLC purification separation was stopped after obtaining approximate 5 mg pure compound.

Synthesis of isatoic anhydride precursors

For the propyl- and acetylated amino-ANT-nucleotide derivatives the corresponding isatoic anhydrides were easily accessible by nucleophilic substitution with propyliodide and for acetylation with acetic acid anhydride by standard protocol respectively.

3.2.2 HPLC analysis of bis-(M)ANT-nucleotides

The samples were filtered using a PTFE filter (Chromafil, O-20/15, organic, pore size 0.2 mm; Machery-Nagel, Düren, Germany). A 10 µl sample was analyzed using a HPLC model 1100 (Agilent Technologies, Waldbronn, Germany) fitted with a C18 analytical column (Phenomenex Luna, particle size 3 µm, 150 x 4.60 mm, Aschaffenburg, Germany) and DAD. Data were analyzed using a HPLC-3D ChemStation Rev. A.10.01 [1635]. Gradient elution was performed with 0.05

Fig. 1: General reaction scheme for the synthesis of mono- and bis-substituted (M)ANT-nucleotides

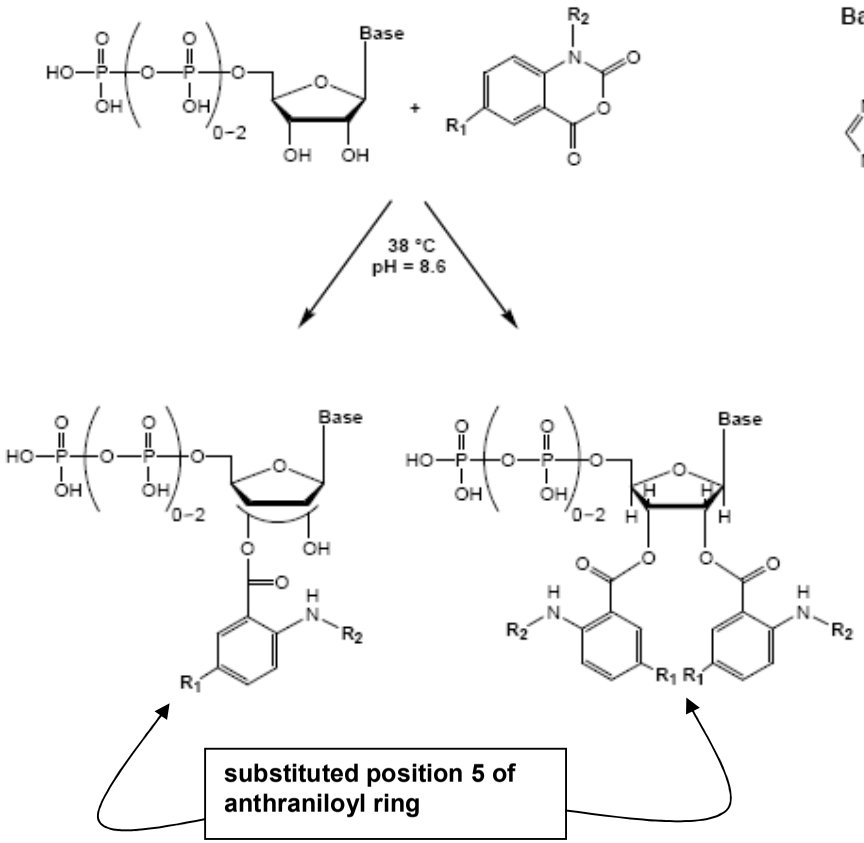

Bases:

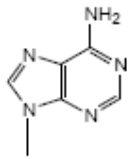
adenine

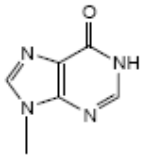
hypoxanthine

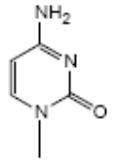
cytosine

Substituent	R_1	R_2
MANT	H	CH_3
ANT	H	H
Cl-ANT	Cl	H
Br-ANT	Br	H
Pr-ANT	H	$CH_2CH_2CH_3$
Ac-NH_2-ANT	NH_2COCH_3	H

ammonium acetate (solvent A) and acetonitrile (solvent B) at a constant flow rate of 1.0 ml/min. A gradient profile with the following proportions of solvent B was applied [t (min), % B]: [0, 5], [10, 5], [30, 45]. [40, 80]. The chromatograms were monitored at UV absorption at 220 and 254 nm. In addition, a fluorescence detector was used for the analysis of the fluorescent anthraniloylic compounds at λ_{ex} of 350 nm and λ_{em} of 450 nm.

3.2.3 LC/MS online coupling

All samples were filtered using a PTFE filter and injected into a HPLC model 1100 (Hewlett- Packard, Waldbronn, Germany). The compound to be analyzed was separated by a C18 column (Phenomenex luna, particle size 3 µm, 150 x 2 mm, Aschaffenburg, Germany). A binary eluent mixture consisting of water (10 mM ammonium acetate) (eluent A) and acetonitrile (eluent B) was pumped with a constant flow of 0.3 ml/min. The following gradient profile was used t [min], % B: [0, 5], [10, 5], [30, 45]. [40, 80]. The injected volume was 3 µl. Using a triple stage mass spectrometer (TSQ 7000, Thermoquest Finnigan, Toronto, Canada) the mass of the respective compound was determined.

3.2.4 Preparative HPLC

Compound mixtures were dissolved in water (concentration: 30-50 mg/ml) and filtered using a PTFE filter. Compounds were separated using a HPLC model 1100 (Agilent Technologies, Waldbronn, Germany) fitted with a C18 preparative column (phenomenex Luna, particle size) 10 µm 21.2 mm). Gradient elution was performed with 0.05 M ammonium acetate (solvent A) and acetonitrile (solvent B) at a constant flow rate of 21 ml/min. The chromatograms were monitored by UV absorption at 220 and 254 nm.

3.2.5 NMR spectrometry

Bruker Avance 400 (^{1}H: 400.1 MHz, ^{13}C: 100.6 MHz, ^{31}P-NMR: 161.9 MHz, T = 300 K), Bruker Avance 300 (^{1}H: 300.1 MHz, ^{13}C: 75.5 MHz, T = 300 K). The chemical shifts are reported in δ [ppm] relative to external standards (solvent residual peak). The spectra were analysed by first order, the coupling constants are given in Hertz [Hz]. Characterisation of the signals: s = singlet, d = doublet, t =

triplet, m = multiplet, dd = double doublet, ddd = double double doublet. Integration is determined as the relative number of atoms. Assignment of signals in ^{13}C-spectra was determined with DEPT-technique (pulse angle: 135°) and given as (+) for CH or CH_3, (-) for CH_2 and (C_{quat}) for quaternary C. Error of reported values: chemical shift: 0.01 ppm for ^{1}H- NMR, 0.1 ppm for ^{13}C-NMR and 0.1 Hz for coupling constants. The solvent used is reported for each spectrum.

3.2.6 Spectroscopy

Absorption spectroscopy was performed using a Varian Cary BIO 50 UV/VIS/NIR spectrometer with a 1 cm quartz cuvette (Hellma) and Uvasol solvents (Merck or Baker). IR spectra were recorded by a Bio-Rad FTS 2000 MX FT-IR. Further mass spectrometry measurements with electron ionization technique were applied by a Varian CH-5.

3.2.7 Synthesized nucleotides:

Cl-ANT-ATP (2'(3')-*O*-5-chloroanthraniloyl-adenosine-5'-triphosphate) or [(2R,3S,4R,5R)-5-(6-aminopurin-9-yl)-4(3)-hydroxy-2-[[hydroxy-(hydroxyl-phosphonooxy-phosphoryl)oxyphosphoryl]oxymethyl]oxolan-3(4)-yl]2-amino-5-chlorobenzoate

For the procedure see general prescription. 100 mg (0.17 mmol) introduced disodium salt of ITP yielded 47 mg (71 µmol, 42 %) pure product after purification. R_f = 0.27 (1- propanol:H_2O:NH_3 (32%) = 2:1:1). HPLC (analytic): R_t = 20.59 min, 20.84 min; k = 13.24, 13.39; LC/MS (ESI, H_2O/CH_3CN): *m/z* = 96.0 [M+$NH_3NH_4^+$] (R_t = 16.77 min, 100 %), 679.0 [M+NH_4^+] (R_t = 16.77 min, 90 %), 662.1 [M+H^+] (R_t = 16.77 min, 5 %); (-ESI, H_2O/CH_3CN): *m/z* = 660.1 [M-H^-] (R_t = 16.77 min, 100 %); HPLC (preparative), gradient (t [min], % B: [0, 14], [6, 14], [15, 38], [20, 80]): R_t = 7.71 min, 8.44 min; UV/Vis (H_2O) λ_{max} (log ε) = 255 nm (14,600), 348 nm (4,500); empirical formula: $C_{17}H_{19}ClN_5O_{15}P_3$; MW = 661.73.

Br-ANT-ATP (2'(3')-*O*-5-bromoanthraniloyl-adenosine-5'-triphosphate) or [(2R,3S, 4R,5R)-5-(6-aminopurin-9-yl)-4(3)-hydroxy-2-[[hydroxy-(hydroxyl-phosphonooxy- phosphoryl)oxyphosphoryl]oxymethyl]oxolan-3(4)-yl]2-amino-5-bromobenzoate

For the procedure see general prescription. 100 mg (0.18 mmol) introduced disodium salt of ATP led to 36 mg (50 µmol, 28 %) pure product after purification. R_f = 0.24 (1- propanol:H_2O:NH_3 (32 %) = 2:1:1). HPLC (analytic): R_t = 20.24 min, 20.39 min; k = 12.18, 12.28; LC/MS (ESI, H_2O/CH_3CN): *m/z* = 724.1 [$M+NH_4^+$] (R_t = 21.21 min, 100 %), 741.2 [$M+NH_3+NH_4^+$] (R_t = 21.21 min, 40%); (-ESI, H_2O/CH_3CN): *m/z* = 705.1 [$M-H^-$] (R_t = 21.21 min, 100 %); HPLC (preparative), gradient (t [min], % B: [0, 17], [8, 17], [10, 25], [15, 38], [20, 80]): R_t = 6.32 min; UV/Vis (H_2O) λ_{max} (log ε) = 256 nm (16,400), 332 nm (3,300); empirical formula: $C_{17}H_{20}BrN_6O_{14}P_3$; MW = 705.20.

Br-ANT-ITP (2'(3')-*O*-5-bromoanthraniloyl-inosine-5'-triphosphate) or [(2R,3S,4R,5R)-5-(6-oxo-1H-purin-9-yl)-4(3)-hydroxy-2-[[hydroxy-(hydroxyl-phosphonooxy-phosphoryl)oxyphosphoryl]oxymethyl]oxolan-3(4)-yl]2-amino-5-bromobenzoate

For the procedure see general prescription. 100 mg (0.17 mmol) introduced disodium salt of ITP yielded 48 mg (68 µmol, 40 %) pure product after purification. R_f = 0.25 (1- propanol:H_2O:NH_3 (32 %) = 2:1:1). HPLC (analytic): R_t = 21.16 min, 21.45 min; k = 13.63, 13.83; LC/MS (ESI, H_2O/CH_3CN): *m/z* = 725.1 [$M+NH_4^+$] (R_t = 18.81 min, 100 %), 742.2 [$M+NH_3+NH_4^+$] (R_t = 18.81 min, 35 %); (-ESI, H_2O/CH_3CN) : *m/z* = 706.1 [$M-H^-$] (R_t = 18.81 min, 100 %); HPLC (preparative), gradient (t [min], % B: [0, 18], [15, 38], [20, 80]): R_t = 4.27 min, 4.53 min; UV/Vis (H_2O) λ_{max} (log ε) = 248 nm (15,000), 328 nm (4,300); empirical formula: $C_{17}H_{19}BrN_5O_{15}P_3$; MW = 706.18.

Pr-ANT-ATP (*N*-propyl-2'(3')-*O*-anthraniloyl-adenosine-5'-triphosphate) or [(2R,3S,4R,5R)-5-(6-aminopurin-9-yl)-4(3)-hydroxy-2-[[hydroxy-(hydroxy-phosphonooxy- phosphoryl)oxyphosphoryl]oxymethyl]oxolan-3(4)-yl]2-propylaminobenzoate

For the procedure see general prescription. 100 mg (0.18 mmol) introduced disodium salt of ATP yielded 29 mg (43 µmol, 24 %) pure product after purification. R_f = 0.31 (1-propanol:H_2O:NH_3 (32 %) = 2:1:1). HPLC (analytic): R_t = 24.93 min, 25.67 min; k = 15.29, 15.78; LC/MS (ESI, H_2O/CH_3CN): *m/z* = 669.0 [M+H^+] (R_t = 23.12 min, 100 %), 686.0 [M+NH_4^+] (R_t = 23.12 min, 15 %); (-ESI, H_2O/CH_3CN): *m/z* = 667.0 [M- H^-] (R_t = 23.12 min, 100 %); HPLC (preparative), gradient (t [min], % B: [0, 5], [20, 45], [25, 80]): R_t = 13.33 min; UV/Vis (H_2O) λ_{max} (log ε) = 257 nm (17,500), 359 nm (4,600); empirical formula: $C_{20}H_{27}N_6O_{14}P_3$; MW = 668.38.

Pr-ANT-ITP (*N*-propyl-2'(3')-*O*-anthraniloyl-inosine-5'-triphosphate) or [(2R,3S,4R,5R)-5-(6-oxo-1H-purin-9-yl)-4(3)-hydroxy-2-[[hydroxy-(hydroxy-phosphonooxy-phosphoryl)oxyphosphoryl]oxymethyl]oxolan-3(4)-yl]2-propylaminobenzoate

For the procedure see general prescription. 100 mg (0.17 mmol) introduced disodium salt of ITP yielded 25 mg (37 µmol, 22 %) pure product after purification. R_f = 0.32 (1- propanol:H_2O:NH_3 (32 %) = 2:1:1). HPLC (analytic): R_t = 24.73 min, 25.16 min; k = 16.10, 16.40; LC/MS (ESI, H_2O/CH_3CN): *m/z* = 687.0 [M+NH_4^+] (R_t = 22.87 min, 100 %), 669.8 [M+H^+] (R_t = 22.87 min, 20 %); (-ESI, H_2O/CH_3CN): *m/z* = 668.0 [M-H^-] (R_t = 22.87 min, 100 %); HPLC (preparative), gradient (t [min], % B: [0, 5], [20, 45], [25, 80]): R_t = 13.12 min; UV/Vis (H_2O) λ_{max} (log ε) = 257 nm (17,500), 359 nm (4,600); empirical formula: $C_{20}H_{26}N_5O_{15}P_3$; MW = 669.37.

Ac-NH_2-ANT-ATP (2'(3')-*O*-5-acetylaminoanthraniloyl-adenosine-5'-triphosphate) or [(2R,3S,4R,5R)-5-(6-aminopurin-9-yl)-4(3)-hydroxy-2-[[hydroxy-(hydroxyl-phosphono- oxyphosphoryl)oxyphosphoryl]-oxymethyl]oxolan-3(4)-yl]2-amino-5-acetylamino- benzoate

For the procedure see general prescription. 100 mg (0.18 mmol) introduced disodium salt of ATP yielded 57 mg (84 µmol, 46 %) pure product after purification. R_f = 0.21 (1-propanol:H_2O:NH_3 (32 %) = 2:1:1). HPLC (analytic): R_t = 8.39 min, 8.75 min; k = 4.48, 4.72; LC/MS (ESI, H_2O/CH_3CN): *m/z* = 683.9 [M+H^+] (R_t = 3.34 min, 100 %), 701.0 [M+NH_4^+] (R_t = 3.34 min, 70 %); (-ESI, H_2O/CH_3CN): *m/z* = 682.0 [M- H^-] (R_t = 3.34 min, 100 %); HPLC (preparative),

gradient (t [min], % B: [0, 6], [5, 7], [23, 14], [24, 80], [29, 80]): R_t = 12.06 min; UV/Vis (H_2O) λ_{max} (log ε) = 259 nm (17,200), 349 nm (3,100);empirical formula: $C_{19}H_{24}N_7O_{15}P_3$; MW = 683.35.

Ac-NH_2-ANT-ITP (2'(3')-*O*-5-acetylaminoanthraniloyl-inosine-5'-triphosphate) or [(2R,3S,4R,5R)-5-(6-oxo-1H-purin-9-yl)-4(3)-hydroxy-2-[[hydroxy-(hydroxy-phosphonooxyphosphoryl)oxyphosphoryl]oxymethyl]oxolan-3(4)-yl]2-amino-5-acetyl- aminobenzoate

For the procedure see general prescription. 100 mg (0.17 mmol) introduced disodium salt of ITP yielded 60 mg (88 µmol, 52 %) pure product after purification. R_f = 0.22 (1- propanol:H_2O:NH_3 (32 %) = 2:1:1). HPLC (analytic): R_t = 7.63 min, 7.99 min; k = 4.28, 4.53; LC/MS (ESI, H_2O/CH_3CN): *m/z* = 702.0 [M+NH_4^+] (R_t = 1.91 min, 100 %), 719.0 [M+NH_3+NH_4^+] (R_t = 1.91 min, 40 %), 684.9 [M+H^+] (R_t = 1.91 min, 25 %); (-ESI, H_2O/CH_3CN): *m/z* = 683.0 [M-H^-] (R_t = 1.91 min, 100 %); HPLC (preparative), gradient (t [min], % B: [0, 5.8], [11, 5.8], [12, 10], [18, 13], [20, 80]): R_t = 9.50 min; UV/Vis (H_2O) λ_{max} (log ε) = 248 nm (11,400; shoulder), 345 nm (2,500); empirical formula: $C_{19}H_{23}N_6O_{16}P_3$; MW = 684.34.

Bis-MANT-ATP (*N*-methyl-2',3'-bis-*O*-anthraniloyl-adenosine-5'-triphosphate) or [(2R,3S,4R,5R)-5-(6-aminopurin-9-yl)-2-[[hydroxy-(hydroxy-phosphonooxy- phosphoryl)oxyphosphoryl]oxymethyl]oxolan-3,4-bis-yl]2-methylaminobenzoate

For the procedure see general prescription. 100 mg (0.18 mmol) introduced disodium salt of ATP led over all purification steps to 21 mg (27 µmol, 15 %) pure product. R_f = 0.32 (1-propanol:H_2O:NH_3 (32 %) = 2:1:1). HPLC (analytic): R_t = 26.95 min; k = 16.61; LC/MS (ESI, H_2O/CH_3CN): *m/z* = 791.2 [M+NH_4^+] (R_t = 28.58 min, 100 %), 774.2 [M+H^+] (R_t = 28.58 min, 40 %); (-ESI, H_2O/CH_3CN): *m/z* = 772.3 [M-H^-] (R_t = 28.58 min, 100 %); HPLC (preparative), gradient (t [min], % B: [0, 11], [2, 11], [5, 30], [15, 31.5], [18, 80]): R_t = 9.91 min; UV/Vis (H_2O) λ_{max} (log ε) = 255 nm (18,000), 359 nm (7,300); empirical formula: $C_{26}H_{30}N_7O_{15}P_3$; MW = 773.48.

Bis-MANT-ITP (*N*-methyl-2',3'-bis-*O*-anthraniloyl-inosine-5'-triphosphate) or [(2R,3S,4R,5R)-5-(6-oxo-1H-purin-9-yl)-2-[[hydroxy-(hydroxy-phosphonooxyphosphoryl)oxyphosphoryl]oxymethyl]oxolan-3,4-bis-yl]2-methylaminobenzoate

For the procedure see general prescription. 100 mg introduced trisodium salt of ITP (0.17 mmol) yielded over all purification steps 18 mg (23 µmol, 14 %) pure product. R_f = 0.33 (1-propanol:H_2O: NH_3 (32 %) = 2:1:1) HPLC (analytic): R_t = 26.74 min; k = 16.52; LC/MS (ESI, H_2O/CH_3CN): *m/z* = 792.3 [M+NH_4^+] (R_t = 28.02 min, 100 %), 775.2 [M+H^+] (R_t = 28.58 min, 15 %); (-ESI, H_2O/CH_3CN): *m/z* = 773.3 [M-H^-] (R_t = 28.08 min, 100 %); HPLC (preparative), gradient (t [min], % B: [0, 11], [2, 11], [5, 30], [15, 31.5], [18, 80]): R_t = 9.72 min; UV/Vis (H_2O) λ_{max} (log ε) = 251 nm (16,400), 358 nm (6,400); empirical formula: $C_{26}H_{29}N_6O_{16}P_3$; MW = 774.46.

Bis-MANT-CTP (*N*-methyl-2',3'-bis-*O*-anthraniloyl-cytosine-5'-triphosphate) or [(2R,3S,4R,5R)-5-(4-amino-2-oxopyrimidin-1-yl)-2-[[hydroxy-(hydroxy-phosphonooxy- phosphoryl)oxyphosphoryl]oxymethyl]oxolan-3,4-bis-yl]2-methylaminobenzoate

100 mg introduced trisodium salt of CTP (0.18 mmol) yielded 35 mg (46 µmol, 26 %) pure product. R_f = 0.29 (1-propanol:H_2O:NH_3 (32 %) = 2:1:1). HPLC (analytic): R_t = 26.83 min; k = 16.60; LC/MS (ESI, H_2O/CH_3CN): *m/z* = 750.0 [M+H^+] (R_t = 25.37 min, 100 %), 767.1 [M+NH_4^+] (R_t = 25.37 min, 10 %); (-ESI, H_2O/CH_3CN): *m/z* = 748.0 [M-H^-] (R_t = 25.37 min, 100 %); HPLC (preparative), gradient (t [min], % B: [0, 14], [6, 14], [11, 35], [15, 40], [20, 80]): UV/Vis (H_2O) λ_{max} (log ε) = 253 nm (14,500), 359 nm (6,600); R_t = 13.19 min; empirical formula: $C_{25}H_{30}N_5O_{16}P_3$; MW = 749.45.

Bis-Cl-ANT-ATP (2',3'-bis-*O*-5-chloroanthraniloyl-adenosine-5'-triphosphate) or [(2R, 3S,4R,5R)-5-(6-aminopurin-9-yl)-2-[[hydroxy-(hydroxy-phosphonooxyphosphoryl)oxyphosphoryl]oxymethyl]oxolan-3,4-bis-yl]2-amino-5-chlorobenzoate

For the procedure see general prescription. 100 mg (0.18 mmol) introduced disodium salt of ATP yielded 31 mg (38 µmol, 21 %) pure product after

purification. R_f = 0.32 (1-propanol:H_2O:NH_3 (32 %) = 2:1:1). HPLC (analytic): R_t = 27.79 min; k = 17.10; LC/MS (ESI, H_2O/CH_3CN): *m/z* = 831.0 [M+NH_4^+] (R_t = 26.24 min, 100 %), 814.1 [M+H^+] (R_t = 26.24 min, 10 %); (-ESI, H_2O/CH_3CN): *m/z* = 812.0 [M-H^-] (R_t = 26.24 min, 100 %); HPLC (preparative), gradient (t [min], % B: [0, 14], [6, 14], [11, 37], [15, 40], [20, 80]): R_t = 13.26 min; UV/Vis (H_2O) λ_{max} (log ε) = 255 nm (16,900), 350 nm (5,100); empirical formula: $C_{24}H_{24}Cl_2N_7O_{15}P_3$; MW = 814.31.

Bis-Cl-ANT-ITP (2',3'-bis-*O*-5-chloroanthraniloyl-inosine-5'-triphosphate) or [(2R,3S,4R,5R)-5-(6-oxo-1H-purin-9-yl)-2-[[hydroxy-(hydroxy-phosphonooxyphosphoryl)oxyphosphoryl]oxymethyl]oxolan-3,4-bis-yl]2-methyl-5-chloroaminobenzoate

For the procedure see general prescription. 100 mg introduced trisodium salt of ITP (0.17 mmol) yielded over all purification steps 30 mg (37 µmol, 22 %) pure product. R_f = 0.35 (1-propanol:H_2O: NH_3 (32 %) = 2:1:1) HPLC (analytic): R_t = 27.46 min; k = 17.99; LC/MS (ESI, H_2O/CH_3CN): *m/z* = 849.1 [M+NH_4^+] (R_t = 25.90 min, 100 %), 832.0 [M+H^+] (R_t = 25.90 min, 90 %); (-ESI, H_2O/CH_3CN): *m/z* = 830.0 [M-H^-] (R_t: 25.90 min, 100 %); HPLC (preparative), gradient (t [min], % B: [0, 14], [6, 14], [15, 38], [20, 80]): R_t = 15.65 min; UV/Vis (H_2O) λ_{max} (log ε) = 249 nm (19,700), 350 nm (6,200); empirical formula: $C_{24}H_{23}Cl_2N_6O_{16}P_3$; MW = 815.30.

Bis-Br-ANT-ATP (2',3'-bis-*O*-5-bromoanthraniloyl-adenosine-5'-triphosphate) or (2R,3S,4R,5R)-5-(6-aminopurin-9-yl)-2-[[hydroxy-(hydroxy-phosphonooxyphosphoryl)oxyphosphoryl]oxymethyl]oxolan-3,4-bis-yl]2-amino-5-bromobenzoate

For the procedure see general prescription. 100 mg introduced disodium salt of ATP yielded 18 mg (20 µmol, 11 %) pure product after purification. R_f = 0.31 (1- propanol:H_2O:NH_3 (32 %) = 2:1:1). HPLC (analytic): R_t = 26.72 min; k = 16.41; LC/MS (ESI, H_2O/CH_3CN): *m/z* = 920.9 [M+NH_4^+] (R_t = 26.24 min, 100 %), 904.0 [M+H^+] (R_t = 26.24 min, 10 %) (-ESI, H_2O/CH_3CN): *m/z* = 90.9 [M-H^-] (R_t: 26.24 min, 100 %); HPLC (preparative), gradient (t [min], % B: [0, 17], [8, 17], [10, 25], [15, 38], [20, 80]): R_t = 16.14 min; UV/Vis (H_2O) λ_{max} (log ε) = 255 nm (14,600), 348 nm (4,500); empirical

formula: $C_{24}H_{24}Br_2N_7O_{15}P_3$; MW = 903.21.

Bis-Br-ANT-ITP (2',3'-bis-*O*-5-bromoanthraniloyl-inosine-5'-triphosphate) or [(2R,3S,4R,5R)-5-(6-oxo-1H-purin-9-yl)-2-[[hydroxy-(hydroxy-phosphonooxyphosphoryl)oxyphosphoryl]oxymethyl]oxolan-3,4-bis-yl]2-methyl-5-bromoaminobenzoate

For the procedure see general prescription. 100 mg introduced trisodium salt of ITP (0.17 mmol) yielded over all purification steps 32 mg (36 µmol, 21 %) pure product. R_f = 0.33 (1-propanol:H_2O: NH_3 (32 %) = 2:1:1) HPLC (analytic): R_t = 28.16 min; k = 18.47; LC/MS (ESI, H_2O/CH_3CN): *m/z* = 921.9 [$M+NH_4^+$] (R_t = 25.89 min, 100 %), 905.0 [$M+H^+$] (R_t = 25.89 min, 15 %); (-ESI, H_2O/CH_3CN): *m/z* = 903.0 [$M-H^-$] (R_t: 25.89 min, 100 %); HPLC (preparative), gradient (t [min], % B: [0, 18], [15, 38], [20, 80]: R_t = 12.39 min; UV/Vis (H_2O) λ_{max} (log ε) = 249 nm (19,000), 348 nm (5,600);empirical formula: $C_{24}H_{23}Br_2N_6O_{16}P_3$; MW = 904.20.

Bis-Pr-ANT-ATP (*N*-propyl-2',3'-bis-*O*-anthraniloyl-adenosine-5'-triphosphate) or [(2R,3S,4R,5R)-5-(6-aminopurin-9-yl)-2-[[hydroxy-(hydroxy-phosphonooxy phosphoryl)oxyphosphoryl]oxymethyl]oxolan-3,4-bis-yl]2-propylaminobenzoate

For the procedure see general prescription. 100 mg introduced disodium salt of ATP (0.18 mmol) yielded over all purification steps 21 mg (25 µmol, 14 %) pure product. R_f = 0.34 (1-propanol:H_2O: NH_3 (32 %) = 2:1:1) HPLC (analytic): R_t = 33.04 min; k = 20.59; LC/MS (ESI, H_2O/CH_3CN): *m/z* = 830.2 [$M+H^+$] (R_t = 30.63 min, 100 %), 847.2 [$M+NH_4^+$] (R_t = 30.63 min, 30 %); (-ESI, H_2O/CH_3CN): *m/z* = 828.1 [$M-H^-$] (R_t = 30.63 min, 100 %); HPLC (preparative), gradient (t [min], % B: [0, 5], [20, 45], [25, 80]): R_t = 20.14 min; UV/Vis (H_2O) λ_{max} (log ε) = 255 nm (16,800), 359 nm (5,800); empirical formula: $C_{30}H_{37}N_6O_{16}P_3$; MW = 829.58.

Bis-Pr-ANT-ITP (*N*-propyl-2',3'-bis-*O*-anthraniloyl-inosine-5'-triphosphate) or [(2R,3S,4R,5R)-5-(6-oxo-1H-purin-9-yl)-2-[[hydroxy-(hydroxy-phosphonooxyphosphoryl)oxyphosphoryl]oxymethyl]oxolan-3,4-bis-yl]2-propylaminobenzoate

For the procedure see general prescription. 100 mg introduced trisodium salt

of ITP (0.17 mmol) yielded over all purification steps 15 mg (19 µmol, 11 %) pure product. R_f = 0.35 (1-propanol:H_2O: NH_3 (32 %) = 2:1:1) HPLC (analytic): R_t = 30.57 min; k = 20.14; LC/MS (ESI, H_2O/CH_3CN): *m/z* = 848.1 [M+NH_4^+] (R_t = 30.60 min, 100 %), 831.1 [M+H^+] (R_t = 30.60 min, 20 %); (-ESI, H_2O/CH_3CN): *m/z* = 829.1 [M-H^-] (R_t = 30.60 min, 100 %); HPLC (preparative), gradient (t [min], % B: [0, 5], [20, 45], [25, 80]): R_t = 19.58 min; UV/Vis (H_2O) λ_{max} (log ε) = 255 nm (14,600), 359 nm (5,300); empirical formula: $C_{30}H_{37}N_6O_{16}P_3$; MW = 830.57.

Bis-Ac-NH_2-ANT-ATP (2',3'-bis-*O*-5-acetylaminoanthraniloyl-adenosine-5'-triphosphate) or [(2R,3S,4R,5R)-5-(6-aminopurin-9-yl)-2-[[hydroxy-(hydroxy-phosphonooxyphosphoryl)oxyphosphoryl]oxymethyl]oxolan-3,4-bis-yl]2-amino-5-acetylaminobenzoate

For the procedure see general prescription. 100 mg introduced disodium salt of ATP (0.18 mmol) yielded over all purification steps 27 mg (32 µmol, 18 %) pure product. R_f = 0.27 (1-propanol:H_2O: NH_3 (32 %) = 2:1:1) HPLC (analytic): R_t = 20.05 min; k = 12.10; LC/MS (ESI, H_2O/CH_3CN): *m/z* = 860.1 [M+H^+] (R_t = 16.79 min, 100 %), 877.2 [M+NH_4^+] (R_t = 16.79 min, 30 %); (-ESI, H_2O/CH_3CN): *m/z* = 858.1 [M-H^-] (R_t = 16.79 min, 100 %); HPLC (preparative), gradient (t [min], % B: [0, 6], [5, 7], [23, 14], [24, 80], [29, 80]): R_t = 21.49 min; UV/Vis (H_2O) λ_{max} (log ε) = 261 nm (23,500), 350 nm (5,700); empirical formula: $C_{28}H_{32}N_9O_{17}P_3$; MW = 859.53.

Bis-Ac-NH_2-ANT-ITP (2',3'-bis-*O*-5-acetylaminoanthraniloyl-inosine-5'-triphosphate) or [(2R,3S,4R,5R)-5-(6-oxo-1H-purin-9-yl)-2-[[hydroxy-(hydroxy-phosphonooxy- phosphoryl)oxyphosphoryl]oxymethyl]oxolan-3,4-bis-yl]2-amino-5-acetylamino- benzoate

For the procedure see general prescription. 100 mg introduced trisodium salt of ITP (0.17 mmol) yielded over all purification steps 16 mg (19 µmol, 11 %) pure product. R_f = 0.29 (1-propanol:H_2O: NH_3 (32 %) = 2:1:1) HPLC (analytic): R_t = 18.80 min; k = 12.00; LC/MS (ESI, H_2O/CH_3CN): *m/z* = 878.1 [M+NH_4^+] (R_t = 8.85 min, 100 %), 895.1 [M+NH_3+NH_4^+] (R_t = 8.85 min, 35 %), 861.1 [M+H^+] (R_t = 8.85 min, 30 %); (-ESI, H_2O/CH_3CN): *m/z* = 859.1 [M-H^-] (R_t = 8.85 min, 100 %); HPLC (preparative), gradient (t [min], % B: [0, 5.8], [11, 5.8], [12, 10], [18, 13], [20, 80]): R_t = 18.43 min; UV/Vis (H_2O) λ_{max} (log ε) = 259 nm (14,300; shoulder), 348

nm (5,200); empirical formula: $C_{28}H_{31}N_8O_{18}P_3$; MW = 860.51.

3.3 AC activity assay

For the determination of the potency of AC toxin inhibitors, assay tubes contained 10 μl of (bis)-(M)ANT-nucleotides at final concentrations from 10 nM to 100 μM as appropriate to obtain saturated inhibition curves and 20 μl of EF3 or EF3(F586A) (10 pM final concentration) in 75 mM Tris/HCl, pH 7.4, containing 0.1% (m/v) bovine serum albumin. Tubes were preincubated for 2 min at 25°C, and reactions were initiated by the addition of 20 μL of reaction mixture consisting of the following components to yield the given final concentrations; 100 mM KCl, 10 μM free Ca^{2+}, 5 mM free Mn^{2+}, 100 μM EGTA, 100 μM cAMP, 100 nM CaM. ATP was added as non-labeled substrate at a final concentration of 40 μM and as radioactive tracer [α–^{32}P]ATP (0.2 μCi/tube). For the determination of K_m and V_{max} values, 10 μM to 1 mM ATP/Mn^{2+} were added, instead of inhibitor, plus 5 mM of free Mn^{2+}, respectively. Tubes were incubated for 10 min at 25°C, and reactions were stopped by the addition of 20 μL of 2.2 N HCl. Denaturated protein was sedimented by a 1-min centrifugation at 13,000 x g. [^{32}P]cAMP was separated from [α–^{32}P]ATP by transferring the samples to columns containing 1.4 g of neutral alumina. [^{32}P]cAMP was eluted by the addition of 4 ml of 0.1 M ammonium acetate solution, pH 7.0. Blank values were about 0.02% of the total amount of [α–^{32}P]ATP added; substrate turnover was < 3% of the total amount of [α–^{32}P]ATP added. Samples collected in scintillation vials were filled up with 10 ml of double-distilled water and Čerenkov radiation was measured in a PerkinElmer Tricarb 2800TR liquid scintillation counter. Free concentrations of divalent cations were calculated with WinMaxC (http://www.stanford.edu/~cpatton/maxc.html). K_i values reported in Tables 1, 2 and 3 were calculated using the Prism 4.02 software (Graphpad, San Diego, CA, USA).

For determination of the potency of AC toxin inhibitors at various EF3 mutants (H577A, N583A, N583Q, N583H, K353A and K353R), the experiments were essentially performed as described for EF3 with some modifications. Specifically, the final enzyme concentrations were increased up to 2 nM in order to account for the lower catalytic activity of the mutants. Moreover, the reaction time

was prolonged to 20 min at 30°C. For the determination of V_{max} and K_m, the ATP/Mn^{2+} concentration ranged from 100 μM to 4 mM. The higher substrate concentrations compared to EF were essential in order to obtain saturated enzyme kinetics

For studying of the inhibition mechanism of the EF3 by Bis-MANT-nucleotides, enzyme saturation experiments were performed in the presence of various inhibitor concentrations as shown in Fig. 3. Assay tubes contained Bis-MANT-nucleotides at final concentrations from 0.5 μM to 10 μM as appropriate according to the potency of the inhibitor. For the basal saturation curve 5 μl of double-distilled water was added instead of the inhibitor. Next, 5 μl of 50 μM to 600 μM ATP/Mn^{2+}, plus 20 μl of 10 pM EF3 in 75 mM Tris/HCl, pH 7.4, containing 0.1% (m/v) bovine serum albumin were added. Tubes were preincubated for 2 min at 25°C, and reactions were initiated by the addition of 20 μL of reaction mixture consisting of the following components to yield the given final concentrations; 100 mM KCl, 10 μM free Ca^{2+}, 5 mM free Mn^{2+}, 100 μM EGTA, 100 μM cAMP, 100 nM CaM, and [α–^{32}P]ATP (0.2 μCi/tube).

3.5 Fluorescence resonance energy transfer (FRET) experiments for monitoring inhibitor binding to EF3 and various EF3 mutants

Fluorescence experiments were performed using quartz UV ultra-microcuvettes from Hellma (Müllheim, Germany, type 105.251- QS, light path length 3 x 3 mm, center 15 mm, total volume 70 μl and type 105.250- QS, light path length 10 x 2 mm, center 15 mm, total volume 150 μl) in a thermostated multicell holder at 25°C in a Varian Cary Eclipse fluorescence spectrometer (Varian, Darmstadt, Germany). In case of 150 μl cuvettes, 140 μl of buffer consisting of 100 mM KCl, 100 μM $CaCl_2$, 10 mM $MnCl_2$ and 25 mM HEPES/NaOH, pH 7.4, was added into the cuvette. Five μl of 10 μM EF3/EF3 mutants (final concentration 300 nM), 5 μl of 10 μM CaM (final concentration 300 nM) and Bis-MANT-ATP or Bis-MANT-CTP (300 nM each) were added. In case of experiments with 70 μl cuvettes, volumes were adjusted stoichiometrically. The results obtained with 70 μl- and 150 μl-cuvettes were identical, with the 70 μl-cuvettes offering an opportunity to save EF3/EF3 mutants proteins.

Steady-state fluorescence emission spectra of nucleotides were recorded at low speed in the scan mode from λ_{em} 300 nm to 550 nm with λ_{ex} 280 nm. Fluorescence recordings were analyzed with the spectrum package of the Varian Cary Eclipse software version 1.1. Baseline fluorescence (buffer alone) and the baseline-corrected nucleotide-dependent emission of each concentration of the ligand (buffer + nucleotide) were subtracted from the spectra shown in panel **A** and **B** of Figs. (4-11). In the competition experiments shown in Fig. 13, bis-MANT-nucleotides were displaced from the EF3 catalytic site using PMEApp.

In direct fluorescence experiments, bis-MANT-nucleotides were excited at λ_{ex} 350 nm and emission spectra were recorded from 380 nm to 550 nm. For an estimation of the hydrophobic properties of the binding site interacting with the MANT-group shown in Fig. 12, direct fluorescence control experiments of the bis-MANT-nucleotides were conducted in the presence of dimethyl sulfoxide ranging from 0 to 100% (v/v).

3.6 Data analysis

All monophasic inhibition and saturation curves summarized in Table 1, 2 and 3 were analyzed by non-linear regression using the Prism 4.0 software (Graphpad, San Diego, CA, USA). Fluorescence spectra were analyzed using the spectrum package of the Varian Cary Eclipse 1.1 software. For the generation of graphs shown in Figs. (4-13), fluorescence data were imported into the Prism software.

4. Results

4.1 Inhibition of the catalytic activity of EF3 by Bis-MANT-nucleotides

The K_i values of various mono- and bis-MANT-NTPs and NMP at EF3 in the presence of Mn^{2+} are summarized in Table 1. In general, the inhibitory potencies of MANT-nucleotides were lower than those of the corresponding bis-MANT-nucleotides except for the base cytosine. For example, Bis-MANT-ATP was 3-fold more potent than MANT-ATP. In contrast, Bis-MANT-CTP was 2-fold less potent than MANT-CTP. Moreover, Bis-MANT-NTPs were more potent than Bis-MANT-NMP. The most striking results was the higher potency of both Bis-MANT-ATP and Bis-MANT-CTP among the studied compounds

Table 1: Inhibitory potencies of Mono- and Bis-MANT-nucleotides at EF3 in the presence of Mn^{2+}

Nucleotides	Mono - K_i (µM)	Bis - K_i (µM)
MANT -ATP	0.58 ± 0.13	0.21 ± 0.02
MANT -CTP	0.11 ± 0.04	0.21 ± 0.01
MANT -ITP	5.90 ± 0.69	4.42 ± 0.2
MANT -IMP	35.60 ± 0.13	8.66 ± 0.14

Inhibitory potencies of various mono- and bis-MANT-nucleotides at EF3 were determined as described under “Materials and Methods”. K_i values are given in µM and are the means ± SD of 3-4 independent experiments performed in triplicates. The K_m value of EF3 for ATP in the presence of Mn^{2+} was 82.6 ± 8.2 µM. Reaction mixtures contained 5 mM $MnCl_2$ or 5 mM $MgCl_2$, 100 mM KCl, 10 µM free Ca^{2+}, 40 µM ATP, [α–^{32}P]ATP (0.2-0.4 µCi/tube), 100 µM cAMP and 100 nM CaM. Nucleotides were added at different concentrations as appropriate to construct saturated concentration-response curves. Inhibition curves were analyzed by non-linear regression using the Prism 4.02 software.

4.2 Inhibition of the catalytic activity of EF, EF3 and various EF3 mutants by Bis-MANT-nucleotides

Table 2 summarizes the K_i values of Bis-MANT-ATP and Bis-MANT-CTP at EF3 and EF3 mutants (H577A, N583A, N583Q, N583H, K353A and K353R) in the presence of Mn^{2+}. Both Bis-MANT-ATP and Bis-MANT-CTP possesses the same inhibitory potencies at EF3. The F586A mutation reduced the inhibitory potencies of Bis-MANT-ATP and Bis-MANT-CTP by 5-6-fold, whereas the H577A mutation did not decrease inhibitor potency. The N583A mutation decreased nucleotide-potency by 6-12-fold. The N583Q substitution reduced the potency of Bis-MANT-ATP by 60-fold and the potency of Bis-MANT-CTP by 120-fold. For the N583H mutant, a 130-230-fold decrease in potency of Bis-MANT-ATP and Bis-MANT-CTP was observed. The K353A substitution reduced the potency of Bis-MANT-ATP and Bis-MANT-CTP by 40-50-fold. The Ki value of Bis-MANT-ATP and Bis-MANT-CTP at EF3(K353R) increased about just 3-fold. The relative potencies of Bis-MANT-ATP and Bis-MANT-CTP at various EF3/EF3 mutants are represented in Fig. 2 taking EF3 as a reference. It is clear that both Bis-MANT-ATP and Bis-MANT-CTP behaved similarly at EF3 and various EF3 mutants. In addition, both F586 and K353 amino acid residues that located at EF3 binding site are critical for Bis-MANT-ATP and Bis-MANT-CTP binding.

Fig. 3 shows the double-reciprocal analysis of EF3 inhibition kinetics by Bis-MANT-ATP and Bis-MANT-CTP according to Lineweaver-Burk. The linear regression lines intersected at the y-axis, i.e. V_{max} remained constant, whereas K_m increased with increasing inhibitor concentration.

Table 2: Inhibitory potencies of Bis-MANT-ATP and Bis-MANT-CTP at EF, EF3 and EF3 mutants in the presence of Mn^{2+}

Toxin	Bis-MANT-ATP K_i (µM)	Bis-MANT-ATP rel. pot.	Bis-MANT-CTP K_i (µM)	Bis-MANT-CTP rel. pot.
EF_3 wild type	0.21± 0.02	100	0.21 ± 0.005	100
EF_3 F586A	1.65 ± 0.08	12.73	1.19 ± 0.001	17.65
EF_3 H577A	0.19 ± 0.02	110.53	0.17 ± 0.026	123.53
EF_3 N583A	1.29 ± 0.02	16.28	2.57 ± 0.029	8.17
EF_3 N583Q	16.38 ± 0.14	1.28	24.49 ± 0.32	0.86
EF_3 N583H	46.30 ± 17.95	0.45	27.68 ± 0.47	0.76
EF_3 K353A	9.90 ± 0.24	2.12	7.96 ± 0.15	2.64
EF_3 K353R	0.51 ± 0.001	41.18	0.50 ± 0.001	42

Inhibitory potencies of Bis-MANT-ATP and Bis-MANT-CTP at EF, EF3 and various EF3 mutants were determined as described under "Materials and Methods". K_i-values are given in µM and are the means ± SD of 3 experiments performed in triplicates. The relative potencies (rel. pot.) of Bis-MANT-ATP and Bis-MANT-CTP are given, too, EF3 being the reference. For determination of the inhibitory potencies of Bis-MANT-ATP and Bis-MANT-CTP at EF, EF3 and EF3(F586A), reaction mixtures contained 10 µM free Ca^{2+}, 5 mM free Mn^{2+}, 100 µM EGTA, 40 µM ATP, 0.2 µCi/tube [α–^{32}P]ATP, 100 µM cAMP, 100 nM CaM and 10 pM enzyme in 75 mM Tris/HCl, pH 7.4. For other EF3 mutants, reaction mixtures contained 0.4 µCi [α–^{32}P]ATP per tube. The enzyme concentration was 2 nM. Nucleotides were added at different concentrations as appropriate to obtain saturated concentration-response curves. Inhibition curves were analyzed by non-linear regression using the Prism 4.02 software.

Fig. 2: Inhibitory potencies of Bis-MANT-ATP and Bis-MANT-CTP at EF3 and various EF3 mutants

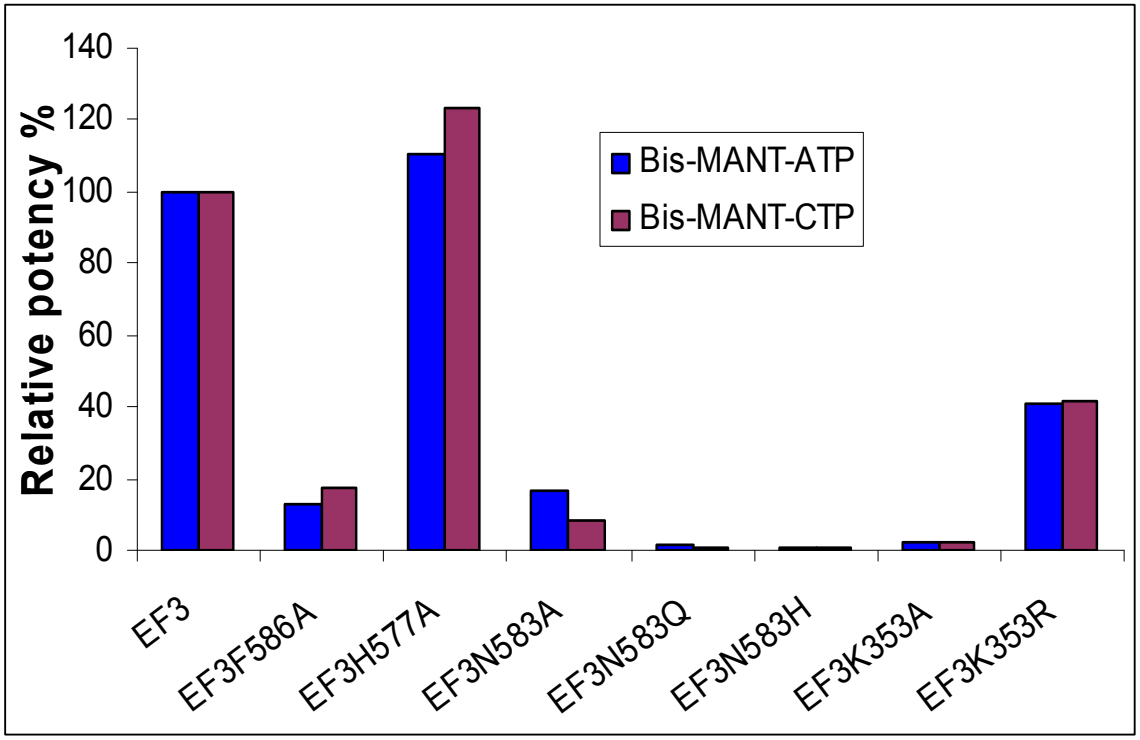

The relative potencies (rel. pot.) of Bis-MANT-ATP (*blue columns*) and Bis-MANT-CTP (*purple columns*) are shown, too, EF3 being the reference. For determination of the inhibitory potencies of Bis-MANT-ATP and Bis-MANT-CTP at EF, EF3 and EF3(F586A), reaction mixtures contained 10 µM free Ca^{2+}, 5 mM free Mn^{2+}, 100 µM EGTA, 40 µM ATP, 0.2 µCi/tube [α–^{32}P]ATP, 100 µM cAMP, 100 nM CaM and 10 pM enzyme in 75 mM Tris/HCl, pH 7.4. For other EF3 mutants, reaction mixtures contained 0.4 µCi [α–^{32}P]ATP per tube. The enzyme concentration was 2 nM. Nucleotides were added at different concentrations as appropriate to obtain saturated concentration-response curves. Inhibition curves were analyzed by non-linear regression using the Prism 4.02 software.

4.3 Inhibition of the catalytic activity of EF3 by various mono- and bis-(propyl)(M)ANT-nucleotides

Table 3 summarizes the K_i values of mono- and bis- propyl-ANT-NTPs and various mono-and bis-MANT-NTPs (substituted at position number 5 of the anthraniloyl ring) at EF3 in the presence of Mn^{2+}. In general, ATP-analogues were about 2-fold more potent than the corresponding ITP-analogues. Moreover, the inhibitory potencies of position-5-substituted-MANT-nucleotides were slightly higher than those of the corresponding bis-MANT-nucleotides. Propyl-ANT-nucleotides were more potent than the corresponding Bis-propyl-ANT-analogues. For example, propyl-ANT-ATP was 13-fold more potent than Bis-propyl-ANT-ATP.

4.4 Direct fluorescence and FRET studies of bis-MANT-nucleotides with EF3

Tryptophan (and tyrosine) residues in proteins are excited at an excitation wavelength of 280 nm (18, 19, 23), resulting in substantial endogenous fluorescence of EF3 with an emission maximum of λ_{em} 350 nm (22) which can then excite the (M)ANT group of nucleotides (26), provided sufficient proximity between donor and acceptor. Such energy transfer results in increased fluorescence of the MANT-group at 420-450 nm in mAC, CyaA and EF3 reflecting the fact that the MANT-group is in a hydrophobic environment (23, 27-29). Previous studies with mAC showed that in the presence of Mn^{2+}, FRET signals were much larger than in the presence of Mg^{2+}(27). All subsequent FRET studies with EF3 were conducted in the presence of Mn^{2+} (see Materials and Methods).

At λ_{ex} 280 and 350 nm, bis-MANT-nucleotides exhibited only minimal endogenous fluorescence, providing an excellent signal-to-noise ratio for FRET studies. In the absence of CaM, EF3/EF3 mutants exhibit a strong emission peak at 350 nm when excited at 280 nm under steady-state conditions (panels A and B of Figs. 4-11). Following the addition of CaM, with Bis-MANT-nucleotides examined, new fluorescence peaks with a maximum of λ_{em} 425–430 nm became apparent. These new peaks reflect FRET from tryptophan and tyrosine residues to the MANT group and were the result of the substantial CaM-induced conformational change in EF (4, 23).

Table 3: Inhibitory potencies of mono- and bis-ANT-nucleotides at EF3 in the presence of Mn^{2+}

Nucleotides	K_i (µM)	Nucleotides	K_i (µM)
Propyl-ANT-ATP	**0.08 ± 0.01**	**Propyl-ANT-ITP**	**0.2 ± 0.02**
Bis- Propyl-ANT-ATP	**1.02 ± 0.15**	**Bis- Propyl-ANT-ITP**	**1.9 ± 0.01**
Br-ANT-ATP	**0.20 ± 0.01**	**Br-ANT-ITP**	**0.4 ± 0.25**
Bis-Br-ANT-ATP	**0.26 ± 0.04**	**Bis-Br-ANT-ITP**	**0.5 ± 0.1**
Cl-ANT-ATP	**0.17 ± 0.02**	**Cl-ANT-ITP**	**0.3 ± 0.05**
Bis-Cl-ANT-ATP	**0.22 ± 0.02**	**Bis-Cl-ANT-ITP**	**0.4 ± 0.09**
AC-NH-ANT-ATP	**0.55 ± 0.01**	**AC-NH-ANT-ITP**	**1.0 ± 0.13**
Bis-AC-NH-ANT-ATP	**0.67 ± 0.03**	**Bis-AC-NH-ANT-ITP**	**1.3 ± 0.25**

Inhibitory potencies of various newly synthesized mono- and bis-ANT-nucleotides at EF3 were determined as described under "Materials and Methods". K_i values are given in µM and are the means ± SD of 3 independent experiments performed in triplicates. The K_m value of EF3 for ATP in the presence of Mn^{2+} was 82.6 ± 8.2 µM. Reaction mixtures contained 10 µM free Ca^{2+}, 5 mM free Mn^{2+}, 100 µM EGTA, 40 µM ATP, 0.2 µCi/tube [α–^{32}P]ATP, 100 µM cAMP, 100 nM CaM and 10 pM enzyme in 75 mM Tris/HCl, pH 7.4. Nucleotides were added at different concentrations as appropriate to obtain saturated concentration-response curves. Inhibition curves were analyzed by non-linear regression using the Prism 4.02 software.

Interestingly, In the FRET experiments of Bis-MANT-ATP and Bis-MANT-CTP, we found a good relation between the maximum intensity of the FRET signal in the FRET assay and the K_i values in the AC assay; i.e., the higher the intensity of the FRET signal, the higher the affinity of the probed Bis-MANT-nucleotides to the binding sites of the EF3/EF3mutants and vice versa. Also, it is noteworthy that the FRET signal with Bis-MANT-CTP was moderately smaller than with Bis-MANT-ATP. Our previous study of EF3/EF3 mutants with MANT-nucleotides showed that in presence of Mn^{2+}, FRET signal with MANT-CTP was moderately smaller than with MANT-ATP (23). These differences in fluorescence were not due to the endogenous differences in responsiveness to hydrophobic environments between nucleotides since hydrophobic environments in the presence of dimethyl sulfoxide ranging from 0 to 100% (v/v) yielded similar relative fluorescence increases with the Bis-MANT-ATP and Bis-MANT-CTP Fig. 12.

In FRET experiments of EF3 (Fig. 4, **A** and **B**) and various EF3 mutants (Figs. 5-11, **A** and **B**) with bis-MANT-.nucleotides, the signal intensities of endogenous tryptophan and tyrosine fluorescence were similar. The mutations F586A, H577A, N586A, N583Q, N583H and K353A differentially alter the FRET signals intensities (difference in fluorescence at an emission wavelength of 427 nm in the presence and absence of calmodulin) of Bis-MANT-ATP and Bis-MANT-CTP. In EF3(F586A), the FRET signal was reduced by 23% (Fig. 5**A**) with Bis-MANT-ATP and 17% With Bis-MANT-CTP (Fig. 5**B**). Moreover, the FRET signal of Bis-MANT-ATP and Bis-MANT-CTP was reduced by 41% and 15% in EF3(N583A) (Fig. 7**A** and **B**). In addition, in EF3(N583Q) and EF3(K353A), the FRET signals with Bis-MANT-ATP were reduced by 45% and 27% (Figs. 8**A** and 10**A**), while with Bis-MANT-CTP no FRET signal was observed (8**B** and 10**B**). The analysis of the EF3 mutants H577A and N583H with Bis-MANT-ATP and Bis-MANT-CTP revealed no FRET at all (Figs. 6 and 9, **A** and **B**), while in K353R mutant, the FRET signal was similar to that in EF3 (Fig. 11, **A** and **B**).

In a classic FRET experiment, the appearance of the new emission peak at λ_{em} 425–430 nm should be accompanied by a corresponding decrease in the endogenous tryptophan- and tyrosine-fluorescence peak at λ_{em} 350 nm (18, 19, 30). However, for bis-MANT-nucleotides, the appearance of the fluorescence peak at λ_{em}

425–430 nm was not accompanied by a decrease at λ_{em} 350 nm. These findings are explained by a model in which part of the endogenous tryptophan and tyrosine fluorescence of EF3 is quenched by surrounding polar amino acids such as aspartate, glutamate and histidine (23, 30). Upon EF3 activation by CaM, a large conformational change in EF3 occurs (4, 23), annihilating, to a large extent, the quenching effects of polar amino acids and masking the predicted decrease in fluorescence at λ_{em} 350 nm.

We also examined the direct bis-MANT-nucleotide fluorescence by using an excitation wavelength of λ_{ex} 350 nm (Figs. 4–11, **C** and **D**) (4, 21-23). At λ_{ex} 350 nm, Bis-MANT-nucleotides exhibited a very low endogenous fluorescence with a maximum at λ_{em} 445-450 nm. Bis-MANT-ATP and Bis-MANT-CTP did not differ from each other in their endogenous fluorescence properties. Moreover, the addition of EF3 to samples did not significantly change this basal fluorescence. However, upon addition of CaM, we observed very large increases in the intensity of the fluorescence signals, about 6-7-fold with Bis-MANT-ATP and 2-3-fold with Bis-MANT-CTP at λ_{em} 440 nm.

In EF3(F586A), the emission maximum at λ_{em} 440 nm was reduced by 35% (Fig. 5**C**) with Bis-MANT-ATP and 15% with Bis-MANT-CTP (Fig. 5**D**). Moreover, the Fluorescence signal of Bis-MANT-ATP and Bis-MANT-CTP was reduced by 50% and 22% in EF3(N583A) (Fig. 7**C** and **D**). In addition, in EF3(N583Q) and EF3(K353A), the fluorescence signals with Bis-MANT-ATP were reduced by 57% and 43% (Figs. 8**C** and 10**C**), while with Bis-MANT-CTP were reduced by 44% and 28% (8D and 10D) respectively. The analysis of the EF3 mutants H577A and N583H with Bis-MANT-ATP and Bis-MANT-CTP at an excitation wavelength λ_{ex} 350 revealed a large reduction in the intensity of fluorescence signal (60%-90%) at λ_{em} 440 (Figs. 6 and 9, **C** and **D**). In the K353R mutant, the fluorescence signal was nearly the same as in case of EF3 (Fig. 11, **A** and **B**).

Increases in direct fluorescence were accompanied by decreases of the emission maximum by about 5 nm, referred to as blue-shift, reflecting transfer of the MANT group into a more hydrophobic environment (21, 23). Previous studies have already shown that MANT-nucleotides are highly sensitive at detecting small

differences in the interaction of ligands with the catalytic site of bacterial AC toxins including EF and mammalian AC (18-20, 23).

Fig. 3: Lineweaver-Burk analysis of the inhibition of EF3 AC activity by Bis-MANT-ATP and Bis-MANT-CTP.

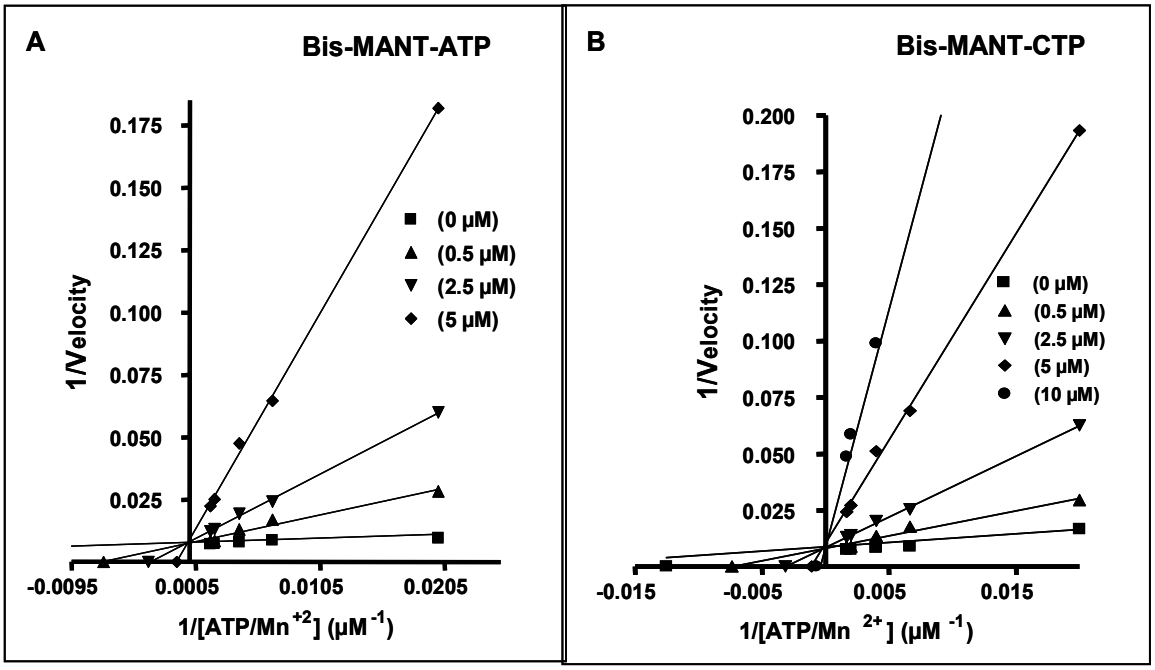

AC activities were determined as described under "Materials and Methods" with the indicated concentrations of Bis-MANT-ATP (0 µM, 0.5 µM, 2.5 µM and 5 µM) (**A**) and MANT-CTP (0 µM, 0.5 µM, 2.5 µM, 5 µM and 10 µM) (**B**). Reaction mixtures contained 10 pM EF3, 100 mM KCl, 10 µM free Ca^{2+}, 5 mM free Mn^{2+}, 100 µM EGTA, 100 µM cAMP, 100 nM calmodulin, 0.2 µCi/tube [α–^{32}P]ATP and unlabeled ATP/Mn^{2+} concentrations indicated in the graph. Data were plotted reciprocally and analyzed by linear regression according to Lineweaver-Burk. Shown are the results of a representative experiment performed in triplicates. Similar results were obtained in two independent experiments.

Fig. 4: Analysis of the interaction of EF3 with Bis-MANT-ATP and Bis-MANT-CTP in fluorescence experiments

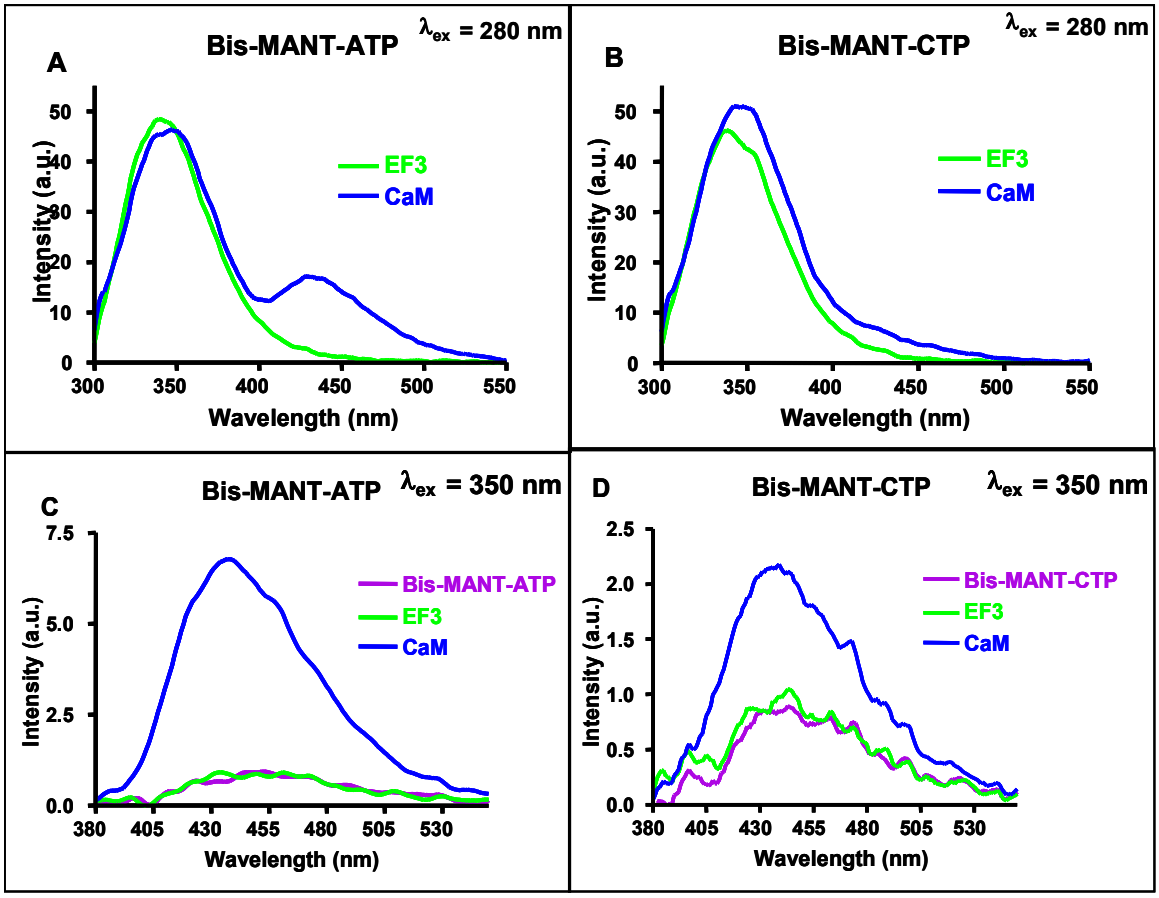

FRET and direct fluorescence experiments were performed as described under "Materials and Methods". The assay buffer consisted of 75 mM HEPES/NaOH, 100 μM $CaCl_2$, 100 mM KCl and 5 mM $MnCl_2$, pH 7.4. Nucleotides were added to the buffer to yield 300 nM final concentrations. EF3 (300 nM final concentration) was added followed by the addition of CaM (1 μM final concentration). Steady state emission spectra were recorded. In FRET studies (panels **A** and **B**) emission was scanned at an excitation wavelength of 280 nm after each addition. In direct fluorescence studies (panels **C** and **D**) emission was scanned at an excitation wavelength of 350 nm after each addition. In panels **A and B,** the buffer and the MANT-nucleotide basal fluorescence were subtracted from the fluorescence after addition of EF3 (*green* line) and CaM (*blue* line). Shown are superimposed recordings of a representative experiment. Similar data were obtained in 5 independent experiments. a.u., arbitrary unit.

Fig. 5: Analysis of the interaction of EF3(F586A) with Bis-MANT-ATP and Bis-MANT-CTP in fluorescence experiments

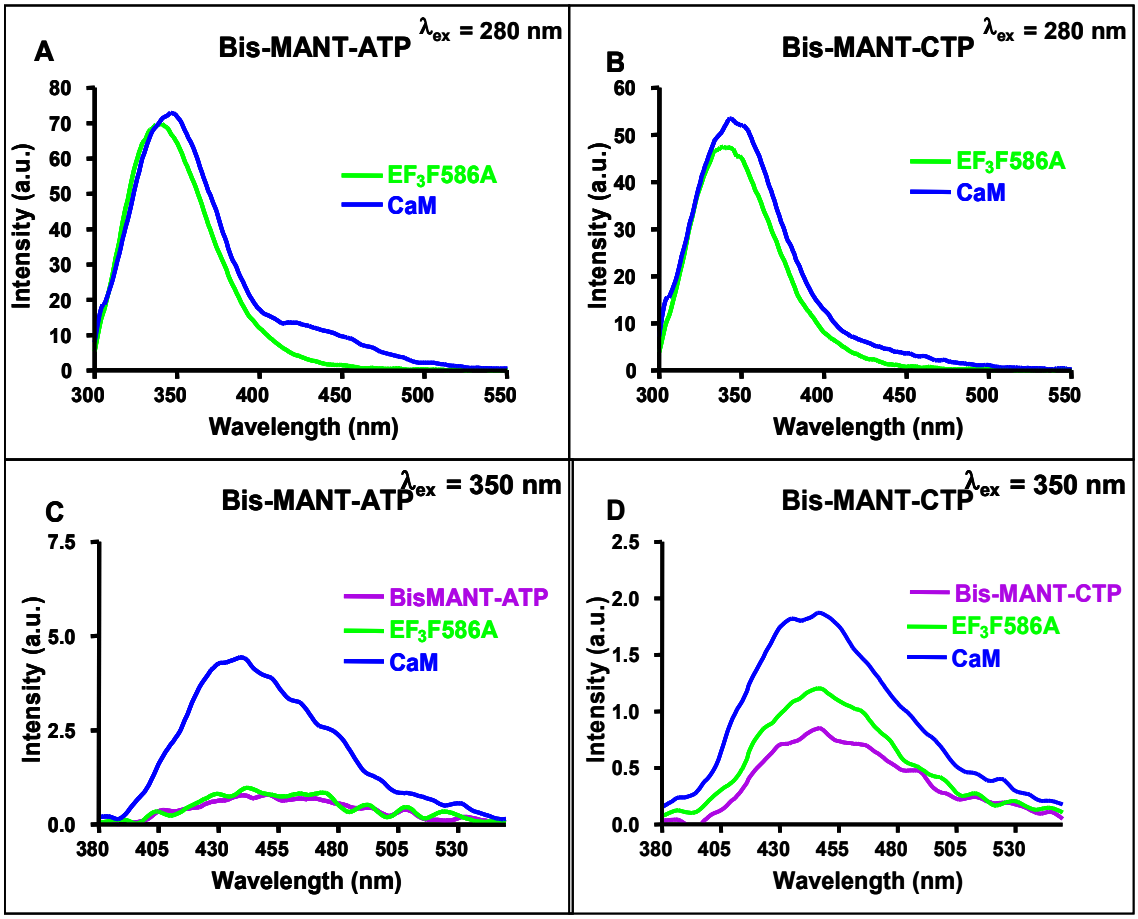

FRET and direct fluorescence experiments were performed as described under "Materials and Methods". The assay buffer consisted of 75 mM HEPES/NaOH, 100 μM $CaCl_2$, 100 mM KCl and 5 mM $MnCl_2$, pH 7.4. Nucleotides were added to the buffer to yield 300 nM final concentrations. EF3(F586A) (300 nM final concentration) was added followed by the addition of CaM (1 μM final concentration). Steady state emission spectra were recorded. In FRET studies (panels **A** and **B**) emission was scanned at an excitation wavelength of 280 nm after each addition. In direct fluorescence studies (panels **C** and **D**), emission was scanned at an excitation wavelength of 350 nm after each addition. In panels **A and B,** the buffer and the MANT-nucleotide basal fluorescence were subtracted from the fluorescence after addition of EF3(F586A) (*green* line) and CaM (*blue* line). Shown are superimposed recordings of a representative experiment. Similar data were obtained in 5 independent experiments. a.u., arbitrary unit.

Fig. 6: Analysis of the interaction of EF3(H577A) with Bis-MANT-ATP and Bis-MANT-CTP in fluorescence experiments

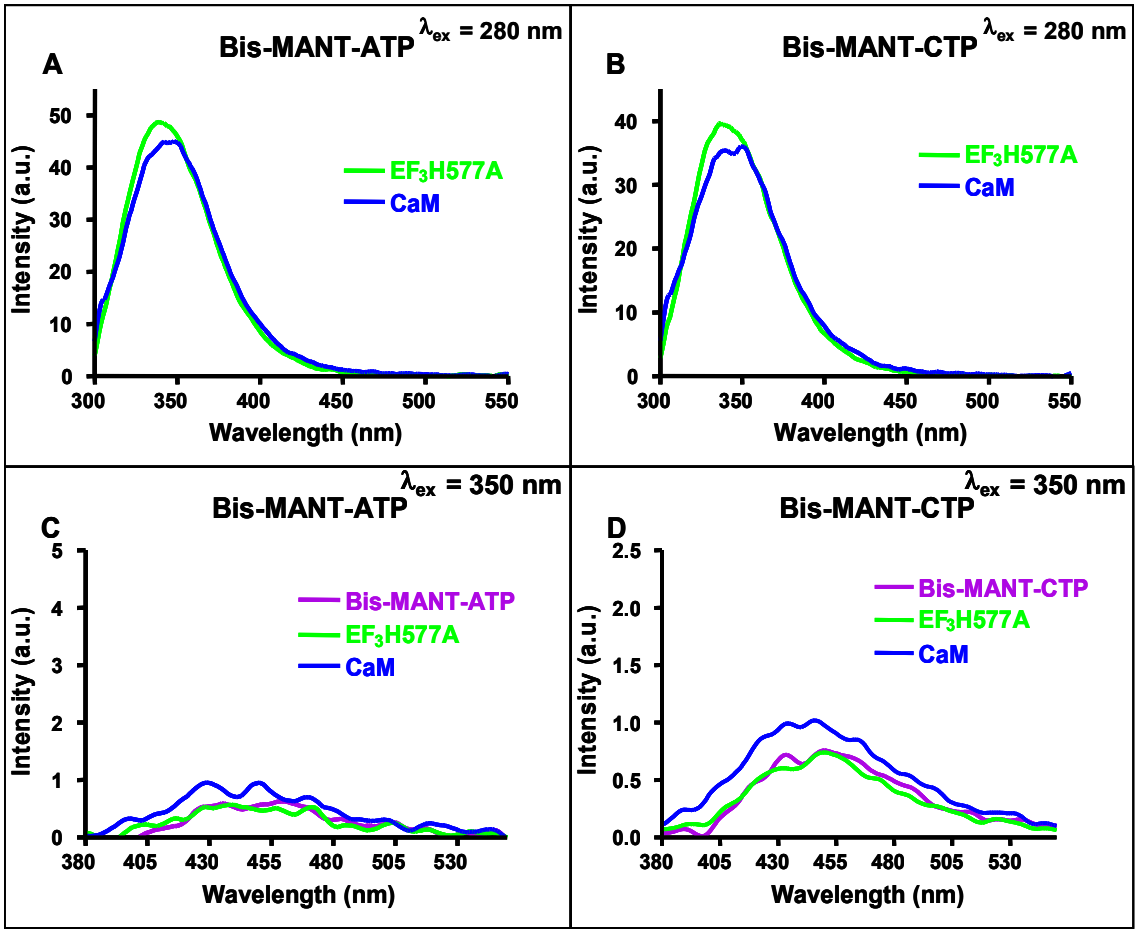

FRET and direct fluorescence experiments were performed as described under "Materials and Methods". The assay buffer consisted of 75 mM HEPES/NaOH, 100 μM $CaCl_2$, 100 mM KCl and 5 mM $MnCl_2$, pH 7.4. Nucleotides were added to the buffer to yield 300 nM final concentrations. EF3(H577A) (300 nM final concentration) was added followed by the addition of CaM (1 μM final concentration). Steady state emission spectra were recorded. In FRET studies (panels **A** and **B**) emission was scanned at an excitation wavelength of 280 nm after each addition. In direct fluorescence studies (panels **C** and **D**), emission was scanned at an excitation wavelength of 350 nm after each addition. In panels **A and B,** the buffer and the MANT-nucleotide basal fluorescence were subtracted from the fluorescence after addition of EF3(H577A) (*green* line) and CaM (*blue* line). Shown are superimposed recordings of a representative experiment. Similar data were obtained in 5 independent experiments. a.u., arbitrary unit.

Fig. 7: Analysis of the interaction of EF3(N583A) with Bis-MANT-ATP and Bis-MANT-CTP in fluorescence experiments

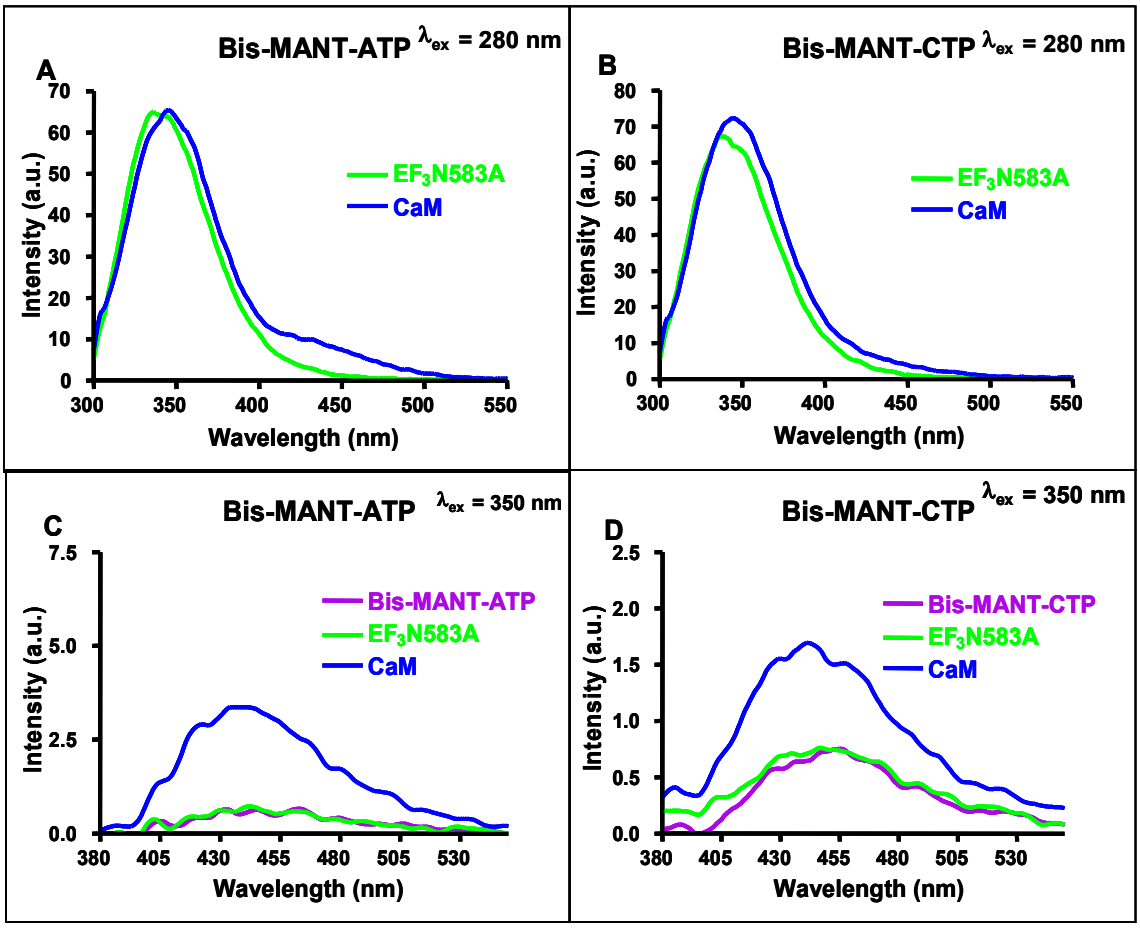

FRET and direct fluorescence experiments were performed as described under "Materials and Methods". The assay buffer consisted of 75 mM HEPES/NaOH, 100 μM $CaCl_2$, 100 mM KCl and 5 mM $MnCl_2$, pH 7.4. Nucleotides were added to the buffer to yield 300 nM final concentrations. EF3(N583A) (300 nM final concentration) was added followed by the addition of CaM (1 μM final concentration). Steady state emission spectra were recorded. In FRET studies (panels **A** and **B**) emission was scanned at an excitation wavelength of 280 nm after each addition. In direct fluorescence studies (panels **C** and **D**), emission was scanned at an excitation wavelength of 350 nm after each addition. In panels **A and B,** the buffer and the MANT-nucleotide basal fluorescence were subtracted from the fluorescence after addition of EF3(N583A) (*green* line) and CaM (*blue* line). Shown are superimposed recordings of a representative experiment. Similar data were obtained in 5 independent experiments. a.u., arbitrary unit.

Fig. 8: Analysis of the interaction of EF3(N583Q) with Bis-MANT-ATP and Bis-MANT-CTP in fluorescence experiments

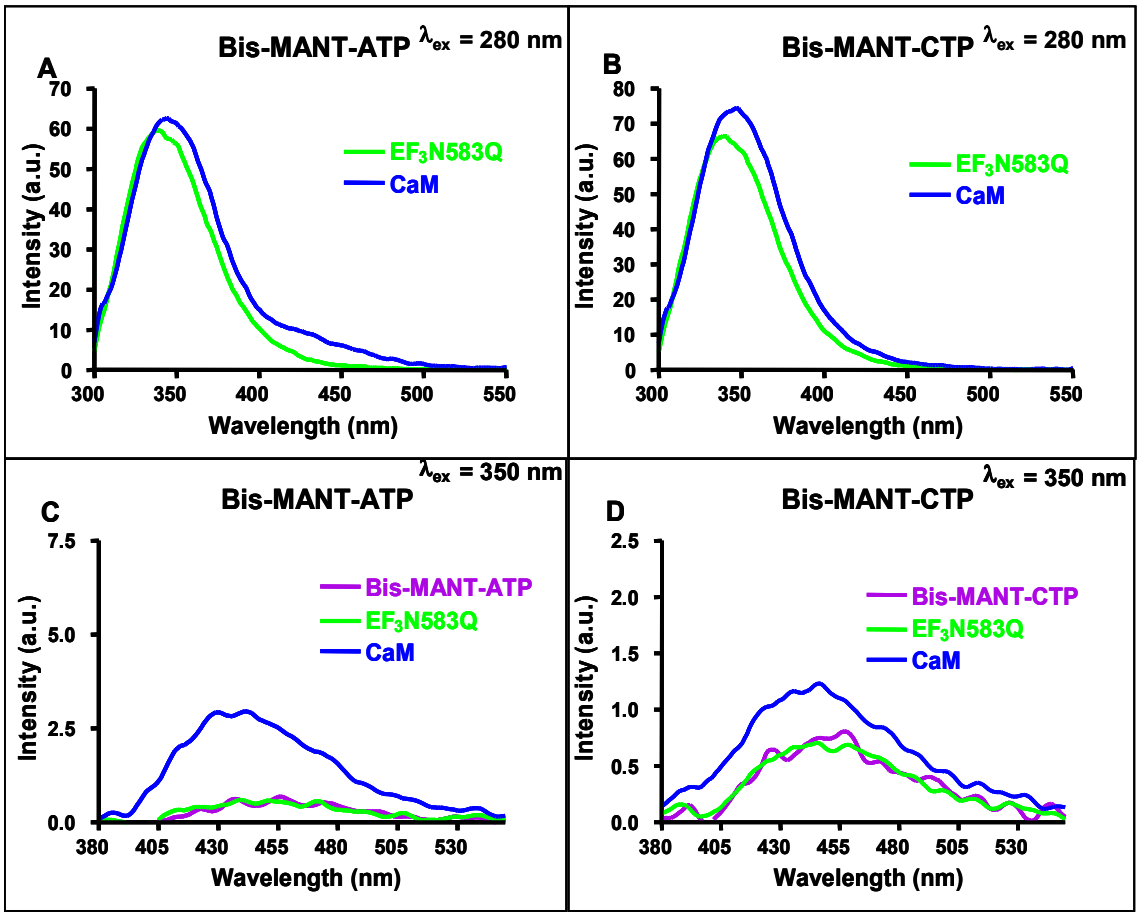

FRET and direct fluorescence experiments were performed as described under "Materials and Methods". The assay buffer consisted of 75 mM HEPES/NaOH, 100 μM $CaCl_2$, 100 mM KCl and 5 mM $MnCl_2$, pH 7.4. Nucleotides were added to the buffer to yield 300 nM final concentrations. EF3(N583Q) (300 nM final concentration) was added followed by the addition of CaM (1 μM final concentration). Steady state emission spectra were recorded. In FRET studies (panels **A** and **B**) emission was scanned at an excitation wavelength of 280 nm after each addition. In direct fluorescence studies (panels **C** and **D**), emission was scanned at an excitation wavelength of 350 nm after each addition. In panels **A and B,** the buffer and the MANT-nucleotide basal fluorescence were subtracted from the fluorescence after addition of EF3(N583Q) (*green* line) and CaM (*blue* line). Shown are superimposed recordings of a representative experiment. Similar data were obtained in 5 independent experiments. a.u., arbitrary unit.

Fig. 9: Analysis of the interaction of EF3(N583H) with Bis-MANT-ATP and Bis-MANT-CTP in fluorescence experiments

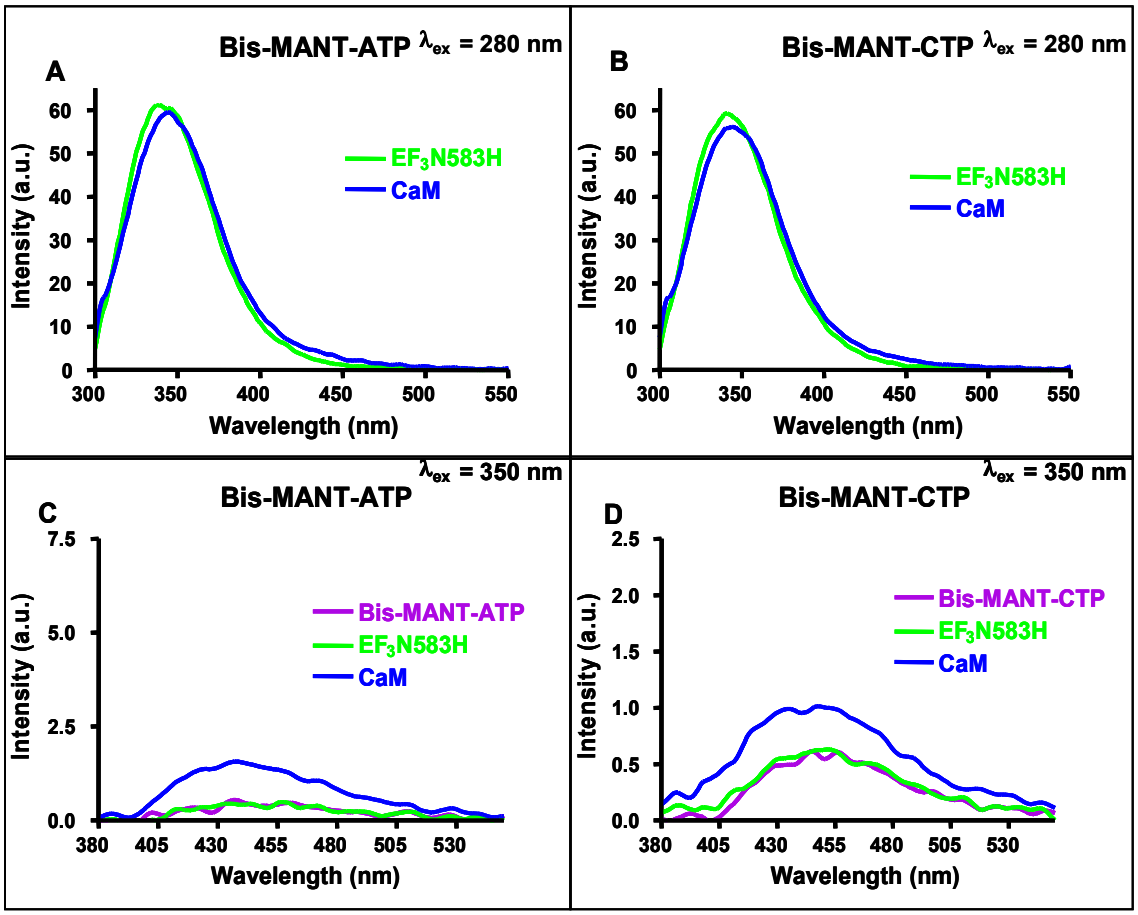

FRET and direct fluorescence experiments were performed as described under "Materials and Methods". The assay buffer consisted of 75 mM HEPES/NaOH, 100 μM $CaCl_2$, 100 mM KCl and 5 mM $MnCl_2$, pH 7.4. Nucleotides were added to the buffer to yield 300 nM final concentrations. EF3(N583H) (300 nM final concentration) was added followed by the addition of CaM (1 μM final concentration). Steady state emission spectra were recorded. In FRET studies (panels **A** and **B**) emission was scanned at an excitation wavelength of 280 nm after each addition. In direct fluorescence studies (panels **C** and **D**), emission was scanned at an excitation wavelength of 350 nm after each addition. In panels **A and B,** the buffer and the MANT-nucleotide basal fluorescence were subtracted from the fluorescence after addition of EF3(N583H) (*green* line) and CaM (*blue* line). Shown are superimposed recordings of a representative experiment. Similar data were obtained in 5 independent experiments. a.u., arbitrary unit.

Fig. 10: Analysis of the interaction of EF3(K353A) with Bis-MANT-ATP and Bis-MANT-CTP in fluorescence experiments

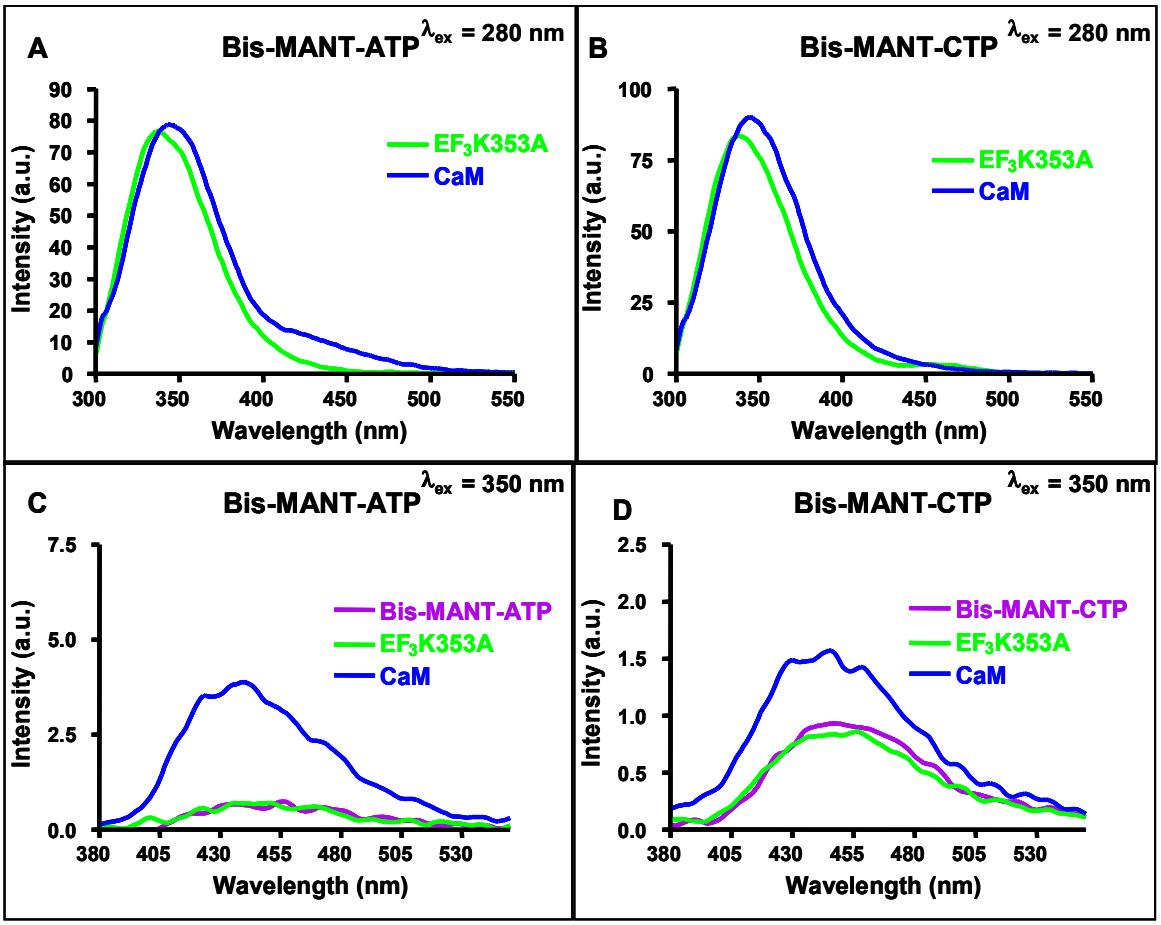

FRET and direct fluorescence experiments were performed as described under "Materials and Methods". The assay buffer consisted of 75 mM HEPES/NaOH, 100 μM $CaCl_2$, 100 mM KCl and 5 mM $MnCl_2$, pH 7.4. Nucleotides were added to the buffer to yield 300 nM final concentrations. EF3(K353A) (300 nM final concentration) was added followed by the addition of CaM (1 μM final concentration). Steady state emission spectra were recorded. In FRET studies (panels **A** and **B**) emission was scanned at an excitation wavelength of 280 nm after each addition. In direct fluorescence studies (panels **C** and **D**), emission was scanned at an excitation wavelength of 350 nm after each addition. In panels **A and B,** the buffer and the MANT-nucleotide basal fluorescence were subtracted from the fluorescence after addition of EF3(K353A) (*green* line) and CaM (*blue* line). Shown are superimposed recordings of a representative experiment. Similar data were obtained in 5 independent experiments. a.u., arbitrary unit.

Fig. 11: Analysis of the interaction of EF3(K353R) with Bis-MANT-ATP and Bis-MANT-CTP in fluorescence experiments

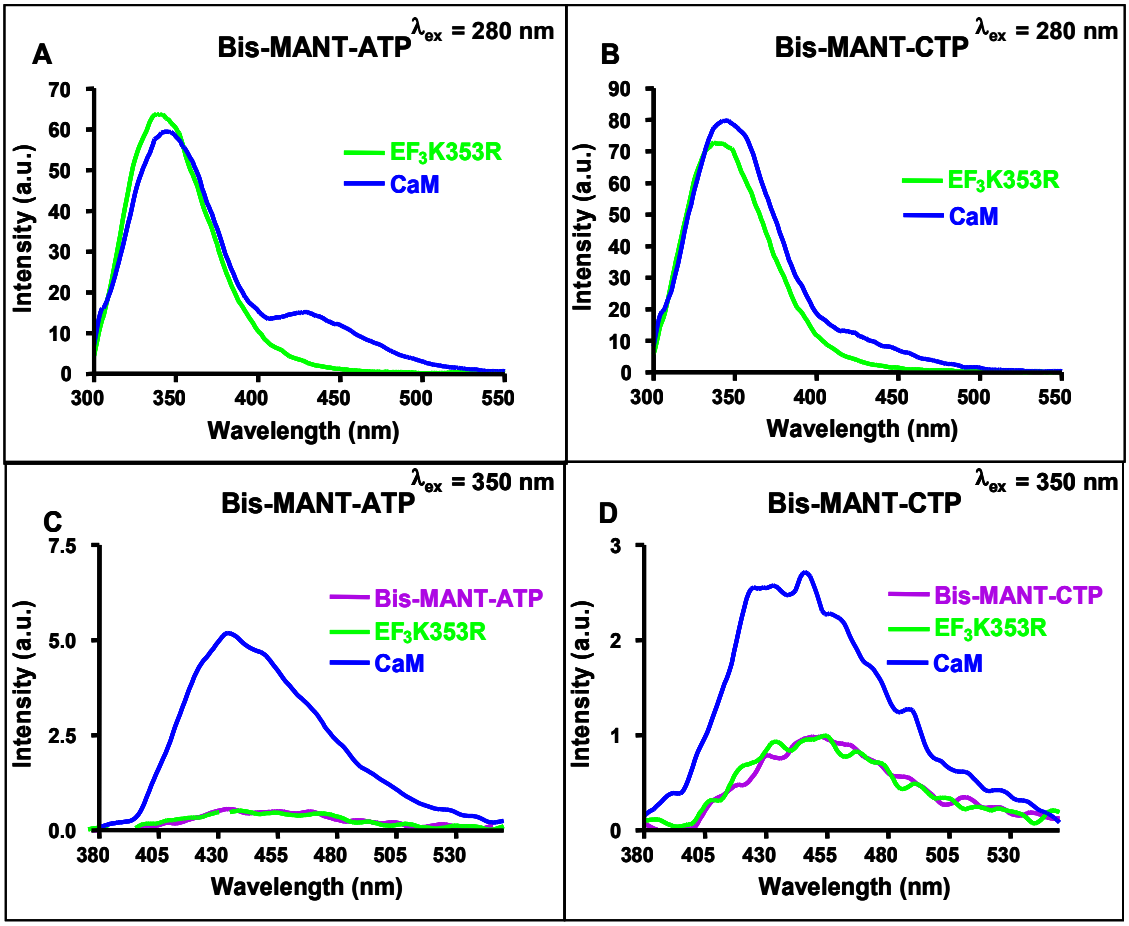

FRET and direct fluorescence experiments were performed as described under "Materials and Methods". The assay buffer consisted of 75 mM HEPES/NaOH, 100 μM $CaCl_2$, 100 mM KCl and 5 mM $MnCl_2$, pH 7.4. Nucleotides were added to the buffer to yield 300 nM final concentrations. EF3(K353R) (300 nM final concentration) was added followed by the addition of CaM (1 μM final concentration). Steady state emission spectra were recorded. In FRET studies (panels **A** and **B**) emission was scanned at an excitation wavelength of 280 nm after each addition. In direct fluorescence studies (panels **C** and **D**), emission was scanned at an excitation wavelength of 350 nm after each addition. In panels **A and B,** the buffer and the MANT-nucleotide basal fluorescence were subtracted from the fluorescence after addition of EF3(K353R) (*green* line) and CaM (*blue* line). Shown are superimposed recordings of a representative experiment. Similar data were obtained in 5 independent experiments. a.u., arbitrary unit.

Fig. 12: Direct fluorescence experiments of Bis-MANT-ATP and Bis-MANT-CTP in the presence of water and different DMSO concentrations

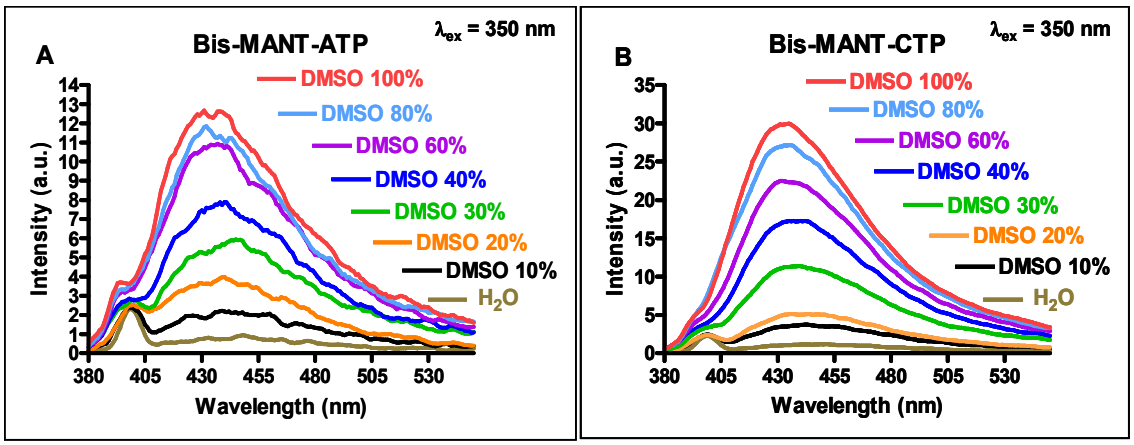

Direct fluorescence experiments of Bis-MANT-nucleotides were performed as described under "Materials and Methods". The excitation wavelength was 350 nm, and emission was scanned from 380 nm to 550 nm. Nucleotides were added to the water and DMSO to yield 300 nM final concentrations. To mimic binding of the Bis-MANT-group to a hydrophobic binding pocket, Bis-MANT-ATP (**A**) and Bis-MANT-CTP (**B**) were directly excited in water plus dimethyl sulfoxide DMSO (10%-100%) (v/v). Shown are superimposed recordings of a representative experiment. Similar data were obtained in 5 independent experiments. a.u., arbitrary unit.

Fig. 13 shows the kinetics of FRET experiments with Bis-MANT-ATP and Bis-MANT- CTP at a fixed emission wavelength of 440 nm. Sequential addition of EF3 and CaM resulted only in small fluorescence increases, reflecting the far end of the tryptophan/tyrosine emission spectrum (see Figs. 4-11). Addition of bis-MANT-nucleotides to cuvettes instantaneously resulted in substantial fluorescence increases, reflecting FRET. Addition of the high-affinity EF inhibitor and non-fluorescent nucleotide analog PMEApp (1 μM) (20, 23) to cuvettes reduced the fluorescence signals with both bis-MANT-nucleotides (300 nM each).

Fig. 13: Kinetic analysis of the interaction of EF3 with Bis-MANT-nucleotides and CaM in FRET experiments

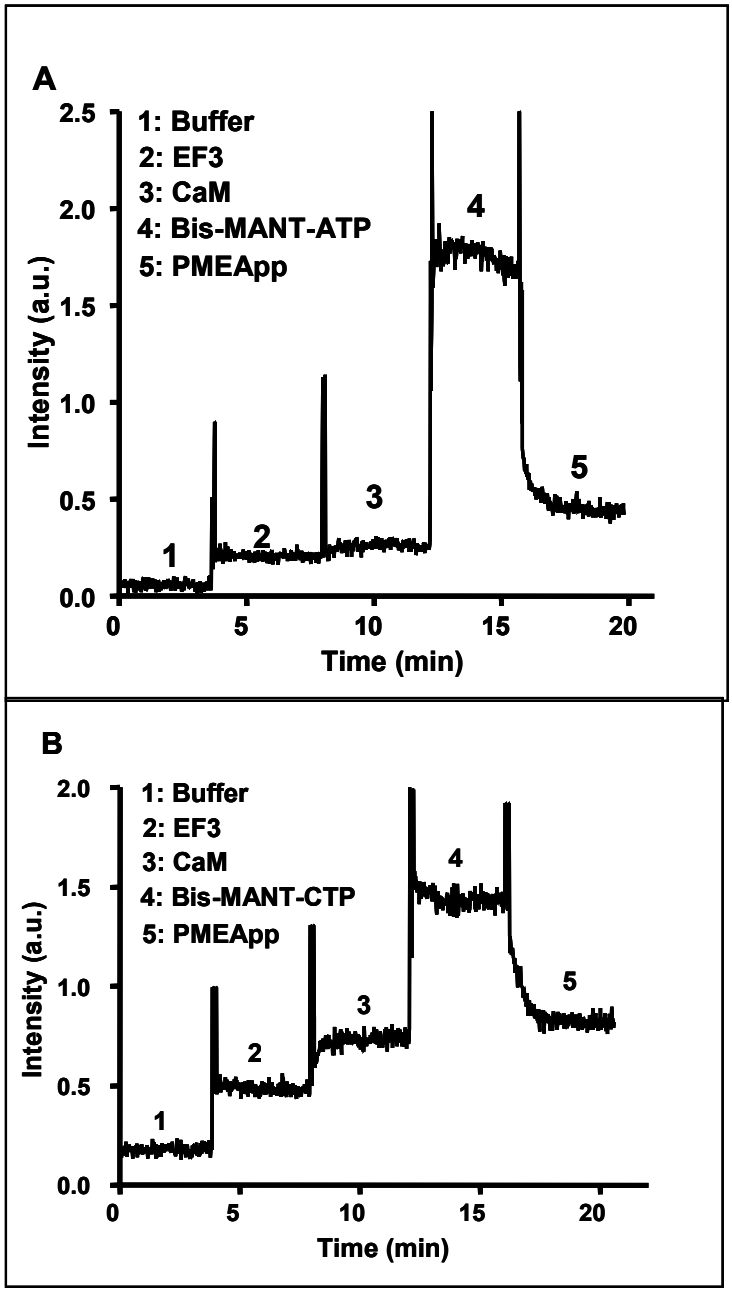

FRET kinetic experiments were performed as described under "Materials and Methods". The excitation wavelength was 280 nm and emission was detected at 430 nm over time. Successively, buffer (**1**), 300 nM EF3 (**2**), 1 µM CaM (**3**), nucleotide (**A**: Bis-MANT-ATP, **B**: Bis-MANT-CTP, 300 nM each) (**4**) and PMEApp (1 µM) (**5**) were added. A recording of a representative experiment is shown. Similar data were obtained in 4 independent experiments. a.u., arbitrary unit.

5. Discussion

In a previous study, the unexpected by-product Bis-MANT-IMP, obtained in synthesis scheme of MANT-ITP, was serendipitously found to possess higher affinity to the nucleotide-binding site of CyaA than the corresponding MANT-IMP (20). The higher affinity of the Bis-MANT-IMP compared with MANT-IMP was attributed to interactions of the 2´MANT-group with a hydrophobic site consisting of P305 and F261 (20). undoubtedly, the introduction of a second MANT-group increased the inhibitor affinity to CyaA. In addition, the introduction of a second MANT-group to MANT-ATP exhibited clear differences in fluorescence responses of MANT- ATP and Bis-MANT-ATP with EF3 in both direct fluorescence and FRET studies.

These findings prompted us to characterize the interaction of the catalytic site of EF with bis-MANT-nucleotides possessing various purine and pyrimidine bases, specifically, Bis-MANT-ATP and Bis-MANT-CTP in order to better dissect the unique preference of EF to base cytosine and better understand the molecular mechanisms of EF inhibition and to provide the basis for the rational development of potent and selective EF inhibitors. Such EF inhibitors could be useful compounds to treat EF toxinemia and antibiotic-resistant *Bacillus anthracis* strains (31).

The structure/activity relationships of (MANT)-nucleotides at EF, CyaA and mAC are different, indicating that in principle, the development of potent and selective EF and AC isoform-specific inhibitors is feasible. Our recent study showed that CTP inhibited EF more than 400-fold more potently than mAC (23, 24). Substitution of the 2'(3')-*O*-ribosyl position of CTP with a MANT group decreased the K_i value from 5 μM to 100 nM, yielding an EF inhibitor that is even 5-10-fold more potent than MANT-ATP in the presence of Mn^{2+}; i.e., EF exhibited high unexpected preference for the base cytosine (23). Surprisingly, among the studied bis-MANT-nucleotides only Bis-MANT-CTP exhibited a lower potency than the corresponding MANT-CTP.

These data prompted us to analyze EF inhibition by Bis-MANT-CTP and Bis-MANT-ATP in more detail. The analysis of enzyme inhibition kinetics revealed

that both Bis-MANT-CTP and Bis-MANT-ATP are competitive EF inhibitors; i.e., they bind to the same site as, and freely compete with, the substrate ATP (Fig. 4). These data ruled out the existence of a hitherto unidentified cytosine base-preferring nucleotide-binding site in the structurally very complex EF protein (4, 15). Kinetic FRET competition experiments with the non-fluorescent ATP analogue PMEApp revealed that both Bis-MANT- ATP and Bis-MANT-CTP reversibly bind to the EF-catalytic site (Fig. 13), corroborating the competitive inhibition mode and the existence of a single nucleotide-binding site in EF. The slower displacement of both Bis-MANT-ATP and Bis-MANT-CTP from EF by PMEApp is explained by the higher affinity of EF for bis-MANT-nucleotides.

Our study demonstrates a noteworthy dissociation between ligand-affinity for EF as assessed by the inhibition of catalysis and FRET on one hand and both the maximum stimulation of direct fluorescence and FRET upon activation of CaM on the other hand. Most notably, both Bis-MANT-ATP and Bis-MANT-CTP possess the same K_i value at EF3 Table 1 and 2. However, in terms of maximum direct fluorescence and FRET signals, Bis-MANT-CTP is clearly surpassed by Bis-MANT-ATP (Fig. 4).In Chapter III, similar dissociations between affinity and maximum fluorescence signals were observed for the comparison of MANT-ATP and MANT-CTP at EF (23). An explanation for these discrepancies could be differences in mobility of the various fluorescence probes, with the more rigidly bound ligands being more effective in terms of direct MANT fluorescence and FRET (20, 23).

A previous study had shown that F586 mediates π-stacking interactions with 2'-deoxy-3'-ANT-ATP, resulting in a fluorescence increase upon excitation of the ANT-group (15). Our previous study also showed that the mutation of F586 resulted in 5-6-fold reduction in potencies of both MANT-ATP and MANT-CTP and largely reduced the CaM-dependent FRET of MANT-ATP. However, the small FRET signal intensity of MANT-CTP with EF3 was slightly reduced in EF3(F586A). The models of the MANT-nucleotides binding mode suggested a similar binding mode of MANT-CTP and its ATP analogue with subtle differences due to the nucleobases occur and may account for the higher potency and the small FRET signal of MANT-CTP. In particular, the cytosine moiety formed water-mediated hydrogen bonds with R329 and E580 and favourably fit to the amide dipole of N583. Additionally, the flexibility of

the bound cytosine was greater than in the case of the bulkier adenine ring. Together with the specific charge distribution in the vicinity of the nucleobase, these might lead to absorption and thus attenuation of the FRET energy which is mainly due to tyrosine and tryptophan residues in switch C.

In agreement with those data, the interaction of Bis-MANT-ATP and Bis-MANTCTP with several EF mutants in terms of enzyme inhibition and fluorescence spectroscopy showed that F586 is also important for the interaction with Bis-MANT-ATP and Bis-MANT-CTP as is revealed by the 5-6-fold reduction in potency (Table 2). Nonetheless, the small FRET and direct fluorescence signal intensities with Bis-MANT-CTP in EF, compared to MANT-ATP, was much smaller, and the F586A mutation had a smaller inhibitory effect on the FRET and direct fluorescence signal intensities (Fig. 5).

H577 plays a crucial role in catalysis as is reflected by the very low catalytic activity of the H577A mutant (4, 23, 32). In addition, Bis-MANT-ATP and Bis-MANT-CTP exhibited no FRET signal at all in H577A mutant (Fig. 6, **A** and **B**), and largely reduced signal intensities in direct fluorescence studies (Fig. 6, **C** and **D**). Nonetheless, this mutation did not exert detrimental effect on substrate- and inhibitor binding per se (Tables 2) (23).

N583 forms a crucial hydrogen bond with the ribosyl moiety of nucleotides bound to the catalytic site of EF (4, 23). Accordingly, replacement of N583 by a non-hydrogen bond-forming amino acid (N583A) or hydrogen bond- forming amino acid with a different spatial arrangement of the bonding partners (N583Q and N383H) substantially decreases catalytic activity of the resulting EF mutants (4, 23). Moreover, N583 mutants substantially reduced the potencies of MANT-ATP and MANT-CTP (23). Similarly, N583 mutants substantially reduced the potencies of Bis-MANT-ATP and Bis-MANT-CTP. Interestingly, N583 mutants reduced the inhibitor potencies of both bis-MANT-nucleotides to a similar extent. Moreover, in N583 mutants, the FRET and direct fluorescence signals intensities were markedly reduced (Figs. 7-9). In addition, the bis-MANT-nucleotides potencies were more strongly reduced by the N583Q and N583H than by N583A mutation. These findings imply a substantial spatial constraint in this part of the binding pocket and

highlight the importance of the spatial arrangement of N583 for the binding of bis-MANT-nucleotides.

We showed previously that the base is locked into the catalytic site by the ionic bond formed between the carboxyl group of E588 and the amino group of K353 (4, 23). In addition, disruption of this ionic bond by the K353A mutation largely reduces catalytic activity and lowers substrate affinity (4, 23) but K353R displayed less severe impairment of catalysis and no change in K_m (23). In the present study, the affinity of Bis-MANT-ATP and Bis-MANT-CTP to the EF-catalytic site is obviously reduced in EF3(K353A) mutant as revealed by higher K_i values (Table 2) and lower intensities of FRET and direct fluorescence signals (Fig. 10). The K353R mutation had only a small effect on inhibitor affinity as revealed by AC and fluorescence assays (Table 2 and Fig. 11). The binding of bis-MANT-nucleotides to the EF-catalytic site was largely affected by disruption of the ionic bond by the K353A mutation. The K353R mutation that alters the spatial arrangement of the catalytic site but still allows ionic bridge formation did not affect the inhibitor potency substantially.

The inhibitory potencies of position-5-substituted-MANT-nucleotides were slightly higher than those of the corresponding bis-MANT-nucleotides (Table 3). Similar data were obtained in case of propyl-ANT-nucleotides; i.e., propyl-ANT-nucleotides were more potent than the corresponding Bis-propyl-ANT-analogues. For example, propyl-ANT-ATP was 13-fold more potent than Bis-propyl-ANT-ATP (Table 3). The most interesting finding is the higher potency of N-propyl-ANT-nucleotides compared to the corresponding MANT-analogues. H351 amino acid interacts with amino function of MANT Substituents. These interactions my account for the higher potency of the compounds possess longer aliphatic chain at the N-position of anthraniloyl ring. It will also be very interesting to examine the effects of the longer aliphatic chain at the N-position of anthraniloyl ring.

Our data have important conceptual implications for future drug development. These results are valuable for the development of potent EF inhibitors with selectivity relative to mammalian membranous ACs. Considering the fact EF exhibits a uniquely high affinity for base cytosine. The analysis of the interaction of PMECpp with EF will be particularly interesting.

Our present data have also practical implications for future EF inhibitor development. Specifically, the lower basal fluorescence of bis-MANT-analogues and the higher CaM-dependent fluorescence signals at the excitation wave length 350 nm (Figs. 4-11, C and D), could be used as non-radioactive high-throughput screening assay for EF inhibitors, including compounds binding to the catalytic site as well as compounds impeding with the interaction of EF and CaM. The establishment of such an assay will be facilitated by the fact that EF can be purified in large quantities. Such FRET assay constitutes a valuable complementation of the sensitive radiometric AC assay.

To the best of our knowledge, this is the first study that systematically compares the interaction of bis-MANT-nucleotides with EF3 and EF3 mutants, using enzymological and biophysical analysis.

6. Conclusion

In conclusion, using enzymatic and fluorescence spectroscopy approaches, our present study shows that bulky bis-MANT- and bis-propyl-ANT-substituted purine and pyrimidine nucleotides are readily accommodated by the nucleotide-binding-site of EF. Thus, the results of this study lend further support to the broad hypothesis that the catalytic sites of various structurally unrelated ACs including mammalian membranous ACs and bacterial AC toxins exhibit substantial degrees of conformational flexibility, allowing for numerous structural modifications in nucleotide inhibitors and the development of EF-potent and selective inhibitors. Our present study also provides valuable insights into the molecular mechanisms of ligand/EF interactions, yields highly sensitive fluorescence probes for EF analysis and facilitates the design of potent and selective EF inhibitors.

7. References

1. Mock M, Fouet A. Anthrax. *Annu Rev Microbiol* 2001; **55**:647-71.
2. Mourez M, Lacy DB, Cunningham K, Legmann R, Sellman BR, Mogridge J, Collier RJ. 2001: a year of major advances in anthrax toxin research. *Trends Microbiol* 2002; **10**:287-93.
3. Leppla SH. Anthrax toxin edema factor: a bacterial adenylate cyclase that increases cyclic AMP concentrations of eukaryotic cells. *Proc Natl Acad Sci USA* 1982; **79**:3162-6.
4. Drum CL, Yan SZ, Bard J, Shen YQ, Lu D, Soelaiman S, Grabarek Z, Bohm A, Tang WJ. Structural basis for the activation of anthrax adenylyl cyclase exotoxin by calmodulin. *Nature* 2002; **415**:396-402.
5. Guidi-Rontani C, Levy M, Ohayon H, Mock M. Fate of germinated *Bacillus anthracis* spores in primary murine macrophages. *Mol Microbiol* 2001; **42**:931-8.
6. Hoover DL, Friedlander AM, Rogers LC, Yoon IK, Warren RL, Cross AS. Anthrax edema toxin differentially regulates lipopolysaccharide-induced monocyte production of tumor necrosis factor alpha and interleukin-6 by increasing intracellular cyclic AMP. *Infect Immun* 1994; **62**:4432-9.
7. Brossier F, Weber-Levy M, Mock M, Sirard JC. Role of toxin functional domains in anthrax pathogenesis. *Infect Immun* 2000; **68**:1781-6.
8. Petosa C, Collier RJ, Klimpel KR, Leppla SH, Liddington RC. Crystal structure of the anthrax toxin protective antigen. *Nature* 1997; **385**:833-8.
9. Duesbery NS, Webb CP, Leppla SH, Gordon VM, Klimpel KR, Copeland TD, Ahn NG, Oskarsson MK, Fukasawa K, Paull KD, Vande Woude GF. Proteolytic inactivation of MAP-kinase-kinase by anthrax lethal factor. *Science* 1998; **280**:734-7.
10. Vitale G, Bernardi L, Napolitani G, Mock M, Montecucco C. Susceptibility of mitogen-activated protein kinase kinase family members to proteolysis by anthrax lethal factor. *Biochem J* 2000; **352**:739-45.

11. Agrawal A, Lingappa J, Leppla SH, Agrawal S, Jabbar A, Quinn C, Pulendran B. Impairment of dendritic cells and adaptive immunity by anthrax lethal toxin. *Nature* 2003; **424**:329-34.

12. Pellizzari R, Guidi-Rontani C, Vitale G, Mock M, Montecucco C. Anthrax lethal factor cleaves MKK3 in macrophages and inhibits the LPS/IFNgamma-induced release of NO and TNFalpha. *FEBS Lett* 1999; **462**:199-204.

13. Dixon TC, Meselson M, Guillemin J, Hanna PC. Anthrax. *N Engl J Med* 1999; **341**:815-26.

14. Atlas RM. Bioterriorism: from threat to reality. *Annu Rev Microbiol* 2002; **56**:167-85.

15. Shen Y, Lee YS, Soelaiman S, Bergson P, Lu D, Chen A, Beckingham K, Grabarek Z, Mrksich M, Tang WJ. Physiological calcium concentrations regulate calmodulin binding and catalysis of adenylyl cyclase exotoxins. *EMBO J* 2002; **21**:6721-32.

16. Shen Y, Zhukovskaya NL, Guo Q, Florian J, Tang WJ. Calcium-independent calmodulin binding and two-metal-ion catalytic mechanism of anthrax edema factor. *EMBO J* 2005; **24**:929-41.

17. Gille A, Lushington GH, Mou TC, Doughty MB, Johnson RA, Seifert R. Differential inhibition of adenylyl cyclase isoforms and soluble guanylyl cyclase by purine and pyrimidine nucleotides. *J Biol Chem* 2004; **279**:19955-69.

18. Mou TC, Gille A, Fancy DA, Seifert R, Sprang SR. Structural basis for the inhibition of mammalian membrane adenylyl cyclase by 2 '(3')-O-(N-methylanthraniloyl)-guanosine 5 '-triphosphate. *J Biol Chem* 2005; **280**:7253-61.

19. Mou TC, Gille A, Suryanarayana S, Richter M, Seifert R, Sprang SR. Broad specificity of mammalian adenylyl cyclase for interaction with 2',3'-substituted purine- and pyrimidine nucleotide inhibitors. *Mol Pharmacol* 2006; **70**:878-86.

20. Göttle M, Dove S, Steindel P, Shen Y, Tang WJ, Geduhn J, König B, Seifert R. Molecular analysis of the interaction of *Bordetella pertussis* adenylyl cyclase with fluorescent nucleotides. *Mol Pharmacol* 2007; **72**:526-35.

21. Hiratsuka T. New ribose-modified fluorescent analogs of adenine and guanine nucleotides available as substrates for various enzymes. *Biochim Biophys Acta* 1983; **742**:496-508.

22. Jameson DM, Eccleston JF. Fluorescent nucleotide analogs: synthesis and applications. *Methods Enzymol* 1997; **278**:363-90.

23. Taha HM, J. Göttle, M. Suryanarayana, S. Shen, Y. Tang, W. J. Gille, A. Geduhn, J. Konig, B. Dove, S. Seifert, R. Molecular analysis of the interaction of anthrax adenylyl cyclase toxin, edema factor, with 2'(3')-O-(N-(methyl)anthraniloyl)-substituted purine and pyrimidine nucleotides. In. *Mol Pharmacol*. 2009; **75**:693-703

24. Gille A, Guo J, Mou TC, Doughty MB, Lushington GH, Seifert R. Differential interactions of G-proteins and adenylyl cyclase with nucleoside 5'-triphosphates, nucleoside 5'-[gamma-thio]triphosphates and nucleoside 5'-[beta,gamma-imido]triphosphates. *Biochem Pharmacol* 2005; **71**:89-97.

25. Wang JL, Guo JX, Zhang QY, Wu JJ, Seifert R, Lushington GH. A conformational transition in the adenylyl cyclase catalytic site yields different binding modes for ribosyl-modified and unmodified nucleotide inhibitors. *Bioorg Med Chem* 2007; **15**:2993-3002.

26. Clark M CRr, Van Opdenbosh N. Validation of the general purpose Tripose 5.2 force field. *J Comput Chem* 1989; **10**:982-1012.

27. Shen Y, Guo Q, Zhukovskaya NL, Drum CL, Bohm A, Tang WJ. Selective inhibition of anthrax edema factor by adefovir, a drug for chronic hepatitis B virus infection. *Proc Natl Acad Sci USA* 2004; **101**:3242-7.

28. Hiratsuka T. Fluorescent and colored trinitrophenylated analogs of ATP and GTP. *Eur J Biochem* 2003; **270**:3479-85.

29. Wolberg G, and Zimmerman, TP. Effects of calmodulin antagonists on immune mouse lymphocytes. *Mol Pharmacol* 1984; **26**:286-92.

30. Lakowizc RJ. Principles of fluorescence spectroscopy. *second edition* , *Principles of* fluorescence spectroscopy. *Kluwer Academic.* 1999

31. Jedrzejas MJ. The structure and function of novel proteins of *Bacillus anthracis* and other spore-forming bacteria: development of novel prophylactic and therapeutic agents. *Crit Rev Biochem Mol Biol* 2002; **37**:339-73.

32. Guo Q, Shen Y, Zhukovskaya NL, Florian J, Tang WJ. Structural and kinetic analyses of the interaction of anthrax adenylyl cyclase toxin with reaction products cAMP and pyrophosphate. *J Biol Chem* 2004; **279**:29427-35.

33. Gille A, Seifert R. 2'(3')-O-(N-methylanthraniloyl)-substituted GTP analogues: a novel class of potent competitive adenylyl cyclase inhibitors. *J Biol Chem* 2003; **278**:12672-9.

Appendix

1. Curriculum Vitae

Personal details

Name	Hesham Hamada Taha Mohammed
Date of birth	August, 31st, 1977
Place of birth	Cairo, Egypt
Nationality	Egyptian
Marital status	Married and have four kids

Scientific Education And Training

09.2006 - 10.2009	PhD program Institute of Chemistry and Pharmacy University of Regensburg, Germany Under supervision of Prof. Dr. R. Seifert Head of the Dept. of Pharmacology and Toxicology
07.2005	Master degree in pharmaceutical Sciences (Biochemistry). The title of the thesis ”Possible therapeutic effects of Cu (I)-nicotinic acid complex on the rat-model with fatty liver” Faculty of Pharmacy University of Assiut- Egypt
08.2001 – 07.2005	Master program in pharmaceutical Sciences (Biochemistry). Dept. of Biochemistry - Faculty of Pharmacy University of Assiut- Egypt
08.2000 – 08.2001	Pharmacist in Dr. Ayman pharmacy Cairo - Egypt
5.2000	Bachelor degree in pharmaceutical sciences with general grade “Excellent with degree of houner” Faculty of Pharmacy, Al-Azhar University, Assiut, Egypt
09.1995 – 05.2000	Study of pharmaceutical sciences Faculty of Pharmacy Al-Azhar University, Assiut, Egypt

Professional Experience

07.2005 – 08.2006	Assistant Lecturer of Biochemistry Dept. of Biochemistry

	Al-Azhar University, Assiut, Egypt
08.2001 – 07.2005	Demonstrator of Biochemistry Dept. of Biochemistry Al-Azhar University, Assiut, Egypt

Professional Training

2002	Advanced course in Instrumental analysis Faculty of Pharmacy University of Assiut- Egypt
2002	Advanced course in physical chemistry Faculty of Pharmacy University of Assiut- Egypt
2003	Advanced course in Mathematics and statistics Faculty of Pharmacy University of Assiut- Egypt
2003	Advanced course in Laboratory safety and waste disposal Faculty of Pharmacy University of Assiut- Egypt
2003	Advanced course in Molecular biology Faculty of Pharmacy University of Assiut- Egypt
2003	Advanced course in General metabolism Faculty of Pharmacy University of Assiut- Egypt
2006	International computer driving license (ICDL) Information Technology center Cairo – Egypt

Scholarship

09.2006 – 11.2009	Scholarship funded from the Egyptian government – Ministry of higher education for obtaining PhD degree

2. Abbreviation List

AC	Adenylyl cyclase
Ac-NH_2	Acetylamino
Ac	Acetyl
AMPCPP	Adenosine 5'-(α, β-methylene)-triphosphate
ANT	Anthraniloyl
ATP	Adenosine 5'-triphosphate
ANTXR1	Anthrax toxin receptor 1
ANTXR2	Anthrax toxin receptor 2
AVA	Anthrax Vaccine Adsorbed
a.u	Arbitrary unit
CaM	Calmodulin
cAMP	Adenosine 3',5'-cyclic monophosphate
CDC	Centers for Disease Control and Prevention
CTP	Cytidine 5'-triphosphate
CyaA	Exotoxin AC of *Bordetella pertussis*
d-	Deoxy
DAD	Diode array detector
DNA	Deoxyribonucleic acid
EDTA	Ethylene diaminetetraacetic acid disodium salt
EF	Full length edema factor, anthrax adenylyl cyclase toxin
EF3	Calmodulin-activated catalytic domain of EF
EGTA	Ethylene glycol tetraacetic acid
EI	Electronic ionisation
eq	Equivalents
EPR	Electron Paramagnetic Resonance
ESI	Electronic spray ionisation
ET	Edema toxin (edema factor and protective antigen)
FDA	Food and drug administration
Fig.	Figure
FPLC	Fast Protein Liquid Chromatography system
FRET	Fluorescent resonance energy transfer
FS	Forskolin
GMPPNP	Guanosine 5'-[β, γ-imido]triphosphate
GPCR	G-protein coupled receptor
GTP	Guanosine 5'-triphosphate
GTP γS	Guanosine 5'-(γ-thio) triphosphate
HEPES	4-(2-hydroxyethyl)- piperazine-1-ethane sulfonic acid
HPLC	High performance liquid chromatography

IC_{50}	Half-maximal inhibition concentration
IR	Infrared spectroscopy
IMAC	Immobilized metal ion-affinity chromatography
IMP	Inosine 5'-monophosphate
IPTG	Isopropyl-1-thio galactopyranoside
ITP	Inosine 5'-triphosphate
ITPγS	Inosine 5'-(γ-thio) triphosphate
J	Coupling constant
K	Capacity factor
kDa	Kilodalton
K_d	Dissociation constant
K_i	Inhibition constant
K_m	Michaelis Menten constant
KO	Knockout
LB medium	Luria-Bertani medium
LC	Liquid chromatography
LF	Lethal factor
LRP6	Low density lipoprotein receptor-related protein 6
LT	Lethal toxin (lethal factor and protective antigen)
LTP	Long-term potentiation
mAC	Membranous adenylyl cyclase
MANT	Methyl anthraniloyl
MAPK	Mitogen–activated protein kinase
mAU	Milli absorbance unit
MEKs	Mitogen–activated protein kinase Kinases
MES	2-(N-morpholino)ethanesulfonic acid
Mp	Melting point
mRNA	Messenger ribonucleic acid
MS	Mass spectroscopy
MW	Molecular weight
m/v	Mass per volume
NDP	Nucleoside 5'-diphosphate
NMP	Nucleoside 5'-mono phosphate
NMR	Nuclear magnetic resonance
NTP	Nucleoside 5'-triphosphate
PA	Protective antigen
PDB	Protein data bank
PKA	Protein kinase A
PKC	Protein kinase C
PMEApp	9-[2-(phosphonomethoxy) ethyl]adenine diphosphate

PMNS	Polymorphonuclear cells
PMSF	Phenyl methyl sulfonyl fluoride
PMT	Photomultiplier
PP_i	Pyrophosphate
PTFE	Polytetrafluorethylene
RAP1	Small GTPase protein
ROS	Reactive oxygen species
rpm	Rrevolution per minute
rPA	Recombinant protective antigen
R_f	Retention factor
R_t	Retention time
sAC	Soluble adenylyl cyclase
SD	Standard deviation
SDS-PAGE	Sodium dodecyl sulfate; polyacrylamide gel electrophoresis
Sf	*Spodoptera frugiperda*
TNP	2,4,6 trinitrophenyl
Tris	Tris(hydroxymethyl)aminomethane
tRNA	Transfere ribonucleic acid
UTP	Uridine 5’-triphosphate
v/v	Volume per volume

Eidesstattliche Erklärung

Ich erkläre hiermit an Eides statt, dass ich die vorliegende Arbeit ohne unzulässige Hilfe Dritter und ohne Benutzung anderer als der angegebenen Hilfsmittel angefertigt habe. Die aus anderen Quellen direkt oder indirekt übernommenen Daten und Konzepte sind unter Angabe des Literaturzitats gekennzeichnet. Weitere Personen waren an der inhaltlich-materiellen Herstellung der vorliegenden Arbeit nicht beteiligt.
Insbesondere habe ich hierfür nicht die entgeltliche Hilfe eines Promotionsberaters oder anderer Personen in Anspruch genommen. Niemand hat von mir weder unmittelbar noch mittelbar geldwerte Leistungen für Arbeiten erhalten, die im Zusammenhang mit dem Inhalt der vorgelegten Dissertation stehen. Die Arbeit wurde bisher weder im In- noch im Ausland in gleicher oder ähnlicher Form einer anderen Prüfungsbehörde vorgelegt.

Regensburg, den _____

Hesham Hamada Taha Mohammed